JPTM

Journal of Pathology and Translational Medicine

May 2022
Vol. 56 / No.3
jpatholtm.org
pISSN: 2383-7837
eISSN: 2383-7845

Central Nervous System

Hemangioblastoma

Journal of Pathology and Translational Medicine

Volume 56 • Number 3 • May 2022 (bimonthly)
Published since 1967
Printed on 11 May 2022 Published on 15 May 2022

J Pathol Transl Med
pISSN: 2383-7837
eISSN: 2383-7845

Aims & Scope

The Journal of Pathology and Translational Medicine is an open venue for the rapid publication of major achievements in various fields of pathology, cytopathology, and biomedical and translational research. The Journal aims to share new insights into the molecular and cellular mechanisms of human diseases and to report major advances in both experimental and clinical medicine, with a particular emphasis on translational research. The investigations of human cells and tissues using high-dimensional biology techniques such as genomics and proteomics will be given a high priority. Articles on stem cell biology are also welcome. The categories of manuscript include original articles, review and perspective articles, case studies, brief case reports, and letters to the editor.

Subscription Information

To subscribe to this journal, please contact the Korean Society of Pathologists/the Korean Society for Cytopathology. Full text PDF files are also available at the official website (https://jpatholtm.org). *Journal of Pathology and Translational Medicine* is indexed by Emerging Sources Citation Index (ESCI), PubMed, PubMed Central, Scopus, KoreaMed, KoMCI, WPRIM, Directory of Open Access Journals (DOAJ), and CrossRef. Circulation number per issue is 50.

Contact the Korean Society of Pathologists/the Korean Society for Cytopathology

Publishers: Nam, Jong Hee, MD, Gong, Gyungyub, MD
Editors-in-Chief: Jung, Chan Kwon, MD, Park, So Yeon, MD
Published by the Korean Society of Pathologists/the Korean Society for Cytopathology

Editorial Office
Room 1209 Gwanghwamun Officia, 92 Saemunan-ro, Jongno-gu, Seoul 03186, Korea
Tel: +82-2-795-3094 Fax: +82-2-790-6635 E-mail: office@jpatholtm.org

#1508 Renaissancetower, 14 Mallijae-ro, Mapo-gu, Seoul 04195, Korea
Tel: +82-2-593-6943 Fax: +82-2-593-6944 E-mail: office@jpatholtm.org

Printed by iMiS Company Co., Ltd. (JMC)
Jungang Bldg. 18-8 Wonhyo-ro 89-gil, Yongsan-gu, Seoul 04314, Korea
Tel: +82-2-717-5511 Fax: +82-2-717-5515 E-mail: ml@smileml.com

Manuscript Editing by InfoLumi Co.
210-202, 421 Pangyo-ro, Bundang-gu, Seongnam 13522, Korea
Tel: +82-70-8839-8800 E-mail: infolumi.chang@gmail.com

Front cover image: Histopathological features of central nervous system hemangioblastoma (p119).

Journal of Pathology and Translational Medicine

J Pathol Transl Med
pISSN: 2383-7837
eISSN: 2383-7845

Volume 56, Number 3, May 2022

CONTENTS

REVIEW

ORIGINAL ARTICLES

CASE REPORTS

CONTENTS CONTINUED

NEWSLETTER

Instructions for Authors for *Journal of Pathology and Translational Medicine* are available at http://jpatholtm.org/authors/authors.php

JPTM
Journal of Pathology and Translational Medicine 2022; 56: 115-125
https://doi.org/10.4132/jptm.2022.04.13

REVIEW

Neuropathologic features of central nervous system hemangioblastoma

Rebecca A. Yoda[1,2], Patrick J. Cimino[1]

[1]Department of Laboratory Medicine and Pathology, Division of Neuropathology, University of Washington, Seattle, WA;
[2]Department of Laboratory Medicine and Pathology, Division of Cytopathology, University of Washington, Seattle, WA, USA

Hemangioblastoma is a benign, highly vascularized neoplasm of the central nervous system (CNS). This tumor is associated with loss of function of the *VHL* gene and demonstrates frequent occurrence in von Hippel-Lindau (VHL) disease. While this entity is designated CNS World Health Organization grade 1, due to its predilection for the cerebellum, brainstem, and spinal cord, it is still an important cause of morbidity and mortality in affected patients. Recognition and accurate diagnosis of hemangioblastoma is essential for the practice of surgical neuropathology. Other CNS neoplasms, including several tumors associated with VHL disease, may present as histologic mimics, making diagnosis challenging. We outline key clinical and radiologic features, pathophysiology, treatment modalities, and prognostic information for hemangioblastoma, and provide a thorough review of the gross, microscopic, immunophenotypic, and molecular features used to guide diagnosis.

Key Words: Hemangioblastoma; von Hippel-Lindau disease; Neuropathology; Cerebellar neoplasms; Brain

Received: March 18, 2022 **Revised:** April 10, 2022 **Accepted:** April 13, 2022
Corresponding Author: Rebecca A. Yoda, MD, Department of Laboratory Medicine and Pathology, University of Washington, 325 9th Avenue, Box 359791, Seattle, WA 98104-2499, USA
Tel: +1-206-744-3145, Fax: +1-206-744-8240, E-mail: byoda@uw.edu
This invited review is a featured collaboration with PathologyOutlines.com.

Hemangioblastoma is a benign neoplasm of the central nervous system (CNS) which most commonly occurs in the cerebellum. This tumor is highly vascular and contains neoplastic stromal cells with typically vacuolar cytoplasm. It is associated with loss or inactivation of the *VHL* gene, with frequent occurrence in von Hippel-Lindau (VHL) disease [1]. This entity has historically been referred to as "capillary hemangioblastoma," "Lindau tumor," and "angioblastoma," although such terminologies are not currently recommended. Hemangioblastoma has an excellent prognosis with complete excision and is assigned a CNS World Health Organization (WHO) grade of 1 in the *World Health Organization classification of CNS tumors* [2]. Diagnosis of hemangioblastoma relies most heavily on histologic and immunophenotypic features with pieces of clinical, radiologic, and molecular information lending additional support.

EPIDEMIOLOGY

Hemangioblastomas are uncommon in the general population, with an overall incidence of 0.141 per 100,000 person-years in the United States [3]. They account for less than 2% of all CNS neoplasms but comprise an estimated 11% of primary posterior fossa tumors [4-6]. Some studies suggest a slightly higher incidence in male than in female patients, while others report no significant sex predilection [3,7,8]. Approximately 70% of cases are believed to be sporadic with the remaining 30% representing VHL-associated familial cases [9,10]. An estimated 60%–80% of patients with VHL disease develop CNS hemangioblastoma during their lifetime [11,12]. The average patient age at presentation varies by genetic subgroup, with VHL-associated tumors presenting on average two decades earlier than sporadic tumors; the mean age of onset is approximately 29 years in VHL-associated hemangioblastomas compared to 47 years in sporadic cases [9]. A comparison of epidemiologic data for sporadic and hereditary hemangioblastomas is summarized in Table 1.

LOCALIZATION

Hemangioblastomas may arise throughout the CNS, most commonly involve the cerebellum, brainstem, and spinal cord, in

pISSN 2383-7837
eISSN 2383-7845

Table 1. Summary of epidemiologic data for sporadic and hereditary hemangioblastomas

	Sporadic	Hereditary
Proportion of total cases (%)	~70	~30
Mean age of onset (yr)	47	29
Sex (M:F)	1–1.25:1	1–1.25:1
No. of tumors	Single	Multiple
Localization	Cerebellum most common	Higher proportion of extracerebellar sites (e.g. spine)
Molecular alterations	Somatic loss of VHL detected in subset of cases	VHL loss of function with germline mutation and somatic alteration

VHL, von Hippel-Lindau.

order of descending frequency [3]. Less common sites of involvement include the supratentorial compartment and spinal nerve roots [13]. Cases of extraneural hemangioblastomas are rare [14,15]. While the cerebellum is still the most common site of hemangioblastoma in VHL patients, a higher proportion of extra-cerebellar sites are seen in VHL-associated cases, including retinal involvement in 28%–50% [16,17]. Patients with VHL disease are more likely to present with multiple hemangioblastomas [10,13,18]. Other VHL-associated neoplasms and their common sites of involvement include clear cell renal cell carcinoma (CCRCC) of the kidneys, paragangliomas of the head and neck, pheochromocytoma of the adrenal gland, neuroendocrine islet cell tumors of the pancreas, endolymphatic sac tumors of the inner ear, and cystadenomas of the epididymis and broad ligament [19].

ETIOPATHOGENESIS

Loss of function of the *VHL* tumor suppressor gene is implicated in most cases of hemangioblastoma, both familial and sporadic. VHL disease is an autosomal dominant tumor predisposition syndrome resulting from inactivating germline mutation in the *VHL* tumor suppressor gene [19,20]. This gene is located on the short arm of chromosome 3 (3p25-26) [21]. Biallelic inactivation of *VHL* is frequently found in familial cases of hemangioblastoma, according to Knudson's "two-hit" hypothesis [22,23]. Under this system, a germline loss of function variant inactivates one copy of the *VHL* gene—the first hit—and loss of function of the remaining functional copy—the second hit—occurs prior to tumorigenesis [22]. The normally functioning VHL protein (pVHL) is involved in multiple cellular functions, including cell cycle regulation, apoptosis, and extracellular matrix formation [24-26]. pVHL also regulates cellular hypoxia signaling via the hypoxia-inducible factor (HIF) complex. Under normoxic conditions, the HIFα subunit undergoes hydroxylation creating a high affinity pVHL binding site [27,28]. As part of a multi-subunit ubiquitin ligase complex, pVHL facilitates HIFα polyubiquitylation and targeting for degradation [27-29]. In contrast, under hypoxic conditions, the HIF complex avoids hydroxylation and ubiquitin-associated degradation [30]. The stabilized complex serves as a transcription factor, upregulating the transcription of multiple growth factors to promote cell survival [31].

While hemangioblastoma pathogenesis is not yet fully understood, the pseudohypoxia hypothesis proposes a mechanism by which VHL loss promotes downstream tumorigenesis. Under this proposed pathway, *VHL* loss of function leads to loss of regulation of the HIF complex, which in turn promotes increased expression of growth factors in the absence of hypoxia, resulting in increased angiogenesis and conditions suitable for neoplastic growth [32].

HIF-independent pathways may also contribute to VHL disease and hemangioblastoma formation. VHL protein has been implicated in several other cellular functions, including regulation of apoptosis, microtubule stabilization, extracellular matrix formation, and cell-cell adhesion; loss of these functions could also contribute to tumorigenesis [33].

While the majority of familial cases demonstrate germline VHL loss, most studies indicate a smaller proportion of sporadic cases show VHL loss of function [34-36]. Historical studies of sporadic hemangioblastomas demonstrated VHL alterations in a minority of cases, although more recent investigation places the rate as high as 78% [36]. Older studies of sporadic hemangioblastoma may have shown erroneously low proportions of VHL loss due to low tumor purity. Since only the neoplastic stromal cells harbor the genetic alterations in sporadic cases, some alterations may evade detection when the stromal cells comprise a small fraction of the sampled tissue [36].

Epigenetic suppression may play a more prominent role in sporadic hemangioblastoma than in familial cases. One investigation found VHL promoter hypermethylation in 33% of sporadic hemangioblastomas but none of the VHL disease-associated cases [37]. Further studies are needed on sporadic cases without demonstrable VHL alterations to elucidate whether VHL loss is present but has not yet been detected, or if alternative pathways are responsible.

https://doi.org/10.4132/jptm.2022.04.13

CLINICAL FEATURES

Clinical signs and symptoms of hemangioblastoma are mainly attributed to the tumor's mass effect on adjacent regions, generalized increase in intracranial pressure, or obstruction of cerebrospinal fluid flow. General symptoms may include manifestations of increased intracranial pressure such as headaches, nausea, and emesis [10,38]. Secondary polycythemia may occur in approximately 5%–40% of cases, owing to ectopic production of erythropoietin [39,40].

Clinical presentation may vary widely based on anatomic localization of the tumor. Cerebellar tumors often present with dysmetria and ataxia [38]. In contrast, patients with spinal hemangioblastomas often present with symptoms associated with radiculopathy and myelopathy, including hypesthesia, weakness, hyperreflexia, pain, and incontinence [41,42]. Patients with brainstem hemangioblastomas may show evidence of cranial nerve impingement as well as increased intracranial pressure [43].

Some radiographic findings appear to correlate with symptomatology. Peritumoral cysts frequently underlie the clinical findings associated with hemangioblastomas, with at least 72% of symptomatic tumors but only 13% of asymptomatic tumors containing cysts [43]. In rare cases, hemangioblastomas may present with intraparenchymal, subarachnoid, or ventricular hemorrhage [44-46].

RADIOLOGIC FEATURES

Radiologic studies of hemangioblastoma generally show a well-demarcated enhancing mass ranging from solid to cystic, frequently presenting as a cyst with an enhancing mural nodule (Fig. 1) [47]. Tumors in the spinal cord are often associated with syrinx formation [48]. Computed tomography imaging demonstrates isodense signal compared to brain within the solid component [49]. Calcification is usually absent [49]. On magnetic resonance imaging, hemangioblastomas tend to appear as a T1 hypointense to isointense, T2 hyperintense nodule (Fig. 1) with serpentine flow voids in the nodular portion [47]. These tumors are often seen abutting the pia [50]. If a cystic component is present, the cyst wall rarely enhances [50].

MACROSCOPIC FEATURES

Grossly, hemangioblastomas appear as solid and/or cystic masses, often seen as a cyst with a mural nodule [43]. The tumors tend to be well-circumscribed and surrounded by a pseudocapsule [43]. Given the highly vascular nature of the neoplasm, cut surfaces may appear red in color, with yellow and orange variegation attributed to the high lipid content in neoplastic cells [51].

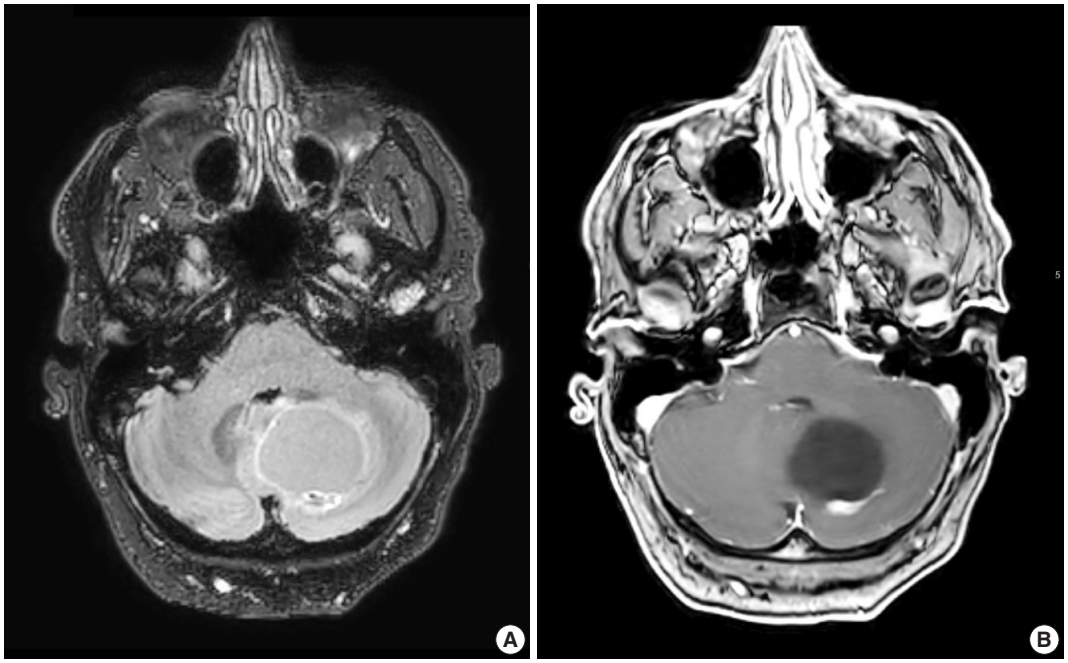

Fig. 1. Representative brain magnetic resonance imaging for hemangioblastoma. (A) T2/FLAIR and (B) T1-weighted post-contrast sequences showing a posterior fossa cystic mass with a mural enhancing nodule.

MICROSCOPIC FEATURES

Cytologic examination via direct smear or squash preparation can be a useful diagnostic aid at the time of intraoperative consultation. Unfortunately, hemangioblastoma samples are frequently resistant to squash preparation, resulting in thick clumps of tissue which may obfuscate cytologic detail (Fig. 2A) [52]. In the case of a successful cytologic smear preparation (or frozen section) with clearly visualized cells, the cytoplasm of neoplastic cells should demonstrate a characteristic foamy or finely vacuolated appearance (Fig. 2B) [52] . Cytoplasmic borders often appear indistinct, and nuclei may be mildly pleomorphic with hyperchromatic, speckled chromatin and occasional nuclear grooves [52]. Hemosiderin deposition is frequently seen, indicative of prior hemorrhage or red blood cell extravasation within these highly vascularized tumors [52].

On histologic sections, hemangioblastomas demonstrate compact, generally non-infiltrative growth patterns with variable lobularity [51]. The neoplastic component of these tumors are the stromal cells which are arranged within a rich network of thin-walled vessels (Fig. 3A) [51]. In these highly vascular tumors, there may be larger branching type vessels (Fig. 3B) and/or areas of hemorrhage (Fig. 3C). The neoplastic stromal cells classically contain clear, foamy cytoplasm with lipid-containing vacuoles (Fig. 3D) [51]. Nuclei may show mild pleomorphism, particularly in cases with degenerative atypia (Fig. 3E). Rare cytoplasmic hyaline globules may also be found [53,54].

Two histologic variants of hemangioblastoma have been described. The first is the more common reticular variant, characterized by a predominance of capillary vessels over stromal cells, and the second and less common variant is the cellular variant, marked by a preponderance of stromal cells and a less prominent vascular component [55].

If present, adjacent neural parenchyma maintains a well-demarcated border with the neoplasm (Fig. 3F), and may show marked reactive changes, including piloid gliosis with Rosenthal fibers [56]. Other helpful but non-essential features include the presence of intratumoral hemorrhage, mast cells, and cyst-like spaces. Extramedullary hematopoiesis may be found in approximately 15% of cases [57]. Mitotic figures are rare to absent.

IMMUNOHISTOCHEMICAL AND ANCILLARY STUDIES

Immunohistochemistry provides a useful and in some cases essential role in the diagnosis of hemangioblastoma and discrimination from histologic mimics.

Positive stains

Hemangioblastoma stromal cells classically show positive staining for inhibin alpha (Fig. 4A), NCAM1 (CD56), S100, and carbonic anhydrase IX & XII (Fig. 4B) [58-64]. Brachyury expression has been reported in 91% of cases and vimentin in 86–100% of cases [65,66]. Other positive stains include aquaporin 1, TFE3, and oil red O [61,62,67]. The background vascular component stains for endothelial cell markers such as CD31 (Fig. 4C) and CD34, while reticulin highlights vessel walls [62].

Negative stains

By immunohistochemistry, the neoplastic cells are typically negative for AE1/AE3, CAM5.2, renal cell carcinoma (RCC) marker, and PAX8 (Fig. 4D) [58,60-62]. Other generally nega-

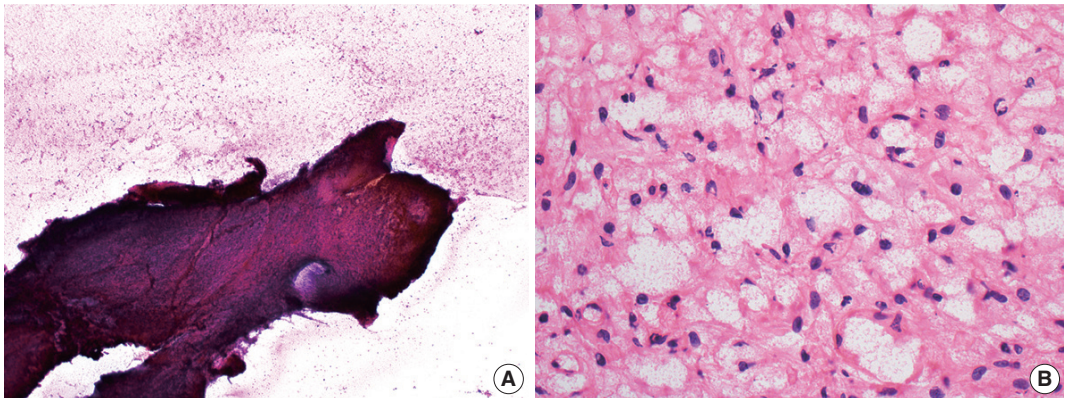

Fig. 2. Intraoperative direct smear and frozen section findings of central nervous system hemangioblastoma. Representative intraoperative analysis of hemangioblastoma demonstrating (A) resistance to smear cytological preparation and (B) the presence of cells with vacuolated cytoplasm on frozen section.

https://doi.org/10.4132/jptm.2022.04.13

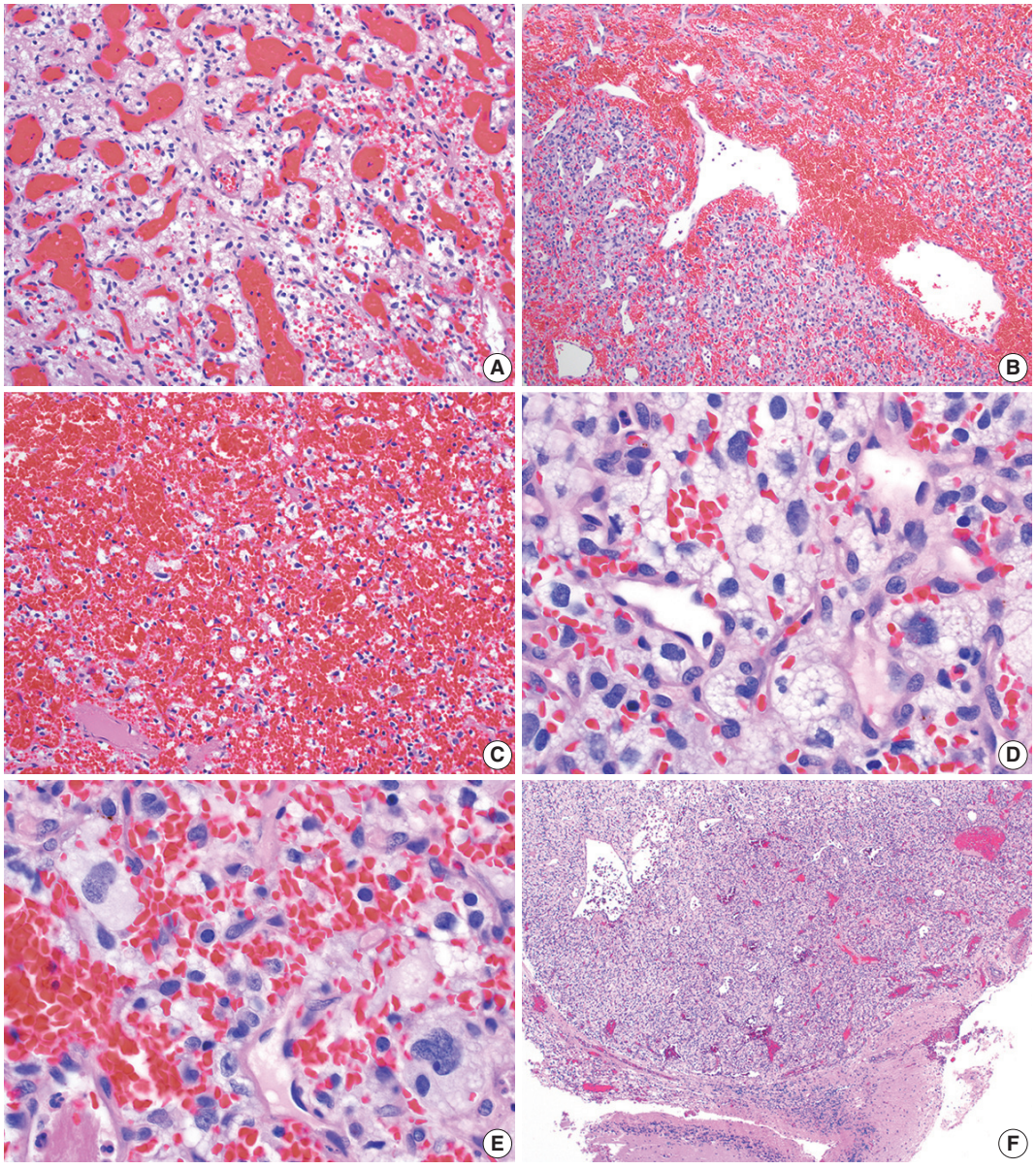

Fig. 3. Histopathological features of central nervous system hemangioblastoma. Representative permanent sections highlighting how hemangioblastomas are highly vascular neoplasms and may contain (A) abundant capillaries, (B) large branching vessels, and/or (C) areas of hemorrhage. (D) Stromal cells contain abundant foamy vacuolated cytoplasm. (E) Nuclear atypia may be seen in some stromal cells. (F) Hemangioblastomas often from well-demarcated border with adjacent brain parenchyma.

tive stains include PAX2 (positive in up to 5%), CD10 (positive in 0%–12%), epithelial membrane antigen (EMA; positive in 0%–36%), neuron-specific enolase (positive in 33%), and glial fibrillary acidic protein (GFAP; positive in scattered individual cells in up to 18%) [58,60,61,63,68].

Electron microscopy

Reports of electron microscopic studies of hemangioblastoma parallels histologic findings, with lipid-laden stromal cells occupying spaces between background capillaries [69].

Molecular and cytogenetic testing

Biallelic inactivation of the *VHL* tumor suppressor gene is present in many hemangioblastomas arising in VHL syndrome patients, with the majority of VHL-associated hemangioblastomas showing loss of heterozygosity of chromosome 3 [34,37]. VHL inactivation has been found in a large proportion of sporadic cases as well, with up to 78% of sporadic cases found to have loss

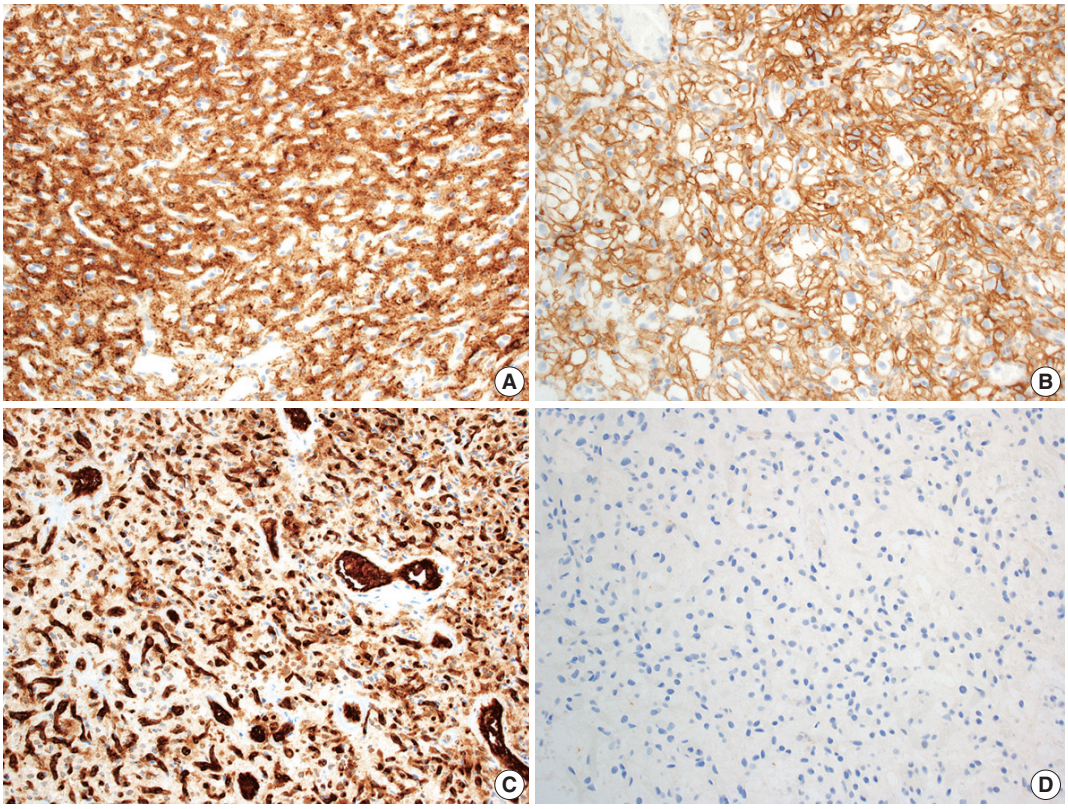

Fig. 4. Immunohistochemical features of central nervous system hemangioblastoma. Immunohistochemical profiling for hemangioblastoma usually includes positivity for (A) inhibin alpha, (B) CAIX, and (C) CD31, with negativity for renal markers such as (D) PAX8.

or inactivation of *VHL* [34-37].

When a suspected hemangioblastoma shows ambiguous histopathologic and immunophenotypic features, newer ancillary studies such as DNA methylation testing and even microRNA (miRNA) analysis could aid diagnostic decision making. Studies of genome-wide DNA methylation array profiling report a distinctive epigenetic classifying signature for hemangioblastoma [69]. In addition, distinctive miRNA signatures have been described in hemangioblastomas, which show elevated miRNA-9 and decreased miRNA-200a expression compared to CCRCCs [70]. At present, these methodologies are not used in routine clinical practice, nor are they intended to replace histologic evaluation. However, there is a potential for more widespread use of these supplemental tests in the future as the technology becomes more accessible.

DIFFERENTIAL DIAGNOSIS

Several entities must be considered in the differential diagnosis of hemangioblastoma on a histopathologic basis. In the VHL disease patient, special care must be taken to exclude certain histologic mimics that are of greater risk due to genetic predisposition.

Clear cell renal cell carcinoma

One of the most common diagnostic challenges is differentiating hemangioblastoma from metastatic CCRCC, both due to the histologic overlap of vascular neoplasms with clear cytoplasm, as well as the increased risk of these entities in the setting of VHL syndrome. In contrast to the benign hemangioblastoma, CCRCC may demonstrate more noticeable cytologic atypia with prominent anaplasia and large nucleoli, although such features may be absent [60]. Other aggressive features that may be seen in CCRCC include mitotic activity and necrosis. Metastatic CCRCC cells typically show clear to eosinophilic cytoplasm but lack the foamy or vacuolated cytoplasm of hemangioblastoma stromal cells. By immunohistochemistry, CCRCC is usually positive for AE1/AE3, CAM5.2, EMA, CD10, PAX2, PAX8, and RCC marker, while negative for inhibin alpha, brachyury, and NCAM1 [59-62,65,71-73].

Meningioma

Certain histologic subtypes of meningioma may be mistaken

https://doi.org/10.4132/jptm.2022.04.13

for hemangioblastoma, particularly the clear cell, microcystic, and angiomatous variants which may demonstrate prominent vasculature and/or clear cytoplasm. In contrast to hemangioblastomas, meningiomas are typically positive for EMA in a weak, patchy, cytoplasmic pattern, along with SSTR2A in a membranous and cytoplasmic pattern [73,74]. Lower grade meningiomas, which would be more easily mistaken for a benign hemangioblastoma, often express nuclear progesterone receptor, although higher grade meningiomas are less likely to show expression [73]. Meningiomas should not express the hemangioblastoma markers inhibin alpha or brachyury [65,73].

Solitary fibrous tumor

Solitary fibrous tumor (SFT) is a fibroblastic tumor with variable histologic patterns. Like hemangioblastoma, it is a mesenchymal neoplasm with prominent vasculature. SFT may occur in a wide range of anatomic sites, although in neuropathologic practice, the intracranial dura is most often affected [75,76]. SFT is genetically defined by a *NAB2* and *STAT6* gene fusion due to inversion at the 12q13 locus [77-79]. This genomic alteration results in STAT6 nuclear immunoreactivity, which is a highly sensitive and specific marker [73,80,81]. SFT is negative for inhibin alpha [73].

Glial neoplasms

Glial neoplasms may occasionally need to be considered in the differential diagnosis of hemangioblastoma given the overlapping sites of disease within the CNS. Some glial neoplasms may also show circumscribed growth. While well preserved and well differentiated examples may be more easily distinguished from one another, pathologists may face greater challenges in the setting of small tissue samples, obscuring artifact, or poor differentiation. Cytologic smear preparations may be especially useful in the case of a well-differentiated glial neoplasm showing elongated glial fibrillary processes and poorly cohesive cells. However, caution must be exercised in interpretation of smears, as reactive astrocytes in gliotic neural parenchyma adjacent to a hemangioblastoma could show similar fibrillary glial processes. Histologic and immunophenotypic features vary more widely by glial tumor type.

Ependymomas generally show circumscribed growth, similar to hemangioblastomas, and may even show clear cell morphology in some cases [82]. In contrast, ependymomas may demonstrate characteristic perivascular pseudorosettes, ependymal rosettes, and ependymal canals. By immunohistochemistry, ependymomas show variable GFAP staining, often with accentuation of cell processes within perivascular pseudorosettes [83]. Of note, hemangioblastomas may also show rare GFAP immunoreactivity in a small number of cells [68]. While not an entirely specific feature, ependymomas may demonstrate paranuclear dot-like or ring-like staining with EMA [83].

Pilocytic astrocytomas, like hemangioblastomas, typically show circumscribed growth patterns. In contrast, pilocytic astrocytomas are characterized by a biphasic appearance, with compact fibrillar portions containing Rosenthal fibers and loose microcystic areas containing eosinophilic granular bodies. Pilocytic astrocytomas are generally positive for GFAP and Olig2 by immunohistochemistry and demonstrate characteristic mitogen-activated protein kinase pathway activating genetic alterations, of which *KIAA1549-BRAF* fusion is the most common [84-86].

Diffuse gliomas encompass a broad spectrum of low- and high-grade neoplasms, now organized into adult and pediatric types in the most recent iteration of the WHO classification of CNS tumors [2]. While the clinical presentation and genomic features of diffuse gliomas vary widely, they are characterized by individual neoplastic glioma cells infiltrating through background brain parenchyma. Entrapped neurons and axons may be detected by histology or by immunohistochemistry in regions with dense neoplastic growth. In contrast to hemangioblastomas, diffuse gliomas are generally positive for GFAP and Olig2 [85,87].

Paraganglioma/pheochromocytoma/cauda equina neuroendocrine tumor

Paragangliomas are circumscribed neuroendocrine neoplasms derived from the paraganglia of the sympathetic and parasympathetic nervous systems classically characterized by nested to organoid architecture of chief cells surrounded by sustentacular cells. Pheochromocytoma is the histologic correlate arising in the adrenal gland. While similar appearing neuroendocrine neoplasms of the cauda equina region have long been designated as paragangliomas, recent data suggests that these cauda equina neuroendocrine neoplasms are biologically distinct from paragangliomas elsewhere in the body based on DNA methylation profiling as well as the lack of SDH mutations [88,89]. Therefore, this entity has been renamed "cauda equina neuroendocrine tumor" in the fifth edition of the WHO classification of CNS tumors [2].

Paragangliomas, pheochromocytomas and cauda equina neuroendocrine tumors may show overlapping cytomorphologic features with hemangioblastomas. All these tumors may contain cells with clear to vacuolated cytoplasm in a richly vascular background [90]. The potential for confusion between these two entities is compounded by the fact that VHL patients are at increased risk of hemangioblastomas, parasympathetic paragangliomas, and

pheochromocytomas. The organoid, "zellballen" architecture of paragangliomas, as well as their neuroendocrine nuclear features with uniform, round nuclei and salt and pepper chromatin may help to differentiate the entities, if these features are well preserved. On immunohistochemistry, paragangliomas and related entities are diffusely positive for synaptophysin and chromogranin, with intervening sustentacular cells staining for S-100 [90].

Hemangioma

Hemangioblastomas share some histologic features in common with hemangiomas, which are benign vascular neoplasms consisting of densely arranged capillaries and cavernous vessels. The tightly packed vessels contain plump endothelial cells which can impart the appearance of solid growth in areas. In the neuropathologic setting, hemangiomas are usually intraosseous, involving the spine and less frequently the skull, but have also been reported in CNS parenchyma [91-93]. If a suspected hemangioma involves the CNS parenchyma, adequate sampling and immunohistochemical workup should be undertaken to exclude the presence of neoplastic stromal cells.

TREATMENT AND PROGNOSIS

Hemangioblastoma is assigned a CNS WHO grade of 1, as complete excision is curative in most cases [2]. Surgical resection is considered the standard of care [94]. However, depending on the location of the tumor, excision may not be feasible. In the case of a symptomatic nonresectable tumor, stereotactic radiosurgery may provide some short-term control, but data on safety and long-term efficacy is currently limited [95-97].

Prospective natural history studies reveal unpredictable growth patterns in CNS hemangioblastoma. The predominant pattern is saltatory with intermittent periods of growth and quiescence [13,98]. Since it is difficult to predict the timeline of tumor growth, and because surgical intervention is not without risk of morbidity and mortality, treatment is often reserved for symptomatic tumors [94,98].

CNS hemangioblastoma carries a good prognosis with complete surgical excision, with significantly longer overall survival observed in patients who underwent gross total resection versus those who did not [96]. Compared to sporadic cases, outcomes are poorer in VHL patients; in this population, CNS hemangioblastomas remain the primary cause of mortality [99,100].

CONCLUSION

CNS hemangioblastoma is an important cause of morbidity and mortality in patients with VHL disease. Further studies are needed to clarify the pathogenesis of this disease, particularly in sporadic cases. Recognizing the basic clinical, radiographic, and pathologic features and considering a relevant differential diagnosis is crucial for making a correct diagnosis and guiding disease management.

Ethics Statement

Not applicable.

Availability of Data and Material

Data sharing not applicable to this article as no datasets were generated or analyzed during the study.

Code Availability

Not applicable.

ORCID

Patrick J. Cimino https://orcid.org/0000-0003-0441-4502
Rebecca A. Yoda https://orcid.org/0000-0001-7866-5625

Author Contributions

Conceptualization: RAY, PJC. Funding acquisition: PJC. Supervision: PJC. Writing—original draft: RAY, PJC. Writing—review & editing: RAY, PJC.

Conflicts of Interest

The authors declare that they have no potential conflicts of interest.

Funding Statement

No funding to declare.

Acknowledgments

PJC is supported by the National Institutes of Health K08 CA245037 award.

References

1. Tse JY, Wong JH, Lo KW, Poon WS, Huang DP, Ng HK. Molecular genetic analysis of the von Hippel-Lindau disease tumor suppressor gene in familial and sporadic cerebellar hemangioblastomas. Am J Clin Pathol 1997; 107: 459-66.
2. WHO Classification of Tumours Editorial Board. Central nervous system tumours. 5th ed. Vol. 6 [Internet]. Lyon: International Agency for Research on Cancer, 2021 [cited 2022 Mar 10]. Available from: https://tumourclassification.iarc.who.int/chapters/45.
3. Yin X, Duan H, Yi Z, Li C, Lu R, Li L. Incidence, prognostic factors and survival for hemangioblastoma of the central nervous system: analysis based on the Surveillance, Epidemiology, and End Results Database. Front Oncol 2020; 10: 570103.
4. Ostrom QT, Cioffi G, Waite K, Kruchko C, Barnholtz-Sloan JS. CBTRUS statistical report: primary brain and other central nervous system tumors diagnosed in the United States in 2014-2018. Neuro Oncol 2021; 23: iii1-105.

5. Surawicz TS, McCarthy BJ, Kupelian V, Jukich PJ, Bruner JM, Davis FG. Descriptive epidemiology of primary brain and CNS tumors: results from the Central Brain Tumor Registry of the United States, 1990-1994. Neuro Oncol 1999; 1: 14-25.
6. Constans JP, Meder F, Maiuri F, Donzelli R, Spaziante R, de Divitiis E. Posterior fossa hemangioblastomas. Surg Neurol 1986; 25: 269-75.
7. Westwick HJ, Giguere JF, Shamji MF. Incidence and prognosis of spinal hemangioblastoma: a Surveillance Epidemiology and End Results study. Neuroepidemiology 2016; 46: 14-23.
8. Nguyen HS, Doan NB, Gelsomino M, et al. Intracranial hemangioblastoma: a SEER-based analysis 2004-2013. Oncotarget 2018; 9: 28009-15.
9. Neumann HP, Eggert HR, Weigel K, Friedburg H, Wiestler OD, Schollmeyer P. Hemangioblastomas of the central nervous system: a 10-year study with special reference to von Hippel-Lindau syndrome. J Neurosurg 1989; 70: 24-30.
10. Conway JE, Chou D, Clatterbuck RE, Brem H, Long DM, Rigamonti D. Hemangioblastomas of the central nervous system in von Hippel-Lindau syndrome and sporadic disease. Neurosurgery 2001; 48: 55-62.
11. Lonser RR, Glenn GM, Walther M, et al. von Hippel-Lindau disease. Lancet 2003; 361: 2059-67.
12. Glasker S, Bender BU, Apel TW, et al. The impact of molecular genetic analysis of the VHL gene in patients with haemangioblastomas of the central nervous system. J Neurol Neurosurg Psychiatry 1999; 67: 758-62.
13. Lonser RR, Butman JA, Huntoon K, et al. Prospective natural history study of central nervous system hemangioblastomas in von Hippel-Lindau disease. J Neurosurg 2014; 120: 1055-62.
14. Doyle LA, Fletcher CD. Peripheral hemangioblastoma: clinicopathologic characterization in a series of 22 cases. Am J Surg Pathol 2014; 38: 119-27.
15. Nonaka D, Rodriguez J, Rosai J. Extraneural hemangioblastoma: a report of 5 cases. Am J Surg Pathol 2007; 31: 1545-51.
16. Maher ER, Yates JR, Harries R, et al. Clinical features and natural history of von Hippel-Lindau disease. Q J Med 1990; 77: 1151-63.
17. Chew EY. Ocular manifestations of von Hippel-Lindau disease: clinical and genetic investigations. Trans Am Ophthalmol Soc 2005; 103: 495-511.
18. Yousef A, Rutkowski MJ, Yalcin CE, Eren OC, Caliskan I, Tihan T. Sporadic and Von-Hippel Lindau disease-associated spinal hemangioblastomas: institutional experience on their similarities and differences. J Neurooncol 2019; 143: 547-52.
19. Maher ER, Neumann HP, Richard S. von Hippel-Lindau disease: a clinical and scientific review. Eur J Hum Genet 2011; 19: 617-23.
20. Maher ER, Iselius L, Yates JR, et al. Von Hippel-Lindau disease: a genetic study. J Med Genet 1991; 28: 443-7.
21. Seizinger BR, Rouleau GA, Ozelius LJ, et al. Von Hippel-Lindau disease maps to the region of chromosome 3 associated with renal cell carcinoma. Nature 1988; 332: 268-9.
22. Knudson AG Jr, Strong LC, Anderson DE. Heredity and cancer in man. Prog Med Genet 1973; 9: 113-58.
23. Kim WY, Kaelin WG. Role of *VHL* gene mutation in human cancer. J Clin Oncol 2004; 22: 4991-5004.
24. Pause A, Lee S, Lonergan KM, Klausner RD. The von Hippel-Lindau tumor suppressor gene is required for cell cycle exit upon serum withdrawal. Proc Natl Acad Sci U S A 1998; 95: 993-8.
25. Sendoel A, Kohler I, Fellmann C, Lowe SW, Hengartner MO. HIF-1 antagonizes p53-mediated apoptosis through a secreted neuronal tyrosinase. Nature 2010; 465: 577-83.
26. Tang N, Mack F, Haase VH, Simon MC, Johnson RS. pVHL function is essential for endothelial extracellular matrix deposition. Mol Cell Biol 2006; 26: 2519-30.
27. Jaakkola P, Mole DR, Tian YM, et al. Targeting of HIF-alpha to the von Hippel-Lindau ubiquitylation complex by O_2-regulated prolyl hydroxylation. Science 2001; 292: 468-72.
28. Ivan M, Kondo K, Yang H, et al. HIFalpha targeted for VHL-mediated destruction by proline hydroxylation: implications for O2 sensing. Science 2001; 292: 464-8.
29. Yu F, White SB, Zhao Q, Lee FS. HIF-1alpha binding to VHL is regulated by stimulus-sensitive proline hydroxylation. Proc Natl Acad Sci U S A 2001; 98: 9630-5.
30. Semenza GL. Oxygen sensing, homeostasis, and disease. N Engl J Med 2011; 365: 537-47.
31. Schodel J, Oikonomopoulos S, Ragoussis J, Pugh CW, Ratcliffe PJ, Mole DR. High-resolution genome-wide mapping of HIF-binding sites by ChIP-seq. Blood 2011; 117: e207-17.
32. Favier J, Gimenez-Roqueplo AP. Pheochromocytomas: the (pseudo)-hypoxia hypothesis. Best Pract Res Clin Endocrinol Metab 2010; 24: 957-68.
33. Li M, Kim WY. Two sides to every story: the HIF-dependent and HIF-independent functions of pVHL. J Cell Mol Med 2011; 15: 187-95.
34. Glasker S, Bender BU, Apel TW, et al. Reconsideration of biallelic inactivation of the VHL tumour suppressor gene in hemangioblastomas of the central nervous system. J Neurol Neurosurg Psychiatry 2001; 70: 644-8.
35. Lee JY, Dong SM, Park WS, et al. Loss of heterozygosity and somatic mutations of the VHL tumor suppressor gene in sporadic cerebellar hemangioblastomas. Cancer Res 1998; 58: 504-8.
36. Shankar GM, Taylor-Weiner A, Lelic N, et al. Sporadic hemangioblastomas are characterized by cryptic VHL inactivation. Acta Neuropathol Commun 2014; 2: 167.
37. Takayanagi S, Mukasa A, Tanaka S, et al. Differences in genetic and epigenetic alterations between von Hippel-Lindau disease-related and sporadic hemangioblastomas of the central nervous system. Neuro Oncol 2017; 19: 1228-36.
38. Jagannathan J, Lonser RR, Smith R, DeVroom HL, Oldfield EH. Surgical management of cerebellar hemangioblastomas in patients with von Hippel-Lindau disease. J Neurosurg 2008; 108: 210-22.
39. Glasker S, Kruger MT, Klingler JH, et al. Hemangioblastomas and neurogenic polyglobulia. Neurosurgery 2013; 72: 930-5.
40. Krieg M, Marti HH, Plate KH. Coexpression of erythropoietin and vascular endothelial growth factor in nervous system tumors associated with von Hippel-Lindau tumor suppressor gene loss of function. Blood 1998; 92: 3388-93.
41. Roonprapunt C, Silvera VM, Setton A, Freed D, Epstein FJ, Jallo GI. Surgical management of isolated hemangioblastomas of the spinal cord. Neurosurgery 2001; 49: 321-7.
42. Chu BC, Terae S, Hida K, Furukawa M, Abe S, Miyasaka K. MR findings in spinal hemangioblastoma: correlation with symptoms and with angiographic and surgical findings. AJNR Am J Neuroradiol 2001; 22: 206-17.
43. Wanebo JE, Lonser RR, Glenn GM, Oldfield EH. The natural his-

tory of hemangioblastomas of the central nervous system in patients with von Hippel-Lindau disease. J Neurosurg 2003; 98: 82-94.
44. Ene CI, Morton RP, Ferreira M Jr, Sekhar LN, Kim LJ. Spontaneous hemorrhage from central nervous system hemangioblastomas. World Neurosurg 2015; 83: 1180.
45. Glasker S, Van Velthoven V. Risk of hemorrhage in hemangioblastomas of the central nervous system. Neurosurgery 2005; 57: 71-6.
46. de San Pedro JR, Rodriguez FA, Niguez BF, et al. Massive hemorrhage in hemangioblastomas literature review. Neurosurg Rev 2010; 33: 11-26.
47. Ho VB, Smirniotopoulos JG, Murphy FM, Rushing EJ. Radiologic-pathologic correlation: hemangioblastoma. AJNR Am J Neuroradiol 1992; 13: 1343-52.
48. Parizel PM, Baleriaux D, Rodesch G, et al. Gd-DTPA-enhanced MR imaging of spinal tumors. AJR Am J Roentgenol 1989; 152: 1087-96.
49. Ganti SR, Silver AJ, Hilal SK, Mawad ME, Sane P. Computed tomography of cerebellar hemangioblastomas. J Comput Assist Tomogr 1982; 6: 912-9.
50. Raz E, Zagzag D, Saba L, et al. Cyst with a mural nodule tumor of the brain. Cancer Imaging 2012; 12: 237-44.
51. Ganeshan D, Menias CO, Pickhardt PJ, et al. Tumors in von Hippel-Lindau syndrome: from head to toe-comprehensive state-of-the-art review. Radiographics 2018; 38: 849-66.
52. Commins DL, Hinton DR. Cytologic features of hemangioblastoma: comparison with meningioma, anaplastic astrocytoma and renal cell carcinoma. Acta Cytol 1998; 42: 1104-10.
53. Wang X, Haines GK 3rd, Mehrotra M, Houldsworth J, Si Q. Primary hemangioblastoma of the kidney with molecular analyses by next generation sequencing: a case report and review of the literature. Diagn Pathol 2022; 17: 34.
54. Shin Y, Kim S, Lee HW, Bang H, Suh YL. Supratentorial hemangioblastoma with unusual features. Korean J Pathol 2014; 48: 462-5.
55. Hasselblatt M, Jeibmann A, Gerss J, et al. Cellular and reticular variants of haemangioblastoma revisited: a clinicopathologic study of 88 cases. Neuropathol Appl Neurobiol 2005; 31: 618-22.
56. Wippold FJ 2nd, Perry A, Lennerz J. Neuropathology for the neuroradiologist: rosenthal fibers. AJNR Am J Neuroradiol 2006; 27: 958-61.
57. Zec N, Cera P, Towfighi J. Extramedullary hematopoiesis in cerebellar hemangioblastoma. Neurosurgery 1991; 29: 34-7.
58. Carney EM, Banerjee P, Ellis CL, et al. PAX2(-)/PAX8(-)/inhibin A(+) immunoprofile in hemangioblastoma: a helpful combination in the differential diagnosis with metastatic clear cell renal cell carcinoma to the central nervous system. Am J Surg Pathol 2011; 35: 262-7.
59. Hoang MP, Amirkhan RH. Inhibin alpha distinguishes hemangioblastoma from clear cell renal cell carcinoma. Am J Surg Pathol 2003; 27: 1152-6.
60. Rivera AL, Takei H, Zhai J, Shen SS, Ro JY, Powell SZ. Useful immunohistochemical markers in differentiating hemangioblastoma versus metastatic renal cell carcinoma. Neuropathology 2010; 30: 580-5.
61. Weinbreck N, Marie B, Bressenot A, et al. Immunohistochemical markers to distinguish between hemangioblastoma and metastatic clear-cell renal cell carcinoma in the brain: utility of aquaporin1 combined with cytokeratin AE1/AE3 immunostaining. Am J Surg Pathol 2008; 32: 1051-9.
62. Polydorides AD, Rosenblum MK, Edgar MA. Metastatic renal cell carcinoma to hemangioblastoma in von Hippel-Lindau disease. Arch Pathol Lab Med 2007; 131: 641-5.
63. Hufnagel TJ, Kim JH, True LD, Manuelidis EE. Immunohistochemistry of capillary hemangioblastoma. Immunoperoxidase-labeled antibody staining resolves the differential diagnosis with metastatic renal cell carcinoma, but does not explain the histogenesis of the capillary hemangioblastoma. Am J Surg Pathol 1989; 13: 207-16.
64. Proescholdt MA, Mayer C, Kubitza M, et al. Expression of hypoxia-inducible carbonic anhydrases in brain tumors. Neuro Oncol 2005; 7: 465-75.
65. Barresi V, Vitarelli E, Branca G, Antonelli M, Giangaspero F, Barresi G. Expression of brachyury in hemangioblastoma: potential use in differential diagnosis. Am J Surg Pathol 2012; 36: 1052-7.
66. Frank TS, Trojanowski JQ, Roberts SA, Brooks JJ. A detailed immunohistochemical analysis of cerebellar hemangioblastoma: an undifferentiated mesenchymal tumor. Mod Pathol 1989; 2: 638-51.
67. Yang Y, Gao H, Zhen T, et al. Hemangioblastoma: clinicopathologic study of 42 cases with emphasis on TFE3 expression. Am J Transl Res 2020; 12: 4498-510.
68. Wizigmann-Voos S, Plate KH. Pathology, genetics and cell biology of hemangioblastomas. Histol Histopathol 1996; 11: 1049-61.
69. Capper D, Stichel D, Sahm F, et al. Practical implementation of DNA methylation and copy-number-based CNS tumor diagnostics: the Heidelberg experience. Acta Neuropathol 2018; 136: 181-210.
70. Venneti S, Boateng LA, Friedman JR, et al. MiRNA-9 and MiRNA-200a distinguish hemangioblastomas from metastatic clear cell renal cell carcinomas in the CNS. Brain Pathol 2012; 22: 522-9.
71. Jung SM, Kuo TT. Immunoreactivity of CD10 and inhibin alpha in differentiating hemangioblastoma of central nervous system from metastatic clear cell renal cell carcinoma. Mod Pathol 2005; 18: 788-94.
72. Sangoi AR, Karamchandani J, Kim J, Pai RK, McKenney JK. The use of immunohistochemistry in the diagnosis of metastatic clear cell renal cell carcinoma: a review of PAX-8, PAX-2, hKIM-1, RCCma, and CD10. Adv Anat Pathol 2010; 17: 377-93.
73. Boulagnon-Rombi C, Fleury C, Fichel C, Lefour S, Marchal Bressenot A, Gauchotte G. Immunohistochemical approach to the differential diagnosis of meningiomas and their mimics. J Neuropathol Exp Neurol 2017; 76: 289-98.
74. Menke JR, Raleigh DR, Gown AM, Thomas S, Perry A, Tihan T. Somatostatin receptor 2a is a more sensitive diagnostic marker of meningioma than epithelial membrane antigen. Acta Neuropathol 2015; 130: 441-3.
75. Gold JS, Antonescu CR, Hajdu C, et al. Clinicopathologic correlates of solitary fibrous tumors. Cancer 2002; 94: 1057-68.
76. Mena H, Ribas JL, Pezeshkpour GH, Cowan DN, Parisi JE. Hemangiopericytoma of the central nervous system: a review of 94 cases. Hum Pathol 1991; 22: 84-91.
77. Chmielecki J, Crago AM, Rosenberg M, et al. Whole-exome sequencing identifies a recurrent NAB2-STAT6 fusion in solitary fibrous tumors. Nat Genet 2013; 45: 131-2.
78. Schweizer L, Koelsche C, Sahm F, et al. Meningeal hemangiopericytoma and solitary fibrous tumors carry the NAB2-STAT6 fu-

 https://doi.org/10.4132/jptm.2022.04.13

sion and can be diagnosed by nuclear expression of STAT6 protein. Acta Neuropathol 2013; 125: 651-8.
79. Robinson DR, Wu YM, Kalyana-Sundaram S, et al. Identification of recurrent NAB2-STAT6 gene fusions in solitary fibrous tumor by integrative sequencing. Nat Genet 2013; 45: 180-5.
80. Doyle LA, Vivero M, Fletcher CD, Mertens F, Hornick JL. Nuclear expression of STAT6 distinguishes solitary fibrous tumor from histologic mimics. Mod Pathol 2014; 27: 390-5.
81. Yoshida A, Tsuta K, Ohno M, et al. STAT6 immunohistochemistry is helpful in the diagnosis of solitary fibrous tumors. Am J Surg Pathol 2014; 38: 552-9.
82. Fouladi M, Helton K, Dalton J, et al. Clear cell ependymoma: a clinicopathologic and radiographic analysis of 10 patients. Cancer 2003; 98: 2232-44.
83. Vege KD, Giannini C, Scheithauer BW. The immunophenotype of ependymomas. Appl Immunohistochem Mol Morphol 2000; 8: 25-31.
84. Tihan T, Ersen A, Qaddoumi I, et al. Pathologic characteristics of pediatric intracranial pilocytic astrocytomas and their impact on outcome in 3 countries: a multi-institutional study. Am J Surg Pathol 2012; 36: 43-55.
85. Ligon KL, Alberta JA, Kho AT, et al. The oligodendroglial lineage marker OLIG2 is universally expressed in diffuse gliomas. J Neuropathol Exp Neurol 2004; 63: 499-509.
86. Zhang J, Wu G, Miller CP, et al. Whole-genome sequencing identifies genetic alterations in pediatric low-grade gliomas. Nat Genet 2013; 45: 602-12.
87. Nakagawa Y, Perentes E, Rubinstein LJ. Immunohistochemical characterization of oligodendrogliomas: an analysis of multiple markers. Acta Neuropathol 1986; 72: 15-22.
88. Schweizer L, Thierfelder F, Thomas C, et al. Molecular characterization of CNS paragangliomas identifies cauda equina paragangliomas as a distinct tumor entity. Acta Neuropathol 2020; 140: 893-906.
89. Ramani B, Gupta R, Wu J, et al. The immunohistochemical, DNA methylation, and chromosomal copy number profile of cauda equina paraganglioma is distinct from extra-spinal paraganglioma. Acta Neuropathol 2020; 140: 907-17.
90. Koch CA, Mauro D, Walther MM, et al. Pheochromocytoma in von hippel-lindau disease: distinct histopathologic phenotype compared to pheochromocytoma in multiple endocrine neoplasia type 2. Endocr Pathol 2002; 13: 17-27.
91. Koga Y, Hamada S, Saito H, Akai T, Kuroda S. Intracranial, intraparenchymal capillary hemangioma: case report. NMC Case Rep J 2020; 7: 43-6.
92. Fish C, Sy J, Wong J. High mitotic activity in a capillary hemangioma of the cauda equina: case report and review of the literature. Clin Neuropathol 2020; 39: 135-8.
93. Kasukurthi R, Ray WZ, Blackburn SL, Lusis EA, Santiago P. Intramedullary capillary hemangioma of the thoracic spine: case report and review of the literature. Rare Tumors 2009; 1: e10.
94. Dornbos D 3rd, Kim HJ, Butman JA, Lonser RR. Review of the Neurological Implications of von Hippel-Lindau Disease. JAMA Neurol 2018; 75: 620-7.
95. Kano H, Shuto T, Iwai Y, et al. Stereotactic radiosurgery for intracranial hemangioblastomas: a retrospective international outcome study. J Neurosurg 2015; 122: 1469-78.
96. Huang Y, Chan L, Bai HX, et al. Assessment of care pattern and outcome in hemangioblastoma. Sci Rep 2018; 8: 11144.
97. Asthagiri AR, Mehta GU, Zach L, et al. Prospective evaluation of radiosurgery for hemangioblastomas in von Hippel-Lindau disease. Neuro Oncol 2010; 12: 80-6.
98. Ammerman JM, Lonser RR, Dambrosia J, Butman JA, Oldfield EH. Long-term natural history of hemangioblastomas in patients with von Hippel-Lindau disease: implications for treatment. J Neurosurg 2006; 105: 248-55.
99. Miyagami M, Katayama Y, Nakamura S. Clinicopathological study of vascular endothelial growth factor (VEGF), p53, and proliferative potential in familial von Hippel-Lindau disease and sporadic hemangioblastomas. Brain Tumor Pathol 2000; 17: 111-20.
100. Binderup ML, Jensen AM, Budtz-Jorgensen E, Bisgaard ML. Survival and causes of death in patients with von Hippel-Lindau disease. J Med Genet 2017; 54: 11-8.

JPTM
Journal of Pathology and Translational Medicine 2022; 56: 126-133
https://doi.org/10.4132/jptm.2022.01.04

ORIGINAL ARTICLE

Frequency of *PIK3CA* mutations in different subsites of head and neck squamous cell carcinoma in southern Thailand

Arunee Dechaphunkul[1], Phatcharaporn Thongwatchara[1], Paramee Thongsuksai[2], Tanadech Dechaphunkul[3], Sarayut Lucien Geater[4]

[1]Holistic Center for Cancer Study and Care (HOCC-PSU), Medical Oncology Unit, Department of Internal Medicine, Faculty of Medicine, Prince of Songkla University, Songkhla; Departments of [2]Pathology and [3]Otorhinolaryngology Head and Neck Surgery, [4]Division of Respiratory and Respiratory Critical Care Medicine, Department of Internal Medicine, Faculty of Medicine, Prince of Songkla University, Songkhla, Thailand

Background: Phosphatidylinositol-4,5-bisphosphate 3-kinase catalytic subunit alpha (*PIK3CA*) mutations have been reported in many cancers, including head and neck squamous cell carcinoma (HNSCC). The frequency of these mutations varies among tumor locations and might be relevant to treatment outcomes among HNSCC. In this study, we examined the frequency of *PIK3CA* mutations in the different subsites of HNSCC. **Methods:** Ninety-six fresh biopsy specimens were investigated for mutations in *PIK3CA* exons 4, 9, and 20 using allele-specific real-time polymerase chain reaction. Patient characteristics and survival were analyzed and compared between specimens with or without *PIK3CA* mutations. **Results:** The study included primary tumors originating from the oral cavity (n=63), hypopharynx (n=23), and oropharynx (n=10). We identified mutations in 10.4% of patients (10 of 96 specimens). The overall mutational frequency was 17.4% (4/23) and 9.5% (6/63) in the hypopharynx and oral cavity, respectively. No patients with oropharyngeal carcinoma had mutations. Among the 10 mutant specimens, five were missense mutations (exon 9 [E545K] in two samples and exon 20 [H1047R] in three samples) and five were silent mutations in exon 20 (T1025T). Mutations were not found in exon 4. Among 84 patients with available clinical data, we found no significant differences in clinical characteristics and survival based on the presence or absence of *PIK3CA* mutations. **Conclusions:** The results indicate that *PIK3CA* mutations are involved in HNSCC carcinogenesis, and the hypopharynx should be considered a primary site of interest for future studies, particularly in Southeast Asian populations.

Key Words: *PIK3CA* mutations; Head and neck squamous cell carcinoma; Oral cavity carcinoma; Hypopharyngeal carcinoma; Oropharyngeal carcinoma

Received: October 27, 2021 **Revised:** December 23, 2021 **Accepted:** January 4, 2022
Corresponding Author: Arunee Dechaphunkul, MD, Holistic Center for Cancer Study and Care (HOCC-PSU), Medical Oncology Unit, Department of Internal Medicine, Faculty of Medicine, Prince of Songkla University, Songkhla 90110, Thailand
Tel: +6674-455856, Fax: +6674-451469, E-mail: dr.arunee@gmail.com

Head and neck cancer includes all tumors that arise from various anatomical subsites, including the oral cavity, oropharynx, nasopharynx, hypopharynx, larynx, paranasal sinuses, and salivary glands. Although histologic subtypes are diverse, malignancies of the epithelial lining, namely squamous cell carcinoma, are the most common [1].

Head and neck squamous cell carcinoma (HNSCC) is the sixth most common malignancy worldwide, with approximately 890,000 new cases diagnosed and 450,000 deaths reported in 2008. Among all HNSCC, the oral cavity is the most common subsite of a primary tumor [2]. The burden of HNSCC varies across regions of the world. In Thailand, HNSCC is one of the most common cancers, with approximately 10,000 new cases diagnosed annually. The age-standardized incidence rates of HNSCC in males and females are 15.7 and 10.7, respectively [3]. The dominant tumor locations of HNSCC in males are the oral cavity, nasopharynx, and larynx; and the most common location in females is the oral cavity [3].

At the time of diagnosis, most patients with HNSCC have locally advanced, unresectable tumors. Despite advanced multidisciplinary treatments, including surgery with either or both radiotherapy and chemotherapy, only modest improvements in outcomes have been achieved over the past 20 years. HNSCC molecular profiling and biomarker studies have provided infor-

pISSN 2383-7837
eISSN 2383-7845

mation regarding rapid diagnosis, prognosis, and surveillance for recurrence and metastasis. However, biomarkers that serve as potential targets of novel therapies to improve survival outcomes are important. Among the signaling pathways associated with tumor proliferation and survival, the phosphoinositide 3-kinase/AKT/mammalian target of rapamycin (PI3K/AKT/mTOR) pathway is the most frequently altered oncogenic pathway in HNSCC [4,5].

The phosphatidylinositol 3-kinase gene (*PI3K*) encodes PI3K enzymes (PI3Ks), which ultimately trigger various downstream signaling pathways that result in cell survival, apoptosis, transformation, metastasis, and cell migration. PI3Ks are classified into three major subclasses (class I, II, and III) that are determined based on PI3K structure and substrate specificity. Phosphatidylinositol-4,5-bisphosphate 3-kinase catalytic subunit alpha (*PIK3CA*) is a 34-kb gene located on chromosome 3q26.3 that consists of 20 exons coding for 1,068 amino acids, yielding a protein with a molecular weight of 124 kDa (p110α catalytic subunit protein, class I) [6]. Several studies previously reported alterations in *PIK3CA* in many cancers. The presence of *PIK3CA* mutations is associated with prognosis and might predict response to PI3K inhibitors [6,7]. In HNSCC, the frequency of *PIK3CA* mutations varies among primary tumor locations [6,8-15]; hence, the frequency of these mutations from different tumor subsites might be relevant to determine treatments and outcomes among HNSCCs. Furthermore, the mutation rate in *PIK3CA* might be diverse among ethnicities [15,16]; the mutation rate is unknown in Southeast Asian populations, including the Thai population. Therefore, in the present study, we evaluated the frequency of *PIK3CA* mutations in patients with squamous cell carcinoma of the oral cavity, oropharynx, and hypopharynx in southern Thailand. Furthermore, the clinical characteristics and survival between patients with or without *PIK3CA* mutations were analyzed and compared.

MATERIALS AND METHODS

Patients and specimens

During 2002–2003, 96 fresh tissues (63 from the oral cavity, 10 from the oropharynx, and 23 from the hypopharynx) were obtained from patients registered at the head and neck clinic of Songklanagarind Hospital. The tissue samples were obtained from a biopsy or sampling of surgical resection specimen, after which they were snap frozen and stored at –80°C until DNA extraction. All collected tissues were subsequently reviewed to ensure cancer site and pathological diagnosis of cancer by a pathologist (P.T). All cases were primary tumors that had not been treated with radiation or chemotherapy.

Clinicopathological parameters of the patients were retrieved from medical records. The patient information extracted from the database was date of birth, sex, vital status, history of smoking and alcohol consumption, date of diagnosis, stage, and treatment. Pathological information was obtained from pathological reports. Date of death was obtained from the national civil registration system.

Mutation detection using conventional polymerase chain reaction and DNA sequencing

Genomic DNA was extracted from fresh tissue using an E.Z.N.A Tissue DNA Kit (Omega Bio-Tek Inc., Norcross, GA, USA), and the procedures were performed according to the manufacturer's instructions. *PIK3CA* gene analysis was performed in exons 4, 9, and 20; 100 ng of DNA was amplified using polymerase chain reaction (PCR) with the following primer sets: *PIK3CA*-exon 4 forward (5'-CATCTTATTCCAGACGCATTTC-3'), *PIK3CA*-exon 4 reverse (5'-AGATTACTGTATAGTGCAAGAAAA-3'), *PIK3CA*-exon 9 forward (5'-CCAGAGGGGAAAAATATGACA-3'), *PIK3CA*-exon 9 reverse (5'-CATTTTAGCACTTACCTGTGAC-3'), *PIK3CA*-exon 20 forward (5'-CATTTGCTCCAAACTGACCA-3'), and *PIK3CA*-exon 20 reverse (5'-TGAGCTTTCATTTTCTCAGTTATCTTTTC-3'). The PCR conditions for *PIK3CA* exons 4 and 9 were denaturation at 95°C for 3 minutes; amplification for 45 cycles at 95°C for 30 seconds, 58°C for 30 seconds, and 72°C for 45 seconds; and extension at 72°C for 7 minutes. The PCR conditions for *PIK3CA* exon 20 were denaturation at 95°C for 3 minutes; amplification for 45 cycles at 95°C for 45 seconds, 58°C for 45 seconds, and 72°C for 1 minute; and extension at 72°C for 7 minutes. All gene sequencing was performed with an ABI PRISM 3730xl Genetic Analyzer (Applied Biosystems, Foster City, CA, USA). DNA sequences were analyzed to ascertain point mutations in *PIK3CA* exons 4, 9, and 20. The conventional PCR technique was performed in certain samples to determine the reference point mutations. Then, allele-specific real-time PCR was performed for the remaining tissue samples.

Allele-specific real-time PCR

Reference point mutations were used to design allele-specific probes (dual-labeled fluorogenic probes) to develop a real-time PCR technique. The allele-specific probes were composed of short DNA sequences covering the mutational areas. The probes were labeled with two fluorescent dyes: HEX for the *PIK3CA*

Table 1. Allele-specific probes

Probe name	Type	Sequence
PIK3CA exon 9 G>A	Wild-type probe	5'-(HEX) CTCTCTGAAATCACTGAGCAGGAGAA (BHQ-1)-3'
PIK3CA exon 9 G>A	Mutated probe	5'-(FAM) CTCTCTGAAATCACTAAGCAGGAGAA (BHQ-1)-3'
PIK3CA exon 20 A>G	Wild-type probe	Anti-sense 5' (HEX) AGCCACCATGATGTGCATCATTC (BHQ-1)-3'
PIK3CA exon 20 A>G	Mutated probe	Anti-sense 5' (FAM) AGCCACCATGACGTGCATCATTC (BHQ-1)-3'
PIK3CA exon 20 C>T	Wild-type probe	5'-(HEX) ACATTCGAAAGACCCTAGCCTTAGAT (BHQ-1)-3'
PIK3CA exon 20 C>T	Mutated probe	5'-(FAM) ACATTCGAAAGACTCTAGCCTTAGAT (BHQ-1)-3'

PIK3CA, phosphatidylinositol-4,5-bisphosphate 3-kinase catalytic subunit alpha.

wild-type allele and FAM for the mutated allele (Sigma-Aldrich, Singapore). BHQ-1 was used as a quencher. For all samples, 20 ng of DNA was obtained and subjected to real-time PCR using previously described primer sets and allele-specific probe sets (Table 1). PCR mixtures contained 10 μL of 2× FastStart Essential DNA Probes Master buffer (Roche Diagnostics, Mannheim, Germany), 0.5 μL forward primer, 0.5 μL reverse primer, 0.25 μL wild-type probe, 0.25 μL mutated probe, 6.5 μL molecular grade water, and 20 ng DNA in a final volume of 20 μL. The real-time PCR conditions for *PIK3CA* exon 9 were 95°C, 3 minutes and (95°C, 10 seconds; 58°C, 30 seconds)×45 cycles. The real-time PCR conditions for *PIK3CA* exon 20 were 95°C, 3 minutes and (95°C, 10 seconds; 62°C, 30 seconds; 72°C, 30 seconds)×45 cycles. Template controls were not included in each real-time PCR run. All samples were subsequently subjected to real-time PCR using the probes. Five mutant specimens served as positive controls.

Statistical analysis

Descriptive statistics were used to compare the data between the two groups of patients. The chi-square test or Fisher exact test was used to compare proportional data, and Student's t test or the Mann-Whitney U test was used to assess the differences in continuous data. Descriptive results are presented as the median (continuous variable) and percentage (categorical variable).

Duration of follow-up and overall survival (OS) time were calculated from the date of diagnosis until the date of last follow-up or date of death from any cause, respectively. The data of patients who were alive at the last date of follow-up, December 20, 2021, were censored. The survival curve was calculated using the Kaplan-Meier method. Comparisons of survival curve among groups were performed using the log-rank test.

Stata/MP ver. 17.0 (StataCorp, College Station, TX, USA) was used to perform all analyses. p-values < .05 were considered statistically significant.

Table 2. Patient demographics and baseline characteristics

Variable	Total (n=84)	Wild-type *PIK3CA* (n=74)	Mutant *PIK3CA* (n=10)	p-value
Age (yr)				.100
Median±SD	68±12.6	68±12.8	70±9.7	
Sex				.307
Male	49 (58.3)	45 (60.8)	4 (40.0)	
Female	35 (41.7)	29 (39.2)	6 (60.0)	
Smoking				.324
Yes	47 (56.0)	43 (58.1)	4 (40.0)	
No	37 (44.0)	31 (41.9)	6 (60.0)	
Alcohol drinking				.182
Yes	44 (52.4)	41 (55.4)	3 (30.0)	
No	40 (47.6)	33 (44.6)	7 (70.0)	
Tumor location				.380
Oral cavity	57 (67.9)	51 (68.9)	6 (60.0)	
Tongue	14 (16.7)	13 (17.6)	1 (10.0)	
Gums	13 (15.4)	12 (16.2)	1 (10.0)	
Buccal mucosa	11 (13.1)	10 (13.5)	1 (10.0)	
Floor of mouth	6 (7.1)	5 (6.7)	1 (10.0)	
Lip	5 (6.0)	3 (4.1)	2 (20.0)	
Hard palate	4 (4.8)	4 (5.4)	0	
Retromolar area	2 (2.4)	2 (2.7)	0	
Oral cavity (unspecified)	2 (2.4)	2 (2.7)	0	
Oropharynx	6 (7.1)	6 (8.1)	0	
Base of tongue	6 (7.1)	6 (8.1)	0	
Hypopharynx	21 (25.0)	17 (23.0)	4 (40.0)	
Pyriform sinus	21 (25.0)	17 (23.0)	4 (40.0)	
Clinical stage				.628
I	16 (19.0)	14 (18.9)	2 (20.0)	
II	17 (20.3)	13 (17.6)	4 (40.0)	
III	19 (22.6)	18 (24.3)	1 (10.0)	
IVa	29 (34.5)	26 (35.1)	3 (30.0)	
IVb	1 (1.2)	1 (1.4)	0	
IVc	2 (2.4)	2 (2.7)	0	
Treatment				.337
Surgery	23 (27.4)	18 (24.3)	5 (50.0)	
Surgery followed by RT	42 (50.0)	38 (51.4)	4 (40.0)	
RT	13 (15.5)	12 (16.2)	1 (10.0)	
Best supportive care	6 (7.1)	6 (8.1)	0	

Values are presented as number (%) unless otherwise indicated.
PIK3CA, phosphatidylinositol-4,5-bisphosphate 3-kinase catalytic subunit alpha; SD, standard deviation; RT, radiotherapy.

https://doi.org/10.4132/jptm.2022.01.04

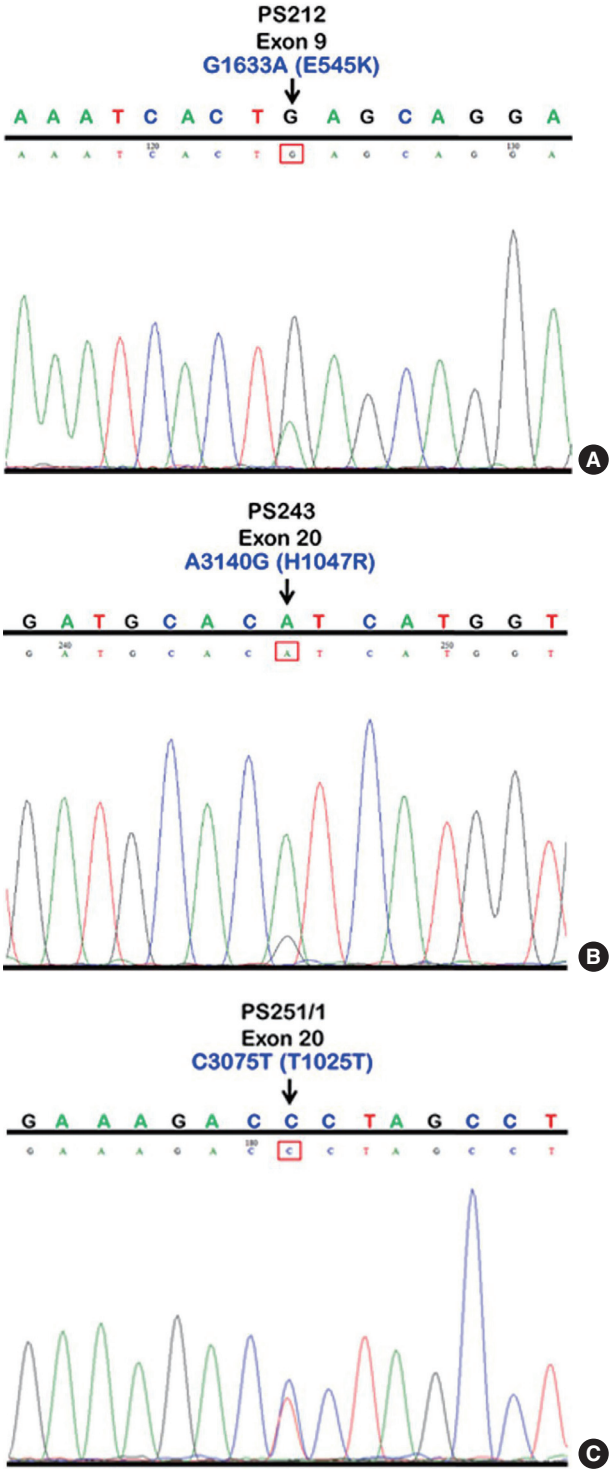

Fig. 1. *PIK3CA* mutations in exons 9 and 20 using conventional PCR as illustrated in sequencing chromatograms showing a missense mutation in sample No. PS212 at position 1633, G>A (E545K) in exon 9 (A), a missense mutation in sample No. PS243 at position 3140, A>G (H1047R) in exon 20 (B), and a silent mutation in sample No. PS251/1, C>T (T1025T) in exon 20 (C). PIK-3CA, phosphatidylinositol-4,5-bisphosphate 3-kinase catalytic subunit alpha; PCR, polymerase chain reaction.

RESULTS

The samples used in this study comprised 96 HNSCC samples diagnosed from 2002–2003. The study included primary tumors originating from the oral cavity (n = 63), hypopharynx (n = 23), and oropharynx (n = 10). The patient demographics and their baseline clinical characteristics were available for 84 cases and are shown in Table 2; 49 cases were male, and the median age at diagnosis was 68 years.

We initially identified three *PIK3CA* point mutations using conventional PCR (Fig. 1A–C): one in exon 9 and two in exon 20. Mutations were not detected in exon 4. We then applied these known mutations as a reference to design allele-specific probes (dual-labeled fluorogenic probes) as shown in Table 1.

We found *PIK3CA* mutations in 10 of 96 samples (10.4%) with all heterozygous mutations. When the patients were classified based on mutational events in the primary tumor location, 17.4% (4/23) with hypopharyngeal squamous cell carcinoma (HPSCC) and 9.5% (6/63) with oral cavity squamous cell carcinoma (OCSCC) had *PIK3CA* mutations. No patient (0/10) with oropharyngeal squamous cell carcinoma (OPSCC) had *PIK3CA* mutations (Table 3). Clinical characteristics between patients with or without *PIK3CA* mutations were not statistically significantly different (Table 2). The patient characteristics and details of *PIK3CA* mutations are shown in Table 4. Two patients had exon 9 mutations (Fig. 2A) and eight had exon 20 mutations (Fig. 2B, C). The 10 mutations were categorized as five missense and five silent mutations, which corresponded to E545K in exon 9 and T1025T and H1047R in exon 20. E545K (GAG1633A-AG) and H1047R (CAT3140CGT) are missense mutations, and T1025T (ACC3075ACT) is a silent mutation.

The majority of patients with wild-type *PIK3CA* (51.4%) underwent surgery followed by adjuvant radiotherapy; however, patients with *PIK3CA* mutations underwent only surgery (50.0%), as shown in Table 2. The median duration of follow-up was 2.11 years (95% confidence interval [CI], 1.21 to 3.26). The 5-year OS rates in the wild-type *PIK3CA* and mutant *PIK3CA* were 35%

Table 3. Frequency of *PIK3CA* mutations in HNSCC by subsite

Subsites of HNSCC	*PIK3CA* mutation		Overall *PIK3CA* mutations
	Exon 9	Exon 20	
Oral cavity	0/63 (0)	6/63 (9.5)	6/63 (9.5)
Oropharynx	0/10 (0)	0/10 (0)	0/10 (0)
Hypopharynx	2/23 (8.7)	2/23 (8.7)	4/23 (17.4)

Values are presented as number (%).
PIK3CA, phosphatidylinositol-4,5-bisphosphate 3-kinase catalytic subunit alpha; HNSCC, head and neck squamous cell carcinoma.

Table 4. Mutational status of *PIK3CA* in HNSCC

Sample No.	Age at diagnosis (yr)	Sex	Tumor location	Exon	Nucleotide	Codon change	Amino acid change	Type of mutation
PS212	76	Male	Pyriform sinus	9	G1633A	GAG to AAG	E545K	Missense
PS220	62	Female	Pyriform sinus	9	G1633A	GAG to AAG	E545K	Missense
PS243	72	Male	Pyriform sinus	20	A3140G	CAT to CGT	H1047R	Missense
PS251/1	63	Male	Pyriform sinus	20	C3075T	ACC to ACT	T1025T	Silent
OR183	58	Female	Buccal mucosa	20	C3075T	ACC to ACT	T1025T	Silent
OR214	90	Female	Tongue	20	C3075T	ACC to ACT	T1025T	Silent
OR378	79	Female	Gums	20	C3075T	ACC to ACT	T1025T	Silent
OR391	69	Male	Floor of mouth	20	C3075T	ACC to ACT	T1025T	Silent
OR205	79	Female	Lip	20	A3140G	CAT to CGT	H1047R	Missense
OR209	66	Female	Lip	20	A3140G	CAT to CGT	H1047R	Missense

PIK3CA, phosphatidylinositol-4,5-bisphosphate 3-kinase catalytic subunit alpha; HNSCC, head and neck squamous cell carcinoma.

(95% CI, 24 to 46) and 58% (95% CI, 23 to 82), respectively (Fig. 3). There was no statistically significant difference in OS rate between the two groups (p = .625).

DISCUSSION

In HNSCC, the PI3K/AKT/mTOR pathway is the most frequently altered oncogenic pathway associated with tumor proliferation and survival [4,5]. Reportedly, *PIK3CA* mutations are associated with advanced stage of HNSCC, particularly in subjects with oral squamous cell carcinoma, indicating that *PIK3CA* mutations play an important role in the carcinogenesis of HNSCC [9,15]. In the present study, we evaluated the frequency of *PIK3CA* mutations in the different subsites of HNSCC in the Thai population.

When divided by primary tumor location, we detected a higher mutation rate in HPSCC than in OCSCC (17.4% vs. 9.5%). We also found a slightly higher *PIK3CA* mutation rate in HPSCC than reported in a study in the Chinese population (13.6%) [16]. The frequency of *PIK3CA* mutations in OCSCC in the present study (9.5%) was slightly higher than the 7.4% frequency reported in the Japanese population [9]. Notably, Kommineni et al. [15] reported a substantially high *PIK3CA* mutation rate of 52% in OCSCC tumor samples from Indian patients. Taken together, these findings might highlight the effect of diverse mutation rates even among Asian populations.

Human papillomavirus (HPV) infection is a well-known risk factor associated with OPSCC. Nichols et al. [17] reported a higher frequency of *PIK3CA* mutations in HPV-related OPSCC than HPV-negative tumors (28% vs. 10%). In the present study, we found no *PIK3CA* mutation in any patient with OPSCC. This result was discordant from those of a study by Beaty et al. [18] showing a *PIK3CA* mutation rate of 21% in patients with HPV-associated OPSCC. The reason for the discordance might be the small sample cohort in the OPSCC subgroup in the present study. Furthermore, information regarding HPV status in these patients was unknown due to the lack of sufficient specimens. However, in previous studies, the proportion of HPV-related OPSCC in Thai patients was remarkably low (15%–20%) [19,20] compared with 40%–60% reported in Western patients [21]. Thus, the correlation between *PIK3CA* mutations and HPV status should be further explored in Asian populations.

In the present study, *PIK3CA* mutations in exon 4 were not detected. In contrast, a previous study reported mutations in exon 4, with a rate of 2.6% in an oral cavity carcinoma cell line (primary tumor originated in the tongue) [8]. In the present study, the overall 10.4% mutation rate of *PIK3CA*, which included 2.1% in exon 9 (E545K) and 8.3% in exon 20 (H1047R and T1025T), was not significantly different from previous studies (9%–13% in non-nasopharyngeal carcinoma), as shown in Table 5. However, a higher mutation rate of 21% in pharyngeal carcinoma and 21% in oropharyngeal carcinoma were reported in two studies [11,18]. In those studies, a more advantageous technique, a novel mutant-enriched sequencing method, was used for analysis, which could explain the difference in results.

We found two of the three types of *PIK3CA* mutations, E545K and H1047R, which have been previously reported as hotspot mutations [22-24]. E545K is located on exon 9 in the helical domain of *PIK3CA*, and H1047R and T1025T are encoded by exon 20 within the kinase domain [25]. The E545K mutation disrupts an inhibitory charge–charge interaction between p110α and the N-terminal SH2 domain of the p85 regulatory subunit, and the H1047R mutation increases the binding affinity between p110α and the negatively charged phosphatidylinositol substrate [26-28]. The functional effect of these two hotspot mutations has been well established in many studies, showing the gain-of-function PI3K activity and downstream signaling *via* the AKT/mTOR pathway [22,23]. Furthermore, the benefit of *PIK3CA* mutations

https://doi.org/10.4132/jptm.2022.01.04

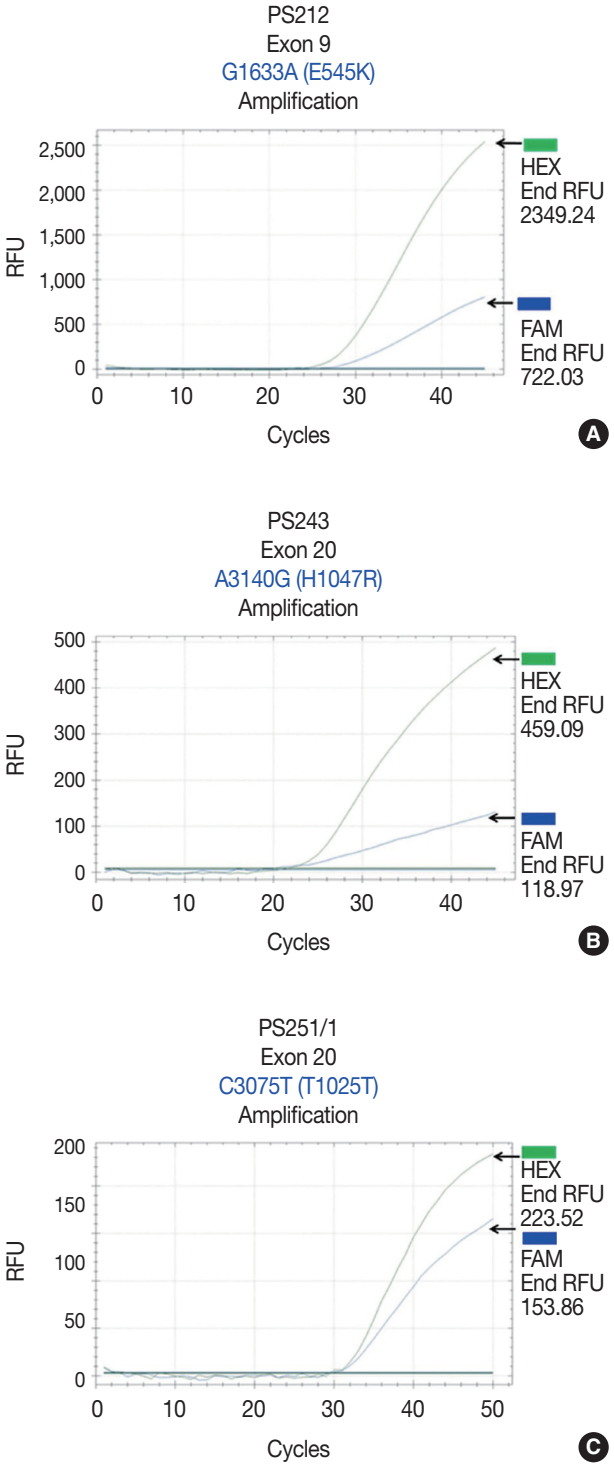

Fig. 2. Amplification plot of allele-specific real-time PCR showing *PIK3CA* mutations in exon 9 and exon 20 and the HEX (green, wild-type PIK3CA allele) and FAM (blue, mutated PIK3CA allele) signals. (A) A missense mutation in sample No. PS212 at position 1633, G>A (E545K) in exon 9. (B) A missense mutation in sample No. PS243 at position 3140, A>G (H1047R) in exon 20. (C) A silent mutation in sample No. PS251/1, C>T (T1025T) in exon 20. PCR, polymerase chain reaction.

as a predictive marker for novel targeted therapies has been demonstrated. Alpelisib, an oral selective PI3K inhibitor, has been implemented in current practice for patients with advanced breast cancer harboring *PIK3CA* mutations [29,30]. The efficacy and safety of PI3K or mTOR inhibitors are being evaluated in several clinical trials for patients with advanced HNSCC [31]. In contrast to the previously mentioned two hotspot mutations, T1025T is categorized as a silent mutation. Notably, we detected the T1025T mutation, which was significantly high in OCSCC, in 4 of 5 mutant cases in the present study. This was concordant with a previous study in which the T1025T mutation was reportedly prominent in OCSCC [15]. However, whether the T1025T silent mutation is the oncogenic driver in HNSCC remains controversial. Kommineni et al. [15] reported a significantly higher frequency of T1025T silent mutation in patients with HNSCC (41.0%) than in healthy controls (16.7%, $p < .001$). In contrast, Dogruluk et al. [28] identified T1025T as a genetic variant in the human germline.

In the present study, clinical significance was not observed based on the presence or absence of *PIK3CA* mutations. This finding was similar to a previous study in which significant difference was not observed in clinical characteristics between patients with wild-type *PIK3CA* or mutant *PIK3CA* OPSCC [18]. However, the presence of a *PIK3CA* mutation in that study was associated with poorer disease-free survival among patients receiving de-intensified definitive chemoradiotherapy for HPV-related OPSCC [18]; survival did not differ between the two groups in the present study. This contradictory finding might be explained by the small sample cohort in the present study. A larger study in which *PIK3CA* mutations are investigated as a potentially prognostic

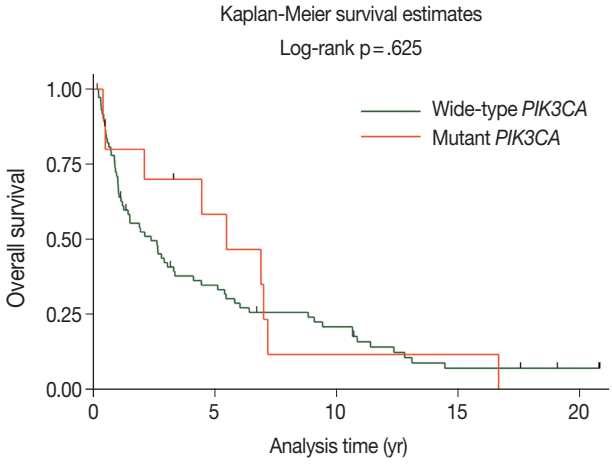

Fig. 3. Kaplan-Meier survival curves of overall survival for patients with wild-type *PIK3CA* or mutant *PIK3CA*. *PIK3CA*, phosphatidylinositol-4,5-bisphosphate 3-kinase catalytic subunit alpha.

Table 5. Previous studies of *PIK3CA* mutations in HNSCC

Authors (year)	Location of HNSCC	*PIK3CA* mutations (%)	Type of mutation	Exons
Qiu et al. (2006) [8]	HNSCC	11 (4/38)	Point mutation	4, 9, and 20
Kozaki et al. (2006) [9]	Oral cavity	9 (11/122)	Point mutation	9 and 20
Qiu et al. (2008) [11]	Pharynx	21 (5/24)	Point mutation	9 and 20
Murugan et al. (2008) [12]	HNSCC	13 (7/54)	Point mutations, frameshift	9 and 20
Kommineni et al. (2015) [15]	HNSCC	60.46	Point mutation	9 and 20
Wu et al. (2017) [16]	Hypopharynx	13.6	Point mutation	9 and 20
Beaty et al. (2020) [18]	Oropharynx	21 (16/77)	Point mutation	9 and 13
Lui et al. (2013) [32]	HNSCC	12.6 (19/151)	Point mutation	9, 20, and novel mutations

PIK3CA, phosphatidylinositol-4,5-bisphosphate 3-kinase catalytic subunit alpha; HNSCC, head and neck squamous cell carcinoma.

factor in patients with OPSCC and non-OPSCC is warranted.

To the best of our knowledge, this is the first study to report the frequency of *PIK3CA* mutations in HNSCC in Thailand. However, the limitations of the study included small sample size, particularly in the OPSCC subgroup, and lack of available data regarding HPV status. The absence of *PIK3CA* mutations in OPSCC might be due to the smaller number of samples tested than those at other subsites. Furthermore, testing for *PIK3CA* mutations in normal tissue from these patients was not performed; hence, conclusions cannot be drawn regarding involvement of the T1025T silent mutation in the pathogenesis of HNSCC or its involvement as a genetic variant in the human germline.

In conclusion, our study showed a higher frequency of *PIK3CA* mutations in HPSCC than in OCSCC. The results suggest that these mutations are involved in carcinogenesis and could serve as biomarkers for novel targeted therapies as well as immunomodulators in the era of immune checkpoint inhibitors. Furthermore, the hypopharynx is suggested as a primary site of interest for further studies, particularly in Southeast Asian populations.

Ethics Statement

This study was approved by the Institutional Review Board of Faculty of Medicine, Prince of Songkla University (REC 56-498-14-1) with a waiver of informed consent.

Availability of Data and Material

All data generated or analyzed during the study are included in this published article (and its supplementary information files).

Code Availability

Not applicable.

ORCID

Arunee Dechaphunkul https://orcid.org/0000-0002-0593-4385
Phatcharaporn Thongwatchara https://orcid.org/0000-0001-5588-8316
Paramee Thongsuksai https://orcid.org/0000-0003-4226-7988
Tanadech Dechaphunkul https://orcid.org/0000-0002-0170-6537
Sarayut Lucien Geater https://orcid.org/0000-0002-3494-8268

Author Contributions

Conceptualization: AD. Data curation: PT (Phatcharaporn Thongwatchara), TD. Formal analysis: AD, PT (Phatcharaporn Thongwatchara), PT (Paramee Thongsuksai), TD, SLG. Funding acquisition: AD. Investigation: PT (Phatcharaporn Thongwatchara). Methodology: PT (Phatcharaporn Thongwatchara), PT (Paramee Thongsuksai). Project administration: AD. Resources: PT (Phatcharaporn Thongwatchara), PT (Paramee Thongsuksai). Supervision: AD, PT (Paramee Thongsuksai). Validation: PT (Phatcharaporn Thongwatchara), PT (Paramee Thongsuksai). Visualization: AD, PT (Paramee Thongsuksai). Writing—original draft: AD, PT (Phatcharaporn Thongwatchara). Writing—review & editing: all authors. Approval of final manuscript: all authors.

Conflicts of Interest

The authors declare that they have no potential conflicts of interest.

Funding Statement

This study was funded by the Faculty of Medicine, Prince of Songkla University, Songkhla, Thailand.

References

1. Cohen N, Fedewa S, Chen AY. Epidemiology and demographics of the head and neck cancer population. Oral Maxillofac Surg Clin North Am 2018; 30: 381-95.
2. Bray F, Ferlay J, Soerjomataram I, Siegel RL, Torre LA, Jemal A. Global cancer statistics 2018: GLOBOCAN estimates of incidence and mortality worldwide for 36 cancers in 185 countries. CA Cancer J Clin 2018; 68: 394-424.
3. Hospital-based cancer registry 2016 [Internet]. Bangkok: National Cancer Institute, Department of Medical Services, Ministry of Public Health, Thailand [cited 2021 Oct 21]. Available from: https://www.nci.go.th/th/File_download/Nci%20Cancer%20Registry/Hospital-Based%20NCI2%202016%20Web.pdf.
4. Cancer Genome Atlas Network. Comprehensive genomic characterization of head and neck squamous cell carcinomas. Nature 2015; 517: 576-82.
5. Wang Z, Valera JC, Zhao X, Chen Q, Gutkind JS. mTOR co-targeting strategies for head and neck cancer therapy. Cancer Metastasis Rev 2017; 36: 491-502.
6. Liu P, Cheng H, Roberts TM, Zhao JJ. Targeting the phosphoinositide 3-kinase pathway in cancer. Nat Rev Drug Discov 2009; 8: 627-44.
7. Karakas B, Bachman KE, Park BH. Mutation of the *PIK3CA* oncogene in human cancers. Br J Cancer 2006; 94: 455-9.
8. Qiu W, Schonleben F, Li X, et al. *PIK3CA* mutations in head and

neck squamous cell carcinoma. Clin Cancer Res 2006; 12: 1441-6.
9. Kozaki K, Imoto I, Pimkhaokham A, et al. *PIK3CA* mutation is an oncogenic aberration at advanced stages of oral squamous cell carcinoma. Cancer Sci 2006; 97: 1351-8.
10. Or YY, Hui AB, To KF, Lam CN, Lo KW. *PIK3CA* mutations in nasopharyngeal carcinoma. Int J Cancer 2006; 118: 1065-7.
11. Qiu W, Tong GX, Manolidis S, Close LG, Assaad AM, Su GH. Novel mutant-enriched sequencing identified high frequency of *PIK3CA* mutations in pharyngeal cancer. Int J Cancer 2008; 122: 1189-94.
12. Murugan AK, Hong NT, Fukui Y, Munirajan AK, Tsuchida N. Oncogenic mutations of the *PIK3CA* gene in head and neck squamous cell carcinomas. Int J Oncol 2008; 32: 101-11.
13. Chou CC, Chou MJ, Tzen CY. *PIK3CA* mutation occurs in nasopharyngeal carcinoma but does not significantly influence the disease-specific survival. Med Oncol 2009; 26: 322-6.
14. Fendri A, Khabir A, Mnejja W, et al. *PIK3CA* amplification is predictive of poor prognosis in Tunisian patients with nasopharyngeal carcinoma. Cancer Sci 2009; 100: 2034-9.
15. Kommineni N, Jamil K, Pingali UR, Addala L, M V, Naidu M. Association of *PIK3CA* gene mutations with head and neck squamous cell carcinomas. Neoplasma 2015; 62: 72-80.
16. Wu P, Wu H, Tang Y, et al. Whole-exome sequencing reveals novel mutations and epigenetic regulation in hypopharyngeal carcinoma. Oncotarget 2017; 8: 85326-40.
17. Nichols AC, Palma DA, Chow W, et al. High frequency of activating *PIK3CA* mutations in human papillomavirus-positive oropharyngeal cancer. JAMA Otolaryngol Head Neck Surg 2013; 139: 617-22.
18. Beaty BT, Moon DH, Shen CJ, et al. *PIK3CA* mutation in HPV-associated OPSCC patients receiving deintensified chemoradiation. J Natl Cancer Inst 2020; 112: 855-8.
19. Arsa L, Siripoon T, Trachu N, et al. Discrepancy in p16 expression in patients with HPV-associated head and neck squamous cell carcinoma in Thailand: clinical characteristics and survival outcomes. BMC Cancer 2021; 21: 504.
20. Argirion I, Zarins KR, McHugh J, et al. Increasing prevalence of HPV in oropharyngeal carcinoma suggests adaptation of p16 screening in Southeast Asia. J Clin Virol 2020; 132: 104637.
21. Mehanna H, Beech T, Nicholson T, et al. Prevalence of human papillomavirus in oropharyngeal and nonoropharyngeal head and neck cancer: systematic review and meta-analysis of trends by time and region. Head Neck 2013; 35: 747-55.
22. Samuels Y, Wang Z, Bardelli A, et al. High frequency of mutations of the *PIK3CA* gene in human cancers. Science 2004; 304: 554.
23. Kang S, Bader AG, Vogt PK. Phosphatidylinositol 3-kinase mutations identified in human cancer are oncogenic. Proc Natl Acad Sci U S A 2005; 102: 802-7.
24. Davoli T, Mengwasser KE, Duan J, et al. Functional genomics reveals that tumors with activating phosphoinositide 3-kinase mutations are dependent on accelerated protein turnover. Genes Dev 2016; 30: 2684-95.
25. Gustin JP, Cosgrove DP, Park BH. The *PIK3CA* gene as a mutated target for cancer therapy. Curr Cancer Drug Targets 2008; 8: 733-40.
26. Miled N, Yan Y, Hon WC, et al. Mechanism of two classes of cancer mutations in the phosphoinositide 3-kinase catalytic subunit. Science 2007; 317: 239-42.
27. Kang S, Bader AG, Zhao L, Vogt PK. Mutated PI 3-kinases: cancer targets on a silver platter. Cell Cycle 2005; 4: 578-81.
28. Dogruluk T, Tsang YH, Espitia M, et al. Identification of variant-specific functions of PIK3CA by rapid phenotyping of rare mutations. Cancer Res 2015; 75: 5341-54.
29. Andre F, Ciruelos E, Rubovszky G, et al. Alpelisib for *PIK3CA*-mutated, hormone receptor-positive advanced breast cancer. N Engl J Med 2019; 380: 1929-40.
30. Andre F, Ciruelos EM, Juric D, et al. Alpelisib plus fulvestrant for *PIK3CA*-mutated, hormone receptor-positive, human epidermal growth factor receptor-2-negative advanced breast cancer: final overall survival results from SOLAR-1. Ann Oncol 2021; 32: 208-17.
31. Jung K, Kang H, Mehra R. Targeting phosphoinositide 3-kinase (PI3K) in head and neck squamous cell carcinoma (HNSCC). Cancers Head Neck 2018; 3: 3.
32. Lui VW, Hedberg ML, Li H, et al. Frequent mutation of the PI3K pathway in head and neck cancer defines predictive biomarkers. Cancer Discov 2013; 3: 761-9.

JPTM
Journal of Pathology and Translational Medicine 2022; 56: 134-143
https://doi.org/10.4132/jptm.2022.02.22

ORIGINAL ARTICLE

Expression of prostate-specific membrane antigen in the neovasculature of primary tumors and lymph node metastasis of laryngeal squamous cell carcinomas

Gamze Erkılınç[1], Hasan Yasan[2], Yusuf Çağdaş Kumbul[2], Mehmet Emre Sivrice[2], Meltem Durgun[1]

Departments of [1]Pathology and [2]Otorhinolaryngology, Süleyman Demirel Univesity, Çünür/Isparta, Turkey

Background: Prostate-specific membrane antigen (PSMA) expression is encountered in tumor-associated neovascularization. **Methods:** PSMA-antibody was applied to the paraffin blocks of 51 patients who were diagnosed with squamous cell carcinoma of the larynx and underwent laryngectomy and one who underwent lymph node dissection. The percentage of vascular expression in tumoral and extratumoral stroma and lymph nodes and intensity score in tumoral epithelium were evaluated and divided into groups according to the level of PSMA expression. Final PSMA expression was determined by multiplying intensity and percentage scores. **Results:** The mean age was 61 ± 10 years. Patients with perineural invasion, cartilage invasion, and local invasion exhibited higher PSMA expression scores. Age, tumor differentiation, tumor diameter, perineural invasion, tumor localization, capsular invasion, depth of invasion, surgical margin status, local invasion, nodal metastasis, TNM classification, and stage were similar in high and low PSMA expression groups. There was no PSMA expression in extratumoral vascular stroma. Significantly higher PSMA expression was observed in the vascular endothelium of metastatic lymph nodes compared with reactive lymph nodes. Patients with advanced-stage disease exhibited higher PSMA vascular expression scores compared to those with earlier stages ($p < .001$). PSMA expression was not correlated with overall survival, disease-specific survival, or disease-free survival ($p > .05$). **Conclusions:** Our study suggests that higher PSMA expression is associated with cartilage invasion, local invasion, and advanced-stage of disease. PSMA expression can be utilized for detection of lymph node metastasis and has some predictive role in cases of neck metastasis.

Key Words: Prostate-specific membrane antigen; Larynx; Lymph nodes; Neovascularization; Immunohistochemistry

Received: April 7, 2021 **Revised:** January 31, 2022 **Accepted:** February 22, 2022

Corresponding Author: Gamze Erkılınç, MD, Department of Pathology, Süleyman Demirel Univesity, Süleyman Demirel Street, 32260, Çünür/Isparta, Turkey
Tel: +90-2462113714, Fax: +90-2462112830, E-mail: gamzecirak@gmail.com

The prevalence and incidence of laryngeal cancers, mostly constituted of squamous cell carcinoma (SCC), have increased by 23.8% and 12%, respectively, in the last 30 years, and the survival of patients with advanced-stage disease remains low [1]. Despite developments in diagnostic and therapeutic techniques, novel and more effective treatment strategies are needed to increase survival, particularly for patients with advanced-stage disease. The microvascular intensity of tumors is positively correlated with T/N category, T/N relapse, and tumor radiosensitivity. Treatment modalities targeting the antigens of active vascular endothelial cells can be beneficial when combined with conventional chemotherapies [2]. Angiogenesis is the formation of new vessels from existing vessels as a response to changes in the circulatory system such as hypoxia. The term neoangiogenesis is also used to define the pathologic angiogenesis of different vessels in the presence of a tumor and other diseases [3]. The relationship between angiogenesis and prognosis in SCC of the larynx (SCCL) was determined in the 1990s [4].

Tumor vessels can be targeted for treatment and prevention of recurrence to protect normal vascular structures from deterioration due to continuous growth and abnormality of tumor vessels. For instance, target-oriented anti–epidermal growth factor receptor treatment has been approved by the United States Food and Drug Administration for treatment of head-neck SCCs [5].

Prostate-specific membrane antigen (PSMA), also known as glutamate carboxypeptidase, is a type 2 transmembrane glycoprotein with a molecular weight of 100 kDa including both intracellular and extracellular domains that have been demonstrated

pISSN 2383-7837
eISSN 2383-7845

to be expressed in prostate cancers and commonly researched in the field of target-oriented treatment [6,7]. There are several complete, ongoing, and interrupted studies on numerous different clones of PSMA (e.g., ADC 2301, ADC BrUOG 263, ADC 1301) within the content of phase 1 and phase 2 trials conducted to investigate the availability of PSMA for use in treatment and imaging procedures. PSMA expression has been confirmed by RNase protection assay, western blot analysis, and immunohistochemical methods [8].

PSMA expression was demonstrated in the neovascularized foci of solid organ tumors (e.g., breast, lung, kidney, brain, thyroid, hepatocellular carcinoma, urothelial carcinoma). PSMA is more commonly encountered in tumor-associated new blood vessels and is not detected in the normal vascular endothelium in solid tumors [9]. The specificity of PSMA for tumor-associated endothelium suggests it as a potential target for treatment of malignancies.

We aimed to evaluate PSMA expression in the vascular endothelium of primary tumors and lymph nodes in patients with SCCL.

MATERIALS AND METHODS

Patients and tissue samples

This study included 51 patients with SCCL who underwent total or partial laryngectomy and neck dissection between January 2010 and January 2020. The hematoxylin and eosin (H&E)-stained sections obtained from all the formalin-fixed paraffin blocks of the patients were re-examined, and appropriate blocks were selected from 17 patients with lymph node metastasis and 34 patients without lymph node metastasis. Neck dissection was performed in patients with clinical and/or radiologic findings suspicious for positive lymph nodes in the neck.

All cases were histopathologically confirmed according to the 4th edition of the *World Health Organization (WHO) classification of head and neck tumors* [10]. The Protocol for the Examination of Specimens from Patients with Cancers of the Larynx 2017 of the College of American Pathologists was used to identify histopathologic subtype, tumor location, tumor size, tumor differentiation, tumor spread, surgical margins, lymphovascular invasion, perineural invasion, and lymphatic spread for SCCL [11]. Tumor stage was determined retrospectively for all patients according to the TNM Classification System of the American Joint Committee on Cancer [11]. Data such as clinical information, age, sex, presence of metastasis, and survival data including disease-free survival (DFS), overall survival (OS), disease-specific survival (DSS), and recurrence were obtained from the hospital database.

Immunohistochemistry

PSMA antibodies were applied to the blocks that represented tumors, and blocks were selected from metastatic lymph nodes or tumor-negative lymph nodes in the absence of metastatic lymph nodes using an immunohistochemical method in the H&E-stained sections (Fig. 1A). PSMA antibodies (clone 3E6, isotype: IgG1, kappa, DAKO flex ready-to-use monoclonal mouse antibody (Carpinteria, CA, USA) provided in liquid form in a buffer containing stabilizing protein and 0.015 mol/L sodium azide) were prepared according to the manufacturer's instructions as expressed in the datasheet. The tissue samples were processed together with prostate tissue samples as an antibody-positive control and a negative control in an automated immunohistochemistry device.

Evaluation of immunohistochemical staining

Immunohistochemically stained slides were evaluated by two pathologists who were experienced in head and neck pathology, with each being blinded to the cases. PSMA immunohistochemically stained slides were examined under a light microscope and accepted as having positive cytoplasmic staining and/or positive cytoplasmic membrane staining.

The percentage of vascular endothelial cells that stained positive for PSMA was stratified as: 0, 0%–5%; 1, 6%–25%; 2, 26%–50%; and 3, >50%. The intensity score was stratified as: 1, weak; 2, moderate; and 3, strong. PSMA expression was scored according to the intensity of the tumor epithelium as: 1, none-weak; 2, moderate; and 3, strong. Final PSMA expression was determined by multiplying intensity and percentage scores. The cases were grouped according to stage and lymph node metastasis. The groups were compared by PSMA expression scores [12,13].

Statistical analysis

The normality of continuous data distribution was tested using the Kolmogorov-Smirnov test or the Shapiro-Wilk test. Continuous data were compared using the independent sample t test or the Mann-Whitney U test. Categorical data were compared using Pearson's chi-square test. Fisher's exact test was used when expected value problems occurred. Kaplan-Meier survival analysis was conducted to predict survival estimates according to PSMA expression score. Receiver operator curve (ROC) analysis was performed to determine the cut off value for PSMA expression in assessing the event of death during follow-up. Patients were classified into two groups according to cut off value as high and low expression of PSMA. A p-value < .05 was regarded as statistically significant. The SPSS ver. 21 software package (IBM Corp., Armonk, NY,

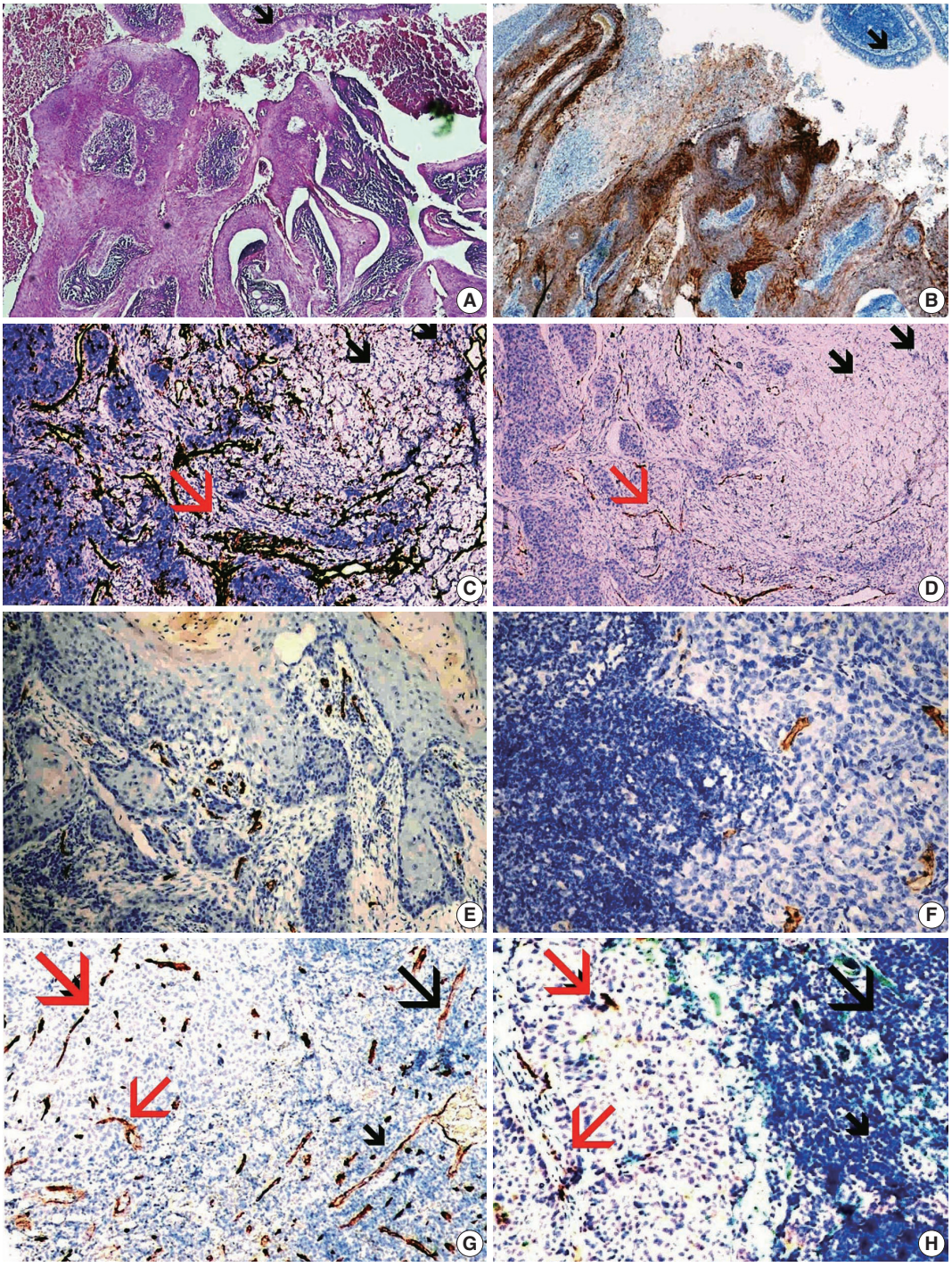

Fig. 1. Hematoxylin and eosin (H&E) and immunohistochemistry (IHC) staining of tumoral and nontummoral tissues. (A) Primary squamous cell carcinoma and respiratory epithelium (arrow) in the neighborhood of the tumor (H&E). (B) High prostate-specific membrane antigen (PSMA) expression score in the epithelium of the primary squamous cell carcinoma, no PSMA expression in the normal respiratory epithelium (arrow). (C) CD34 expression in the vessels of the tumoral stroma (red arrow) and non-tumoral stroma (black arrow). (D) High PSMA expression score in the vessels of the tumoral stroma (red arrow) and no expression of PSMA in the vessels of the normal tissue (black arrows). (E) PSMA expression in the vessels of the primary tumor (F) and expression in the vessels of the metastatic lymph node. (G) CD31 expression in the stromal vessels of the metastatic focus (red arrows) and non-metastatic focus (black arrow) of the same lymph node. (H) PSMA expression in the stromal vessels of the metastatic focus (red arrows) and no expression in the vessels of the non-metastatic focus (black arrow) of the same lymph node.

https://doi.org/10.4132/jptm.2022.02.22

USA) was used for statistical analysis.

RESULTS

All but one patient were male (98%). The mean age was 61 ± 10 years. Of the primary tumors, 37.3%, 43.1%, and 19.6% were well-differentiated, moderately differentiated, and poorly differentiated, respectively. Fifty (29.4%), 12 (23.5%), one (2%), six (11.8%), eight (15.7%), and nine (17.6%) tumors were located in the supraglottic, glottic, infraglottic, supraglottic+glottic, glottic+infraglottic, and transglottic regions, respectively. Table 1 shows the demographic data of the patients. Age was similar between the high and low vascular expression groups. Tumor differentiation was similar between the high and low vascular expression score groups. Tumor diameter and perineural invasion was similar between the groups. Supraglottic localization was more frequent in the low vascular score group compared to the high group. Transglottic localization was more frequent in the high vascular score group. Capsular invasion, depth of invasion, lymphovascular invasion, surgical margin positivity, and local spread nodal metastasis were similar between the groups. The presence of T4 tumors and stage 4 disease was more frequent in the high vascular PSMA expression group. Comparison of the high and low vascular PSMA expression groups is shown in Table 2.

We evaluated the expression of PSMA in tumoral epithelium and divided the patients according to expression levels. Age, tumor differentiation, tumor diameter, perineural invasion, tumor localization, capsular invasion, depth of invasion, surgical margin status, local invasion, nodal metastasis, TNM classification, and stage were similar in the high and low intratumoral PSMA expression groups. PSMA expression in tumoral epithelium is shown in Table 3.

ROC analysis revealed that PSMA was a significant marker of death. A PSMA cut off value of 3 exhibited the highest sensitivity and specificity (area under the curve, 0.705; sensitivity, 81%; specificity, 51%). Patients were divided into two groups according to PSMA expression as high (≥3) and low (< 3).

PSMA expression in the vascular epithelium of lymphatic metastasis was significantly higher compared with that in patients with tumor-negative lymph nodes ($p < .001$) (Table 4). Most patients with lymphatic metastasis exhibited higher primary tumoral PSMA expression. However, no significant difference was found between patients with and without lymph node metastasis in terms of PSMA expression.

A higher vascular expression score of PSMA was observed in pT4 tumors. Similarly, higher vascular PSMA scores were observed in stage 4 tumors. No significant correlation with pN was detected for PSMA score.

PSMA expression in the epithelium of the primary SCCL is

Table 1. Clinical findings, histopathological findings, and clinical stages of the cases

	No. (%)
Age, mean ± SD (yr)	61 ± 10
Tumor differentiation	
Well	19 (37.3)
Moderately	22 (43.1)
Poor	10 (19.6)
Tumor diameter (cm), median (range)	2.5 (0.6–8.5)
Perineural invasion	
No	46 (90.2)
Yes	5 (9.8)
Tumor localization	
Supraglottic	15 (29.4)
Glottic	12 (23.5)
Infraglottic	1 (2)
Glottic + supraglottic	6 (11.8)
Glottic + infraglottic	8 (15.7)
Transglottic	9 (17.6)
Capsular invasion	
No	44 (86.3)
Yes	7 (13.7)
Depth of invasion, mean ± SD, cm	1.3 ± 0.9
Lymphovascular invasion	
No	42 (82.4)
Yes	9 (17.6)
Cartilage invasion	
No	19 (37.3)
Yes	32 (62.7)
Surgical margin	
No	48 (94.1)
Yes	3 (5.9)
Soft tissue invasion	
No	28 (54.9)
Yes	23 (45.1)
T category	
1	6 (11.8)
2	14 (27.5)
3	6 (11.8)
4	25 (49)
N category	
0	32 (62.7)
1	5 (9.8)
2	5 (9.8)
3	9 (17.6)
Stage	
1	4 (7.8)
2	12 (23.1)
3	3 (5.9)
4	32 (62.7)

SD, standard deviation; T, tumor; N, node.

Table 2. The correlative evaluation between clinical findings, histopathological findings, and clinical stages of the cases and PSMA expression scores in the intratumoral vessels

	PSMA score <3 (%)	PSMA score ≥3 (%)	p-value
Age (yr)	61±12	60±9	.844
Tumor differentiation			
Well	8 (44.4)	11 (33.3)	.744
Moderately	6 (33.3)	16 (48.5)	
Poor	4 (22.2)	6 (18.2)	
Tumor diameter (cm)	2.5±1.6	3±1.6	.367
Perineural invasion			
No	18 (100)	28 (84.8)	.148
Yes	0	5 (15.2)	
Tumor localization			
Supraglottic	9 (50)	6 (18.2)	.017
Glottic	4 (22.2)	8 (24.2)	>.99
Infraglottic	0	1 (3.0)	>.99
Glottic+supraglottic	3 (16.7)	3 (9.1)	.652
Glottic+infraglottic	2 (11.1)	6 (18.2)	.696
Transglottic	0	9 (27.3)	.019
Capsular invasion			
No	17 (94.4)	27 (81.8)	.398
Yes	1 (5.6)	6 (18.2)	
Depth of invasion	1.09±0.9	1.4±0.6	.227
Lymphovascular invasion			
No	16 (88.9)	26 (78.8)	.464
Yes	2 (11.1)	7 (21.2)	
Cartilage invasion			
No	12 (66.7)	7 (21.2)	.001
Yes	6 (33.3)	26 (78.8)	
Surgical margin			
No	17 (94.4)	31 (93.9)	>.99
Yes	1 (5.6)	2 (6.1)	
Soft tissue invasion			
No	13 (72.2)	15 (45.5)	.066
Yes	5 (27.8)	18 (54.5)	
Lymph node metastasis			
No	14 (77.8)	19 (57.6)	.149
Yes	4 (22.2)	14 (42.4)	
T category			
1	3 (16.7)	3 (9.1)	.652
2	9 (50.0)	5 (15.2)	.019
3	4 (22.2)	2 (6.1)	.168
4	2 (11.1)	23 (69.7)	<.001
N category			
0	14 (77.8)	18 (54.5)	.135
1	1 (5.6)	4 (12.1)	.645
2	2 (11.1)	3 (9.1)	>.99
3	1 (5.6)	8 (24.2)	.134
Stage			
1	2 (11.1)	2 (6.1)	.607
2	9 (50.0)	3 (9.1)	.001
3	2 (11.1)	1 (3.0)	.282
4	5 (27.8)	27 (81.8)	<.001

Values are presented as mean±SD or number (%).
PSMA, prostate-specific membrane antigen; T, tumor; N, node; SD, standard deviation.

Table 3. The correlative evaluation between clinical findings, histopathological findings, and clinical stages of the cases and PSMA expression scores in the tumoral epithelium

	PSMA score <3 (%)	PSMA score ≥3 (%)	p-value
Age (yr)	61±10	60±10	.823
Tumor differentiation			
Well	18 (41.9)	1 (12.5)	
Moderately	17 (39.5)	5 (62.5)	.210
Poor	8 (18.6)	2 (25.0)	
Tumor diameter (cm)	2.8±1.7	2.6±1.5	.736
Perineural invasion			
No	39 (90.7)	7 (87.5)	>.99
Yes	4 (9.3)	1 (12.5)	
Tumor localization			
Supraglottic	12 (27.9)	3 (37.5)	.679
Glottic	12 (27.9)	0	.179
Infraglottic	1 (2.3)	0	>.99
Glottic+supraglottic	5 (11.6)	1 (12.5)	>.99
Glottic+infraglottic	5 (11.6)	3 (37.5)	.099
Transglottic	8 (18.6)	1 (12.5)	>.99
Capsular invasion			
No	36 (83.7)	8 (100)	.579
Yes	7 (16.3)	0	
Depth of invasion	1.3±0.9	1.3±0.9	.997
Lymphovascular invasion			
No	35 (81.4)	7 (87.5)	>.99
Yes	8 (18.6)	1 (12.5)	
Cartilage invasion			
No	15 (34.9)	4 (50.0)	.450
Yes	28 (65.1)	4 (50.0)	
Surgical margin			
No	41 (95.3)	31 (93.9)	>.99
Yes	2 (4.7)	2 (6.1)	
Soft tissue invasion			
No	24 (55.8)	7 (87.5)	.407
Yes	19 (44.2)	1 (12.5)	
Lymph node metastasis			
No	27 (62.8)	6 (75.0)	.696
Yes	16 (37.2)	2 (25.0)	
T category			
1	6 (14.0)	0	.572
2	12 (27.9)	2 (25.0)	>.99
3	5 (11.6)	1 (12.5)	>.99
4	20 (46.5)	5 (62.5)	.465
N category			
0	26 (60.5)	6 (75.0)	.694
1	3 (7.0)	2 (25.0)	.170
2	5 (11.6)	0	.580
3	9 (20.9)	0	.322
Stage			
1	4 (9.3)	0	>.99
2	10 (23.3)	2 (25.0)	>.99
3	2 (4.7)	1 (12.5)	.407
4	27 (62.8)	5 (62.5)	>.99

Values are presented as mean±SD or number (%).
PSMA, prostate-specific membrane antigen; T, tumor; N, node; SD, standard deviation.

https://doi.org/10.4132/jptm.2022.02.22

Table 4. The comparison between percentage scores of prostate-specific membrane antigen expression in metastatic and reactive lymph nodes

Lymph node	Score 0	Score 1	Score 2	Score 3	p-value
Reactive lymph node	21 (61.8)	13 (38.2)	0	0	<.001
Metastatic lymph node	0	2 (11.8)	9 (52.9)	6 (35.3)	

Values are presented as number (%).

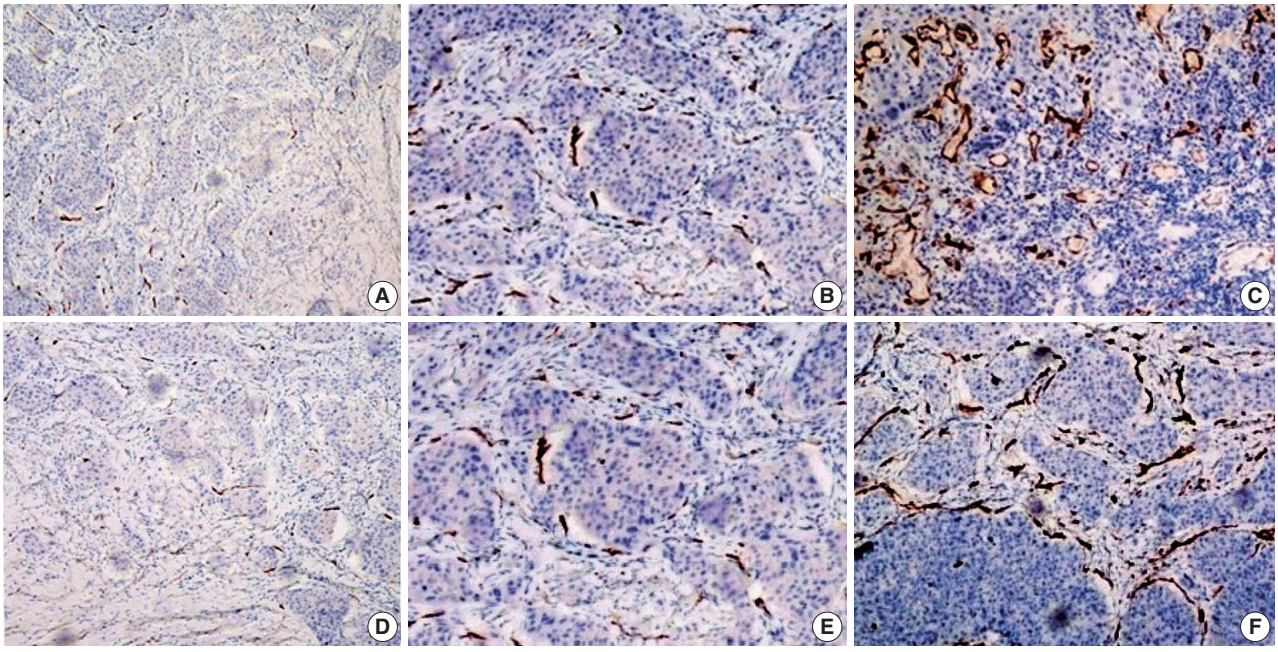

Fig. 2. PSMA expression scores in tumoral and nontumoral tissues. (A) Prostate-specific membrane antigen (PSMA) percentage score of 1 in the vessels of the tumoral stroma. (B) PSMA percentage score of 2 in the vessels of the tumoral stroma. (C) PSMA percentage score of 3 in the vessels of the tumoral stroma. (D) PSMA intensity score of 1 in the vessels of the tumoral stroma. (E) PSMA intensity score of 2 in the vessels of the tumoral stroma. (F) PSMA intensity score of 3 in the vessels of the tumoral stroma.

shown in Fig. 1B. Staining with CD34 demonstrated the difference between normal and tumoral vessels as shown in Fig. 1C. PSMA expression in the vessels of the tumoral stroma are shown on Fig. 1D. PSMA expression in the vessels of a primary tumor (Fig. 1E) and PSMA expression in the vessel cells of the metastatic focus are shown in Fig. 1F. CD31 expression in stromal vessels of the metastatic focus and non-metastatic focus of the same lymph node are shown in Fig. 1G, and PSMA expression in the stromal vessels of the metastatic focus are shown in Fig. 1H. The intratumoral vascular PSMA percentage scores are shown in Fig. 2A–C. Intratumoral PSMA intensity scores are shown in Fig. 2D–F.

No distant organ metastasis was detected in any of the cases. Vascular PSMA expression in metastatic lymph nodes and primary tumors was similar ($p = .383$). No significant correlation was detected between PSMA expression scores in the tumoral vessels and OS, DSS, and DFS ($p > .05$) (Figs. 3, 4).

DISCUSSION

We separately analyzed the expression of PSMA in the stroma of primary tumors, metastatic lymph nodes, non-metastatic lymph nodes, vascular endothelium in the stroma of extratumoral foci, and tumoral epithelium of SCCLs. Many studies have evaluated PSMA expression in intratumoral neovascularized foci [9,14-16]. However, no study has reported PSMA expression in SCCL, and we also compared PSMA expression in metastatic lymph nodes and vascular endothelium in the primary tumoral stroma.

Abnormal stromal cells and neovascularized dysfunctional angiogenic vessels continuously contribute to the microenvironment of the tumor. Certain cancer types that metastasize through hematogenous and lymphatic patterns were reported to be affected by tumor neovascularization [17]. The metastasis, growth, and progression of solid tumors require angiogenesis. In addition to tumoral nutrition, angiogenesis plays an important role in obtaining treatment responsiveness from chemoradiotherapy depending

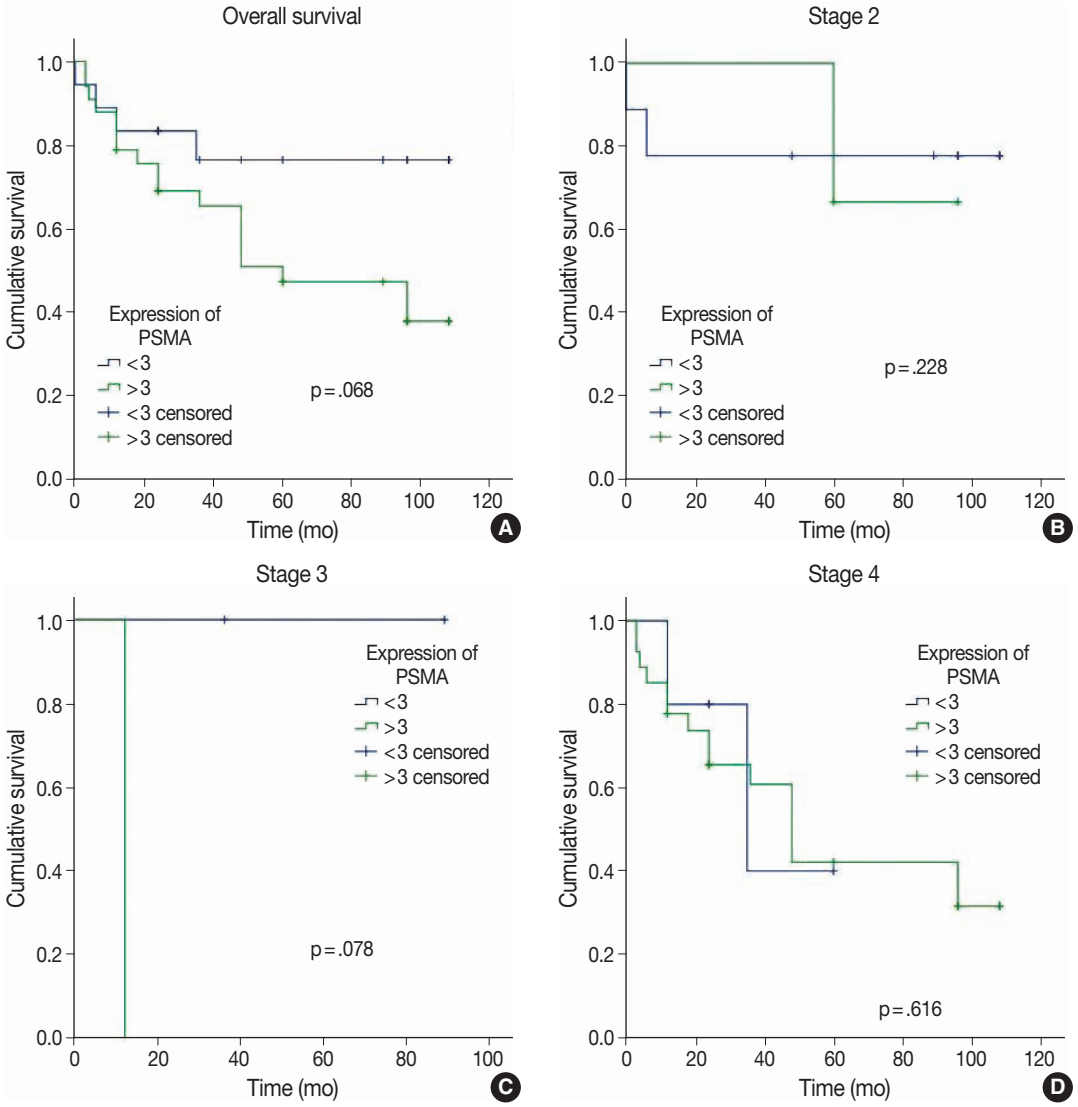

Fig. 3. Overall survival analysis in patients with high and low prostate-specific membrane antigen (PSMA) expression scores according to disease stage. (A) Comparison of overall survival in stage 1 patients according to PSMA expression. (B) Comparison of overall survival in stage 2 patients according to PSMA expression. (C) Comparison of overall survival in stage 3 patients according to PSMA expression. (D) Comparison of overall survival in stage 4 patients according to PSMA expression.

on the quality of the intratumoral vessels. Therefore, a balance between pro- and anti-angiogenic factors should be established [18]. Our study included patients with SCCL who underwent cervical lymph node dissection, and metastatic lymph nodes were detected in 17 of 51 patients, about one-third of the cases.

Angiogenesis is crucial in tumor metastasis [19]. In this respect, it is proposed that antiangiogenic treatment will be of importance in treatment of tumor metastases in the future [20]. In our study, none of the cases exhibited diffuse strong staining with PSMA in the extratumoral normal vascular structures. New investigations of PSMA-ligated treatment strategies could be attempted in cases of advanced tumors when surgical treatment options are impossible.

A proangiogenic microenvironment is considered to increase lymphatic metastatic risk. Even though the 5-year survival rate is commonly high in patients with low T-category and without metastatic lymph nodes, detection of high vascular endothelial growth factor (VEGF) expression has been interpreted to be high risk for poor prognosis and recurrence. Therefore, it is anticipated that these patient groups will benefit from targeted treatment modalities [20]. In our study, the percentage and intensity scores of PSMA expression in intratumoral vessels were significantly high in cases with advanced T-category. PSMA expression scores were 0 and 1 in vessels with a non-metastatic focus in lymph nodes that main-

 https://doi.org/10.4132/jptm.2022.02.22

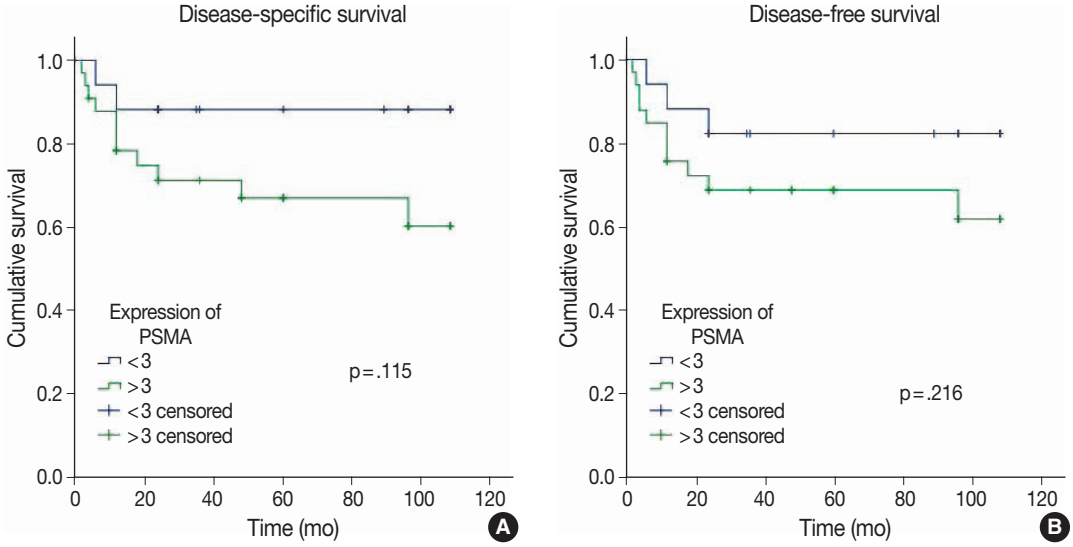

Fig. 4. Disease-specific survival (A) and disease-free survival (B) analyses in patients with high and low prostate-specific membrane antigen (PSMA) expression scores.

tained normal lymph node morphology, whereas PSMA expression scores were significantly higher at scores 2 and 3 in neovascularized vessels in metastatic foci. Therefore, PSMA seems to be a new key factor in the specific target-oriented treatment of both primary tumors and lymph node metastatic foci, but further studies are necessary to confirm this hypothesis.

A significant level of VEGF expression was encountered, whereas no expression was detected in intratumoral stromal cells in another study that investigated the relationship of VEGF expression with angiogenesis in SCCL. Those authors concluded that progression of SCC was compliant with VEGF expression [21]. By contrast, in another study, no correlation was observed between prognosis and angiogenesis in SCCL [22]. In our study, PSMA expression in tumoral vascular endothelium was associated with poor clinical parameters including cartilage invasion, local invasion, and advanced-stage disease.

PSMA positivity was observed in 151 of 779 tumors in a study that evaluated PSMA expression in bone and soft tissue tumors in tumor-associated vascular structures. A higher concentration of PSMA expression was observed in high-grade tumors compared to intermediate and low-grade tumors. However, it was reported that false-negative expression might be present because a tissue microarray system was used in the study [23]. Similarly, in another study, it was reported that neovascular PSMA expression was significantly higher in malignant tumors of the thyroid gland compared to benign lesions, and that expression rates increased in poorly differentiated and undifferentiated tumors [24]. In our study, we identified no correlation between PSMA expression score and differentiation of SCCL.

Our study showed that the intensity and percentage scores of PSMA expression in the vascular endothelium of primary tumor stroma were significantly higher in cases with cartilage and local tumor invasion. It was additionally noted that PSMA expression scores were significantly high with scores 2 and 3 in the intratumoral vessels of pT4 tumors. However, we found no correlation between the expression scores of PSMA in intratumoral vessels and OS, DSS, and DFS.

Specific target-oriented molecular therapies present a crucial necessity for treatment of tumor-associated vessels [25]. Vascular PSMA expression was determined to be correlated with several cancer types with respect to clinicopathologic and prognostic features. No PSMA expression was identified in 24 of 96 patients with SCC of the oral cavity, whereas PSMA expression was observed in less and more than 50% of tumor-associated vessels in 24 and 24 cases, respectively. Therefore, high vascular expression of PSMA was correlated with poor prognosis in oral SCC [13]. Vascular PSMA expression was correlated with the Ki67 proliferation index, which has prognostic importance in breast cancer [12]. PSMA expression in the vascular endothelium was determined to be significantly correlated with TNM, the Ki67 proliferation index, tumor differentiation, and positivity of lymph node metastasis in 103 patients with hepatocellular carcinoma [25]. Similarly, PSMA expression has been evaluated in gynecologic cancers and was encountered in the neovascular foci of specific and high-grade tumors in endometrial, ovarian, and cervical SCC, while vulval SCC exhibited no such phenomenon [13].

PSMA expression was identified in tumor-associated vessels in 46% (31/68) of patients with breast cancer and metastasis

[16]. The relationship of PSMA expression with distant organ metastasis could not be analyzed in our study because no distant organ metastasis was present in any of our patients.

Early diagnosis and treatment of tumors are important to avoid surgery with high comorbidity for patients such as laryngectomy. Researchers have found that the use of nitric oxide synthase blockers is a promising tool in the scope of antiangiogenic therapy in SCCL [26]. Similarly, PSMA can be considered a target in early-stage tumors because it exhibits specific expression in the vessels of the neoplastic foci.

The limitation of this study was that our study was retrospective, observational, and included patients who underwent neck dissection for SCCL, limiting the number of cases. Heterogeneity of sex was another limitation, which was caused by the male dominance of larynx tumors. In our study, there was only one female patient. Therefore, the relationship between expression of PSMA and sex could not be evaluated. Our study included patients that were followed for a period between 12 and 120 months. The survival analysis revealed no difference between the groups in terms of PSMA expression. However, this might be due to the limited follow-up of the patients that were included in the study in recent years.

Both proangiogenetic and antiangiogenetic drugs will be introduced in the near future as alternative treatment options to suppress tumor blood circulation and halt tumor progression [24]. Numerous preclinical animal studies and case reports of patients with cancer have supported the validity of antiangiogenic therapy [27-29]. The rapidly increasing amount of information on tumor angiogenesis, current information on the biologic behavior of cancer, and implementation of imaging studies to display clinical interventions and tumoral vascularity support antiangiogenic therapy as a new treatment method by facilitating its development. Novel developments will be achieved using innovative molecular analysis technologies to display neovascularization using imaging techniques such as positron emission tomography, computed tomography and magnetic resonance imaging to confirm tumor mass. We anticipate that PSMA will be used as a target of alternative or adjuvant treatment options to surgical procedures for treatment of cancer and metastases. However, this anticipation will only be realized with further prospective studies.

PSMA expression in tumoral vascular endothelium was associated with poor clinical parameters including cartilage invasion, local invasion, and advanced stage. PSMA expression can be used for detection of lymph node metastasis. PSMA seems to be a mediator for novel diagnostic and treatment options in the targeted therapy of advanced-stage laryngeal tumors and their metastases.

Ethics Statement

The study protocol was approved by the institutional review board (258-11.09.2020). The study was designed as a retrospective study; therefore, informed consent was not obtained from the patients.

Availability of Data and Material

The datasets generated or analyzed during the study are available from the corresponding author on reasonable request.

Code Availability

Not applicable.

ORCID

Gamze Erkılınç https://orcid.org/0000-0003-4704-7415
Hasan Yasan https://orcid.org/0000-0002-5470-6784
Yusuf Çağdaş Kumbul https://orcid.org/0000-0002-0713-2933
Mehmet Emre Sivrice https://orcid.org/0000-0002-2396-6794
Meltem Durgun https://orcid.org/0000-0002-0391-7071

Author Contributions

Conceptualization: GE, HY, MES. Data curation: YÇK, MD, GE. Formal analysis: HY, MES. Funding acquisition: GE. Investigation and evaluation of slides: GE, MD. Methodology: GE, HY, MES, YÇK, MD. Supervision: GE. Validation: GE, HY, MES, YÇK, MD. Writing—original draft: GE, HY, MES, YÇK. Writing—review & editing: GE, HY, MES. Approval of final manuscript: all authors.

Conflicts of Interest

The authors declare that they have no potential conflicts of interest.

Funding Statement

This study was funded by The Coordinatorship of Scientific Research Projects Department (BAP), Süleyman Demirel University by the number of TSG-2020-8134.

References

1. Nocini R, Molteni G, Mattiuzzi C, Lippi G. Updates on larynx cancer epidemiology. Chin J Cancer Res 2020; 32: 18-25.
2. Prince A, Aguirre-Ghizo J, Genden E, Posner M, Sikora A. Head and neck squamous cell carcinoma: new translational therapies. Mt Sinai J Med 2010; 77: 684-99.
3. Rieger J, Kaessmeyer S, Al Masri S, Hunigen H, Plendl J. Endothelial cells and angiogenesis in the horse in health and disease: a review. Anat Histol Embryol 2020; 49: 656-78.
4. Beatrice F, Valente G, Cammarota R, et al. Laryngeal cancer and angiogenesis. Acta Otorhinolaryngol Ital 1996; 16: 355-62.
5. Chen X, Liang R, Zhu X. Anti-EGFR therapies in nasopharyngeal carcinoma. Biomed Pharmacother 2020; 131: 110649.
6. de Vries LH, Lodewijk L, Braat A, et al. (68)Ga-PSMA PET/CT in radioactive iodine-refractory differentiated thyroid cancer and first treatment results with (177)Lu-PSMA-617. EJNMMI Res 2020; 10: 18.
7. Rowe SP, Gorin MA, Pomper MG. Imaging of prostate-specific membrane antigen using [(18)F]DCFPyL. PET Clin 2017; 12: 289-96.
8. Bradbury R, Jiang WG, Cui YX. The clinical and therapeutic uses of MDM2 and PSMA and their potential interaction in aggressive

cancers. Biomark Med 2015; 9: 1353-70.
9. Van de Wiele C, Sathekge M, de Spiegeleer B, et al. PSMA expression on neovasculature of solid tumors. Histol Histopathol 2020; 35: 919-27.
10. Gale N, Poljak M, Zidar N. Update from the 4th Edition of the World Health Organization classification of head and neck tumours: what is new in the 2017 WHO blue book for tumours of the hypopharynx, larynx, trachea and parapharyngeal space. Head Neck Pathol 2017; 11: 23-32.
11. Seethala RR, Weinreb I, Bullock MJ, et al. Protocol for the examination of specimens from patients with carcinomas of the larynx. Northfield: College of American Pathologists, 2019.
12. Wernicke AG, Varma S, Greenwood EA, et al. Prostate-specific membrane antigen expression in tumor-associated vasculature of breast cancers. APMIS 2014; 122: 482-9.
13. Wernicke AG, Kim S, Liu H, Bander NH, Pirog EC. Prostate-specific membrane antigen (PSMA) expression in the neovasculature of gynecologic malignancies: implications for PSMA-targeted therapy. Appl Immunohistochem Mol Morphol 2017; 25: 271-6.
14. Haffner MC, Laimer J, Chaux A, et al. High expression of prostate-specific membrane antigen in the tumor-associated neo-vasculature is associated with worse prognosis in squamous cell carcinoma of the oral cavity. Mod Pathol 2012; 25: 1079-85.
15. Silver DA, Pellicer I, Fair WR, Heston WD, Cordon-Cardo C. Prostate-specific membrane antigen expression in normal and malignant human tissues. Clin Cancer Res 1997; 3: 81-5.
16. Kasoha M, Unger C, Solomayer EF, et al. Prostate-specific membrane antigen (PSMA) expression in breast cancer and its metastases. Clin Exp Metastasis 2017; 34: 479-90.
17. Lin PP. Aneuploid circulating tumor-derived endothelial cell (CTEC): a novel versatile player in tumor neovascularization and cancer metastasis. Cells 2020; 9: 1539.
18. Butkiewicz D, Gdowicz-Klosok A, Krzesniak M, et al. Association of genetic variants in ANGPT/TEK and VEGF/VEGFR with progression and survival in head and neck squamous cell carcinoma treated with radiotherapy or radiochemotherapy. Cancers (Basel) 2020; 12: 1506.
19. Kupisz K, Chibowski D, Klatka J, Klonowski S, Stepulak A. Tumor angiogenesis in patients with laryngeal cancer. Eur Arch Otorhinolaryngol 1999; 256: 303-5.
20. Schluter A, Weller P, Kanaan O, et al. CD31 and VEGF are prognostic biomarkers in early-stage, but not in late-stage, laryngeal squamous cell carcinoma. BMC Cancer 2018; 18: 272.
21. Sawatsubashi M, Yamada T, Fukushima N, Mizokami H, Tokunaga O, Shin T. Association of vascular endothelial growth factor and mast cells with angiogenesis in laryngeal squamous cell carcinoma. Virchows Arch 2000; 436: 243-8.
22. Rodrigo JP, Cabanillas R, Chiara MD, Garcia Pedrero J, Astudillo A, Suarez Nieto C. Prognostic significance of angiogenesis in surgically treated supraglottic squamous cell carcinomas of the larynx. Acta Otorrinolaringol Esp 2009; 60: 272-7.
23. Heitkotter B, Trautmann M, Grunewald I, et al. Expression of PSMA in tumor neovasculature of high grade sarcomas including synovial sarcoma, rhabdomyosarcoma, undifferentiated sarcoma and MPNST. Oncotarget 2017; 8: 4268-76.
24. Heitkotter B, Steinestel K, Trautmann M, et al. Neovascular PSMA expression is a common feature in malignant neoplasms of the thyroid. Oncotarget 2018; 9: 9867-74.
25. Jiao D, Li Y, Yang F, et al. Expression of prostate-specific membrane antigen in tumor-associated vasculature predicts poor prognosis in hepatocellular carcinoma. Clin Transl Gastroenterol 2019; 10: 1-7.
26. Franchi A, Gallo O, Paglierani M, et al. Inducible nitric oxide synthase expression in laryngeal neoplasia: correlation with angiogenesis. Head Neck 2002; 24: 16-23.
27. White CW, Sondheimer HM, Crouch EC, Wilson H, Fan LL. Treatment of pulmonary hemangiomatosis with recombinant interferon alfa-2a. N Engl J Med 1989; 320: 1197-200.
28. Folkman J. Seminars in Medicine of the Beth Israel Hospital, Boston. Clinical applications of research on angiogenesis. N Engl J Med 1995; 333: 1757-63.
29. Eisen T, Boshoff C, Mak I, et al. Continuous low dose thalidomide: a phase II study in advanced melanoma, renal cell, ovarian and breast cancer. Br J Cancer 2000; 82: 812-7.

JPTM
Journal of Pathology and Translational Medicine 2022; 56: 144-151
https://doi.org/10.4132/jptm.2022.03.13

ORIGINAL ARTICLE

Prognostic and clinicopathological significance of *Fusobacterium nucleatum* in colorectal cancer: a systemic review and meta-analysis

Younghoon Kim[1,2], Nam Yun Cho[1], Gyeong Hoon Kang[1,2]

[1]Laboratory of Epigenetics, Cancer Research Institute, Seoul National University College of Medicine, Seoul;
[2]Department of Pathology, Seoul National University College of Medicine, Seoul, Korea

Background: *Fusobacterium nucleatum* has been identified to promote tumor progression in colorectal cancer (CRC). However, association between *F. nucleatum* and prognostic or clinicopathological features has been diverse among studies, which could be affected by type of biospecimen (formalin-fixed paraffin-embedded or fresh frozen [FF]). **Methods:** Articles were systemically reviewed for studies that included the correlation between *F. nucleatum* and prognosis or clinicopathological features in CRC. **Results:** Ten articles, eight studies with survival-related features involving 3,199 patients and nine studies with clinical features involving 2,655 patients, were eligible for the meta-analysis. Overall survival, disease-free survival, and cancer-specific survival were all associated with worse prognosis in *F. nucleatum*–high patients ($p < .05$). In subgroup analysis, only studies with FF tissues retained prognostic significance with *F. nucleatum.* In meta-analysis of clinicopathological variables, *F. nucleatum* level was associated with location within colon, pT category, *MLH1* hypermethylation, microsatellite instability status, and *BRAF* mutation regardless of type of biospecimen. However, lymph node metastasis and *KRAS* mutation was only associated with *F. nucleatum* level in FF-based studies. **Conclusions:** In conclusion, type of biospecimen could affect the role of *F. nucleatum* as a biomarker associated with clinicopathological features and prognosis.

Key Words: Fusobacteria; Colorectal neoplasms; Prognosis

Received: December 1, 2021 **Revised:** February 10, 2022 **Accepted:** March 13, 2022
Corresponding Author: Gyeong Hoon Kang, MD, PhD, Department of Pathology, Seoul National University College of Medicine, 103 Daehak-ro, Jongno-gu, Seoul 03080, Korea
Tel: +82-22-740-8272, Fax: +82-2-765-5600, E-mail: ghkang@snu.ac.kr

In recent years, it has been established that gut microbiota is closely linked to various intestinal human disease including colorectal cancer (CRC) via microbiome dysbiosis [1-3]. Among the heterogeneous microbiota, *Fusobacterium nucleatum*, an anaerobic, gram-negative bacteria, has been enriched in CRC tumor tissues and stool specimen compared with normal tissues [4,5]. Abundance of *F. nucleatum* is gradually increased from normal to precancerous adenomatous lesions to carcinoma in CRC and suggests a significant role of *F. nucleatum* in tumor progression of CRC [6,7].

F. nucleatum has various mechanisms that influence carcinogenesis which includes promoting of E-cadherin/β-catenin signaling via adhesion protein FadA [8], adhering to cancer cells, colonizing, and inhibiting immunity by leptin Fap2 [2,9], inducing development of CRC by mircoRNA-21–mediated pathway [10], and increasing chemoresistance via autophagy [11,12]. Recently, it has been reported that *F. nucleatum* is positive in CRC cells in liver metastases, which suggests that *F. nucleatum* may also act as an integral component in CRC metastasis [13]. Furthermore, in xenograft tumor model, treating *F. nucleatum* with antibiotics resulted in reduction of tumor growth.

Even though *F. nucleatum* plays a key role in CRC progression and metastasis, studies that report the characteristics of *F. nucleatum* in prognosis and clinicopatholigcal features by using CRC tissues, nevertheless, has shown conflicting results. Several studies considered *F. nucleatum* level as a suitable biomarker for worse survival [14-16] in CRC patients while other studies did not detect correlation between *F. nucleatum* level and prognosis in overall CRC patients [17,18]. Similar discrepancies between studies arise from other clinicopathological studies such as *KRAS* mutation,

pISSN 2383-7837
eISSN 2383-7845

tumor location, and microsatellite instability (MSI) status. Although the reason for discordance could be due to heterogeneity in CRC patient populations [19], this could also be affected by the type of biospecimen used for each study, namely formalin-fixed paraffin-embedded (FFPE) tissue or fresh frozen (FF) tissue. A recent article addresses differences between paired FFPE and FF samples when detecting *F. nucleatum* in CRC [20], but a systemic review that discuss the impact of biospecimen in detecting *F. nucleatum* has not been available.

In this study, we conducted a systemic review and meta-analysis to determine the prognostic and clinicopathological significance of *F. nucleatum* in CRC. Our aim is to clarify how the selection of biospecimen could allocate different roles of microbiome of CRC by affecting the association between *F. nucleatum* level and survival or clinicopathological features.

MATERIALS AND METHODS

Literature search strategy

Articles relevant with the subject were retrieved from electronic databases, PubMed, Embase, and Web of Science until December 3 of 2020. Search terms were, "Fusobacterium nucleatum, Fusobacterium, Fusobacteria, or *F. nucleatum*" and "colorectal cancer, colon cancer, rectal cancer, colorectal carcinoma, or CRC". Each article was examined carefully to determine studies with identical patient population. When multiple studies present overlapping patient data, we selected the studies with the largest patient cohort for clinical data and survival data, respectively.

Inclusion and exclusion criteria

Studies that were eligible for the inclusion in this meta-analysis were as follows: (1) full length articles published in English that detected Fusobacterium nucleatum from human tumor samples derived from CRC tissue, (2) studies with CRC samples divided into high and low (or high and low/negative) according to *F. nucleatum* level, (3) studies that included clinicopathological, molecular, or survival-associated data that were correlated with *F. nucleatum* level. Studies that only contain abstract or posters, studies could not be arranged as dichotomized *F. nucleatum* level data, studies with insufficient data, studies that used more than one type of biospecimen to detect *F. nucleatum* level, and studies that detected *F. nucleatum* level in stools were excluded.

Data extraction and quality assessment

Two reviewers (Y.K. and G.H.K.) independently collected data from eligible articles according to the criteria. Newcastle-Ottawa Scale was used to evaluate study quality. A score higher than six out of nine criteria was defined as qualified. Name of author, year of publication, number of total patients, number of *F. nucleatum* positive patients, type of biospeicmen (FFPE or FF), method of *F. nucleatum* level detection, survival data, and clinicopathological data associated with *F. nucleatum* level were collected from each study. Survival data were extracted as hazard ratio [HR] and 95% confidence intervals [CIs] from univariate Cox analysis. When only Kaplan-Meier curves were presented for survival analysis, HR and 95% CIs were estimated by using Engauge Digitizer V9.8 (http://digitizer.sourceforge.net) and spreadsheets provided by Tierney et al. [21]. When a three-tier survival was given (negative, low, and high) we pooled negative and low as reference to calculate HR and 95% CIs for high and rearranged it into two-tier (low/negative and high).

Statistical analysis

Meta-analysis was conducted using R software ver. 3.5.3 (https://cran.r-project.org/). Pooled HR and 95% CIs for overall survival (OS), disease-free survival (DFS), and cancer-specific survival (CSS) and pooled odds ratio and 95% CIs for clinicopathological features were analyzed via R package 'meta' and 'dmetar'. Subgroup analysis was performed if multiple types of biospecimen existed within a pooled analysis. Statistic heterogeneity was determined by Cochran's Q and I^2. When heterogeneity was observed ($p < .05$ or $I^2 > 50\%$) random effect model was used for the analysis instead of fixed effect model. A graphical funnel plot was used to evaluate publication bias.

RESULTS

Literature search and study characteristics

Four hundred and thirty-two records were collected from PubMed, Embase, and Web of Science (Fig. 1). After removing 76 duplications, 356 records were screened by abstract and 32 records were categorized as being relevant with the subject. These records were reviewed in detail and 10 articles, eight studies with survival-related features involving 3,199 patients [14-18,22-24] and nine studies with clinical features involving 2,655 patients [14-17,22-25], were selected eligible for the meta-analysis (Table 1). Seven studies were included in the meta-analysis for both survival-related and clinical features [14-17,22-24]. Two studies had overlapping patients but were used for meta-analysis of either clinical or survival-related features, respectively [18,25]. Six out of the 10 articles assessed *F. nucleatum* level with FFPE tissues [6,16-18,24,25] and four articles used FF tissues

to detect *F. nucleatum* [14,15,22,23].

Meta-analysis between *F. nucleatum* level and survival

The meta-analysis between *F. nucleatum* level and prognostic values of OS (Fig. 2A), DFS (Fig. 2B), and CSS (Fig. 2C) in CRC has shown that high *F. nucleatum* level is associated with poor OS, DFS, and CSS (OS: HR, 1.58; 95% CI, 1.28 to 1.94; p < .001; DFS: HR, 1.76; 95% CI, 1.06 to 2.93; p = .030; CSS: HR, 1.72; 95% CI, 1.05 to 2.83; p = .031, respectively). In subgroup analysis, studies with FF samples (p < .001), but not those with FFPE samples (p = .168) retained prognostic significance between *F. nucleatum* level and OS (Table 2, Supplementary Fig. S1). Furthermore, studies with FFPE samples did not show significant correlation between *F. nucleatum* level and DFS (p = .214). Analyzing studies with stage I though IV CRC did not affect prognostic significance between *F. nucleatum* level and OS (HR, 1.41; 95% CI, 1.11 to 1.80; p = .005).

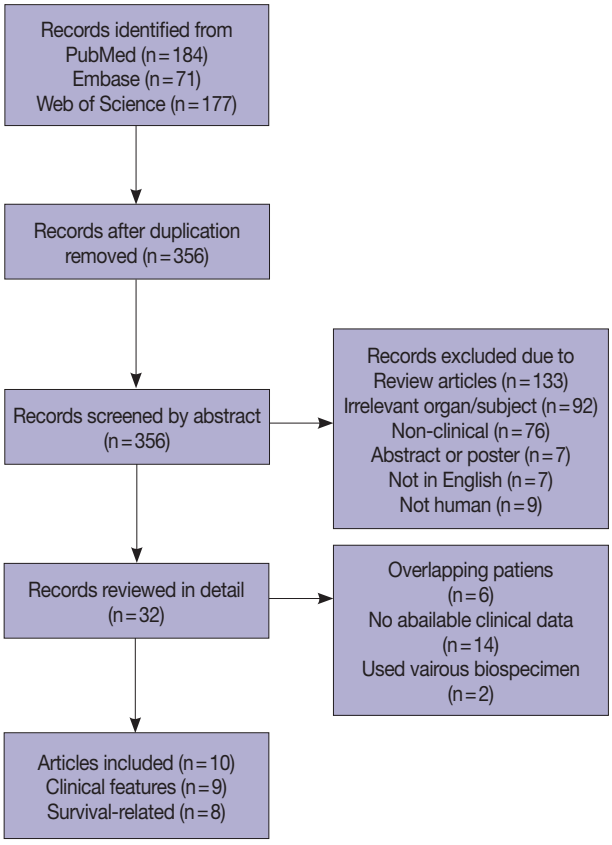

Fig. 1. Flow chart of literature search and study selection.

Meta-analysis between *F. nucleatum* level and clinicopathological features

Meta-analysis for correlation between *F. nucleatum* level and clinicopathological features of CRC are assessed in Table 3. High *F. nucleatum* level was associated with proximal colon location (p < .001), worse tumor differentiation (p = .002), high pT category (p < .001), presence of distal metastasis (p = .007), *MLH1* hypermethylation (p < .001), and MSI-high CRC (p = .001) when all studies were considered. In subgroup analysis (Table 4), studies with FFPE samples showed significant correlation between high *F. nucleatum* level and proximal colon location (p = .001), worse tumor differentiation (p = .015), high pT category (p < .001), *MLH1* hypermethylation (p < .001), CpG island methylator phenotype (CIMP)–high status (p < .001), and MSI-high status (p < .001). Studies with FF samples, on the other hand, demonstrated that high *F. nucleatum* level is significantly correlated with high pT category (p = .001), presence of lymph node metastasis (p = .001), and presence of *KRAS* mutation (p = .007), which showed borderline significance with high *F. nucleatum* level in overall studies (p = .052).

Publication bias

Begg's funnel plot was evaluated for presence of potential publication bias in meta-analysis associated with survival (Fig. 3). Visible asymmetry was observed with Egger's test reporting p-

Table 1. Characteristics of articles included in the meta-analysis

Authors	Year	No. of patients	No. of positives	Biospecimen	Method	Survival	Clinical	Stage
Yan et al. [16]	2017	280	187	FFPE	qPCR	O	O	III/IV
Wei et al. [14]	2016	180	90	FF	qPCR	O	O	I–III
Yamaoka et al. [15]	2018	100	50	FF	ddPCR	O	O	I–IV
Samkamoto et al. [18]	2018	1,069	67	FFPE	qPCR	O		I–IV
Sun et al. [22]	2016	152	59	FF	qPCR	O	O	I–IV
Kunzmann et al. [23]	2019	190	61	FF	qPCR	O	O	I–IV
Oh et al. [17]	2019	593	204	FFPE	qPCR	O	O	II/III
Chen et al. [24]	2019	91	25	FFPE	qPCR	O	O	II/III
Ito et al. [6]	2015	511	143	FFPE	qPCR		O	I–IV
Mima et al. [25]	2015	1,102	69	FFPE	qPCR		O	I–IV

FFPE, formalin-fixed paraffin-embedded; qPCR, quantitative polymerase chain reaction; FF, fresh frozen; ddPCR, droplet digital polymerase chain reaction.

https://doi.org/10.4132/jptm.2022.03.13

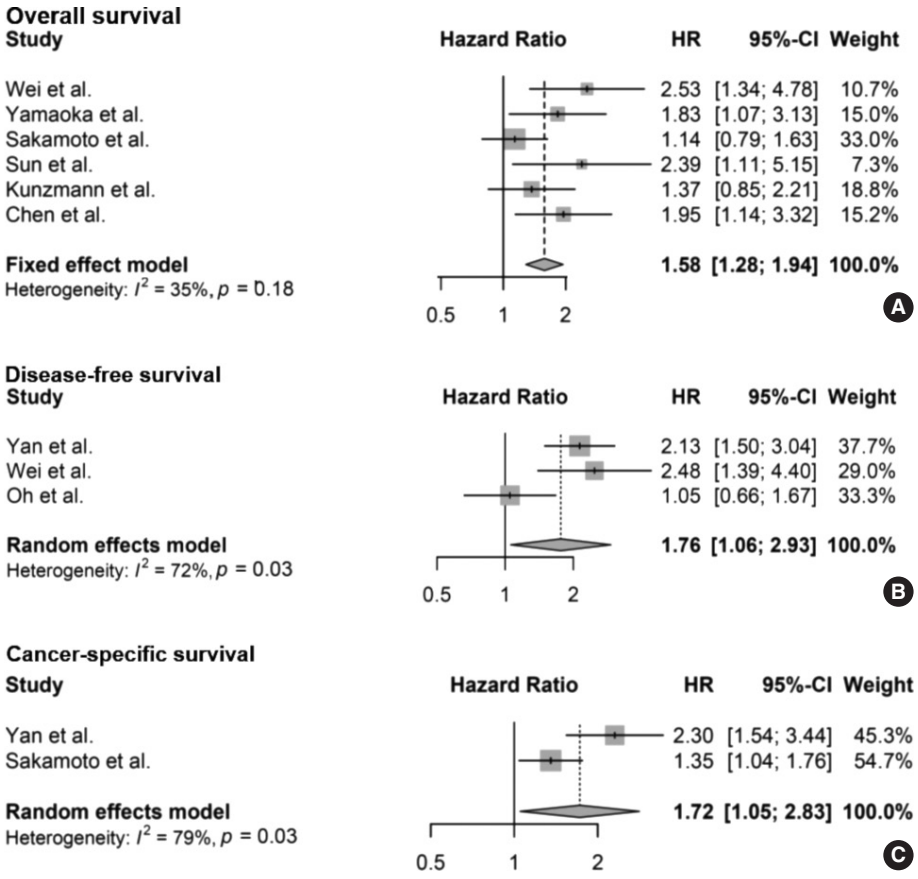

Fig. 2. Forest plot for the correlation between *Fusarium nucleatum* and survival in colorectal cancer [14-18,22-24]: (A) overall survival, (B) disease-free survival, and (C) cancer-specific survival. HR, hazard ratio; CI, confidence interval.

Table 2. Subgroup analysis associated with survival

Survival	Specimen	Study	HR	95% CI	p-value
Overall survival	FFPE	2	1.43	0.85–2.42	.168
	FF	4	1.84	1.36–2.48	<.001
Disease-free survival	FFPE	2	1.52	0.76–3.04	.214

HR, hazard ratio; CI, confidence interval; FFPE, formalin-fixed paraffin-embedded; FF, fresh frozen.

value of .006 for OS but not for DFS (p = .935).

DISCUSSION

F. nucleatum has been associated with cancer development and progression of CRC, as well as a potential target of cancer treatment. *F. nucleatum* is abdudnant in CRC tissues from patients with metastasis than those from non-metastatic CRC patients [26]. Presence *F. nucleatum* was essential in establishment of CRC patients-derived xenografts in mice [13]. Not only does infection of *F. nucleatum* has promoted metastasis in CRC cells via autophage but also is found in distant metastasis sites including liver, lung, and lymph nodes, although the mechanism is yet to be unveiled [9,13,26,27]. Moreover, previous studies have suggested that *F. nucleatum* provoke chemoresistance inhibiting caspase cascade and activating autophagy pathway to prevent apoptosis in CRC cells [11,28].

It is still unclear if *F. nucleatum* is a significant driver of tumor initiation and *F. nucleatum* level detected from CRC tissues and association with prognosis and clinicopathological variables has not been consistent among studies. Herein, we hypothesized that this could be partially caused by different type of biospecimen being used for each study and investigated its affect by a systemic review and meta-analysis with the difference between FFPE and FF into consideration.

High *F. nucleatum* level was associated with worse survival in

OS, DFS, and CSS in overall meta-analysis. Subgroup analysis revealed that studies with FF show a significant correlation between *F. nucleatum* level and OS. However, studies with FFPE tissues show that a significant correlation between *F. nucleatum* and OS or DFS is not observed.

Association between *F. nucleatum* level and clinicopathological features are much more diverse. A pooled analysis of FFPE and FF studies together shows that high *F. nucleatum* level samples

Table 3. Meta-analysis associated with clinical features

Clinical feature	Study	OR	95% CI	p-value
Age	5	0.993	0.787–1.254	.954
Sex (female/male)	9	1.087	0.910–1.299	.356
Proximal/Distal colon	4	1.642	1.252–2.153	<.001
Rectum/Colon	5	1.184	0.899–1.560	.229
Tumor size	2	0.897	0.592–1.360	.609
Differentiation	7	1.547	1.166–2.052	.002
Vascular invasion	2	0.627	0.337–1.167	.141
Perineural invasion (FFPE only)	2	1.022	0.722–1.448	.900
pT category	5	2.253	1.633–3.108	<.001
Lymph node metastasis	5	1.308	0.979–1.748	.069
Distant metastasis	4	1.912	1.196–3.058	.007
Stage	6	1.110	0.885–1.394	.367
CIMP status (FFPE only)	3	2.612	1.849–3.690	<.001
MLH1 hypermethylation	3	2.852	1.987–4.095	<.001
MSI status	5	2.982	2.175–4.086	<.001
KRAS mutation	5	1.248	0.998–1.561	.052
BRAF mutation	4	1.869	1.273–2.745	.001
PIK3CA mutation	3	1.440	0.965–2.147	.074

OR, odds ratio; CI, confidence interval; FFPE, formalin-fixed paraffin-embedded; CIMP, CpG island methylator phenotype; MSI, microsatellite instability.

Table 4. Subgroup analysis for clinical features

Clinical feature	Specimen	Study	OR	95% CI	p-value
Age	FFPE	2	1.158	0.871–1.539	.312
	FF	3	0.720	0.478–1.086	.117
Sex	FFPE	5	1.096	0.891–1.349	.386
	FF	4	1.063	0.753–1.501	.727
Proximal/Distal colon	FFPE	2	1.676	1.220–2.303	.001
	FF	2	1.554	0.925–2.612	.096
Rectum/Colon	FFPE	2	1.259	0.841–1.884	.263
	FF	3	1.120	0.767–1.636	.557
Differentiation	FFPE	4	1.513	1.083–2.112	.015
	FF	3	1.632	0.958–2.778	.071
pT category	FFPE	2	2.187	1.437–3.329	<.001
	FF	3	2.354	1.428–3.880	.001
Lymph node metastasis	FFPE	2	0.832	0.549–1.262	.387
	FF	3	2.009	1.337–3.017	.001
Distant metastasis	FF	3	1.669	0.863–3.228	.128
Stage	FFPE	2	0.917	0.673–1.251	.586
	FF	4	1.389	0.993–1.943	.055
MLH1 hypermethylation	FFPE	2	3.210	2.208–4.667	<.001
MSI status	FFPE	4	2.757	1.987–3.824	<.001
KRAS mutation	FFPE	3	1.125	0.881–1.436	.345
	FF	2	2.220	1.246–3.954	.007
BRAF mutation	FFPE	3	1.882	1.260–2.811	.002
PIK3CA mutation	FFPE	2	1.464	0.960–2.233	.076

OR, odds ratio; CI, confidence interval; FFPE, formalin-fixed paraffin-embedded; FF, fresh frozen; MSI, microsatellite instability.

https://doi.org/10.4132/jptm.2022.03.13

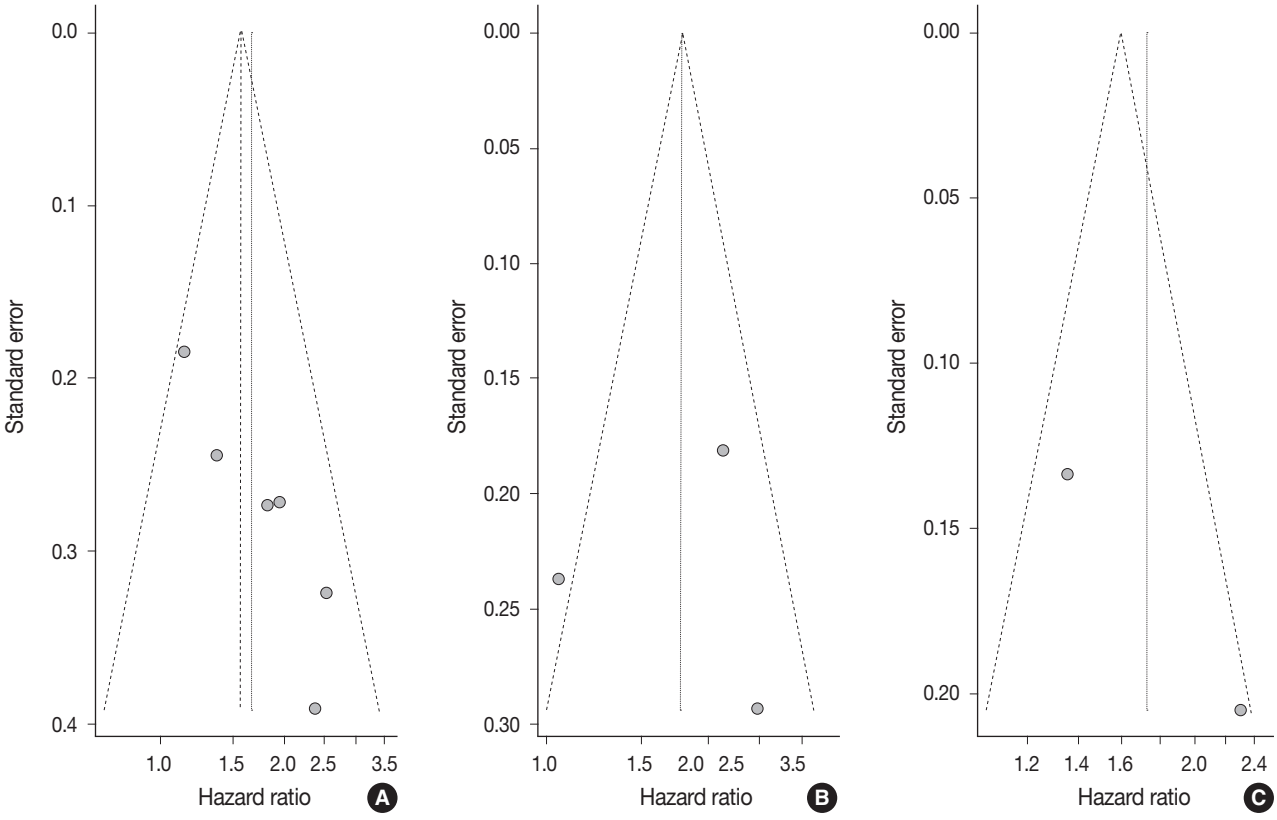

Fig. 3. Funnel plot for studies included in meta-analysis between *Fusarium nucleatum* level and survival: (A) overall survival, (B) disease-free survival, and (C) cancer-specific survival.

are significantly enriched in proximal colon, but on subgroup analysis, only studies using FFPE samples retain statistical significance for the same variable. Similar findings could be observed for correlation between *F. nucleatum* level and distant metastasis. On the contrary, pT category, *MLH1* hypermethylation, and MSI status remained its positive correlation with *F. nucleatum* level regardless of the biospecimen being used. Lymph node metastasis and *KRAS* mutation were only significant in FF tissues and *MLH1* hypermethylation was only significant in FFPE tissues but not in its amalgamated state. Interestingly, the aforementioned features are all considered as hallmark characteristics of MSI-high CRC [29]. These findings emphasize that regardless of type of specimen, high *F. nucleatum* level is strongly indicative of MSI-high status.

There are several putative explanations for discrepancy of results between biospecimen. Mean patient number for studies with FFPE tissue (515.4 patients per study) is more than three times larger than the mean patient number for studies with FF tissues (155.5 patients per study). On the contrary, *F. nucleatum* positivity is significantly higher in studies with FF tissues compared with those of FFPE tissue (41.8% and 24.4%. respectively) which may be a result of a lower threshold in studies with FF tissues to compensate for smaller sample size. This may allude to the fact that features with relatively low incidence such as *KRAS* mutation, could have a higher chance of being categorized as high *F. nucleatum* level sample in studies with FF compared with studies with FFPE.

As an alternative explanation, lower *F. nucleatum* positivity in FFPE tissues may reflect the inherited nature of FFPE samples rather than inflation of threshold in studies with FF tissues. In a study that measured *F. nucleatum* level in paired FFPE and FF tissues of CRC, FF tissues had higher detection rate of overall *F. nucleatum* resulting in difference in survival and clinicopathological features from FFPE-measured samples [20]. Furthermore, concordance between *F. nucleatum* positive cases in FF and those in FFPE samples were low. Discrepancy between DNA results of FFPE and FF samples has also been reported in other paired tumor tissues [30]. This was in part due to inter-strand crosslink between complementary DNA strands which could be aggravated by prolonged fixation [31]. Other potential factors of low *F. nucleatum* detection in FFPE samples includes fragmentation and degeneration of DNA, paraffin embedding, and storage process

[25,32].

Recently, two articles analyzed the correlations between *F. nucleatum* level and prognosis in CRC with meta-analysis [33,34]. Both articles showed a significant correlation between *F. nucleatum* level and OS, but only one study showed a significant correlation between *F. nucleatum* level and DFS. Herein, we suggest that type of biospecimen that was included in each meta-analysis could have affected the discrepancy between the articles.

Limitation of our study is that we cannot identify pathological and molecular discrepancies between FF and FFPE tissues such as correlation between *F. nucleatum* level and T cell density, CIMP, and various immunohistochemical results due to lack of studies with FF that obtain related data. Moreover, although meta-analysis provides evidence that discordance between FF and FFPE samples are present in detecting *F. nucleatum*, we could not narrow down the cause of the misalignment between the two biospecimen.

In conclusion, *F. nucleatum* level is significantly associated with pathological and molecular features including pT category, *MLH1* hypermethylation, and MSI status regardless of biospecimen, but other survival, clinical, and molecular features, such as location of tumor within the colon, distant metastasis, and *KRAS* mutation, could be affected by type of biospecimen in CRC. Therefore, although a strong association between MSI and *F. nucleatum* is always evident, selection of biospecimen could affect the role of *F. nucleatum* as a biomarker in CRC to predict and monitor tumor progression and prognosis as well as evaluate treatment effect.

Supplementary Information

The Data Supplement is available with this article at https://doi.org/10.4132/jptm.2022.03.13.

Ethics Statement

Not applicable.

Availability of Data and Material

All data generated or analyzed during the study are included in this published article (and its supplementary information files).

Code Availability

Not applicable.

ORCID

Younghoon Kim https://orcid.org/0000-0003-4656-0188
Nam Yun Cho https://orcid.org/0000-0002-5736-2956
Gyeong Hoon Kang https://orcid.org/0000-0003-2380-6675

Author Contributions

Conceptualization: YK. Methodology: YK, GHK. Resources: NYC. Writing—original draft: YK. Writing—review & editing: GHK. Approval of final manuscript: all authors.

Conflicts of Interest

The authors declare that they have no potential conflicts of interest.

Funding Statement

This work was financially supported by a grant from the National Research Foundation (NRF) funded by the Korean Ministry of Science and ICT (2019R1F1A1061227) and a grant from the Korea Health Technology R&D Project through the Korea Health Industry Development Institute (KHIDI), funded by the Ministry of Health & Welfare, Republic of Korea (grant number: HI14C1277).

References

1. Wu Y, Wu J, Chen T, et al. *Fusobacterium nucleatum* potentiates intestinal tumorigenesis in mice via a Toll-like receptor 4/p21-activated kinase 1 cascade. Dig Dis Sci 2018; 63: 1210-8.
2. Kostic AD, Chun E, Robertson L, et al. *Fusobacterium nucleatum* potentiates intestinal tumorigenesis and modulates the tumor-immune microenvironment. Cell Host Microbe 2013; 14: 207-15.
3. Marchesi JR, Adams DH, Fava F, et al. The gut microbiota and host health: a new clinical frontier. Gut 2016; 65: 330-9.
4. Kostic AD, Gevers D, Pedamallu CS, et al. Genomic analysis identifies association of *Fusobacterium* with colorectal carcinoma. Genome Res 2012; 22: 292-8.
5. Castellarin M, Warren RL, Freeman JD, et al. *Fusobacterium nucleatum* infection is prevalent in human colorectal carcinoma. Genome Res 2012; 22: 299-306.
6. Ito M, Kanno S, Nosho K, et al. Association of *Fusobacterium nucleatum* with clinical and molecular features in colorectal serrated pathway. Int J Cancer 2015; 137: 1258-68.
7. McCoy AN, Araujo-Perez F, Azcarate-Peril A, Yeh JJ, Sandler RS, Keku TO. *Fusobacterium* is associated with colorectal adenomas. PLoS One 2013; 8: e53653.
8. Rubinstein MR, Wang X, Liu W, Hao Y, Cai G, Han YW. *Fusobacterium nucleatum* promotes colorectal carcinogenesis by modulating E-cadherin/beta-catenin signaling via its FadA adhesin. Cell Host Microbe 2013; 14: 195-206.
9. Abed J, Emgard JE, Zamir G, et al. Fap2 mediates *Fusobacterium nucleatum* colorectal adenocarcinoma enrichment by binding to tumor-expressed Gal-GalNAc. Cell Host Microbe 2016; 20: 215-25.
10. Yang Y, Weng W, Peng J, et al. *Fusobacterium nucleatum* increases proliferation of colorectal cancer cells and tumor development in mice by activating Toll-like receptor 4 signaling to nuclear factor-kappaB, and up-regulating expression of microRNA-21. Gastroenterology 2017; 152: 851-66.
11. Yu T, Guo F, Yu Y, et al. *Fusobacterium nucleatum* promotes chemoresistance to colorectal cancer by modulating autophagy. Cell 2017; 170: 548-63.
12. Mandip KC, Steer CJ. Novel mechanisms of chemoresistance by *Fusobacterium nucleatum* involve not so novel pathways of microRNAs and autophagy. Transl Cancer Res 2018; 7(Suppl 1): S10-5.
13. Bullman S, Pedamallu CS, Sicinska E, et al. Analysis of *Fusobacterium* persistence and antibiotic response in colorectal cancer. Science 2017; 358: 1443-8.
14. Wei Z, Cao S, Liu S, et al. Could gut microbiota serve as prognostic biomarker associated with colorectal cancer patients' survival? A pilot study on relevant mechanism. Oncotarget 2016; 7: 46158-72.
15. Yamaoka Y, Suehiro Y, Hashimoto S, et al. *Fusobacterium nucleatum* as a prognostic marker of colorectal cancer in a Japanese pop-

ulation. J Gastroenterol 2018; 53: 517-24.
16. Yan X, Liu L, Li H, Qin H, Sun Z. Clinical significance of *Fusobacterium nucleatum*, epithelial-mesenchymal transition, and cancer stem cell markers in stage III/IV colorectal cancer patients. Onco Targets Ther 2017; 10: 5031-46.
17. Oh HJ, Kim JH, Bae JM, Kim HJ, Cho NY, Kang GH. Prognostic impact of *Fusobacterium nucleatum* depends on combined tumor location and microsatellite instability status in stage II/III colorectal cancers treated with adjuvant chemotherapy. J Pathol Transl Med 2019; 53: 40-9.
18. Sakamoto Y, Mima K, Daitoku N, et al. *Fusobacterium nucleatum* in colorectal cancer liver metastasis and patient prognosis. Cancer Sci 2018; 109: 1360.
19. Chernyavskiy P, Kennerley VM, Jemal A, Little MP, Rosenberg PS. Heterogeneity of colon and rectum cancer incidence across 612 SEER counties, 2000-2014. Int J Cancer 2019; 144: 1786-95.
20. de Carvalho AC, de Mattos Pereira L, Datorre JG, et al. Microbiota profile and impact of *Fusobacterium nucleatum* in colorectal cancer patients of Barretos Cancer Hospital. Front Oncol 2019; 9: 813.
21. Tierney JF, Stewart LA, Ghersi D, Burdett S, Sydes MR. Practical methods for incorporating summary time-to-event data into meta-analysis. Trials 2007; 8: 16.
22. Sun Y, An QM, Tian XY, et al. *Fusobacterium nucleatum* infection is correlated with tumor metastasis and postoperative survival of colorectal cancer patients in China. Transl Cancer Res 2016; 5: 579-88.
23. Kunzmann AT, Proenca MA, Jordao HW, et al. *Fusobacterium nucleatum* tumor DNA levels are associated with survival in colorectal cancer patients. Eur J Clin Microbiol Infect Dis 2019; 38: 1891-9.
24. Chen Y, Lu Y, Ke Y, Li Y. Prognostic impact of the *Fusobacterium nucleatum* status in colorectal cancers. Medicine (Baltimore) 2019; 98: e17221.
25. Mima K, Sukawa Y, Nishihara R, et al. *Fusobacterium nucleatum* and T cells in colorectal carcinoma. JAMA Oncol 2015; 1: 653-61.
26. Chen Y, Chen Y, Zhang J, et al. Fusobacterium nucleatum promotes metastasis in colorectal cancer by activating autophagy signaling via the upregulation of CARD3 expression. Theranostics 2020; 10: 323-39.
27. Wang S, Liu Y, Li J, et al. *Fusobacterium nucleatum* acts as a pro-carcinogenic bacterium in colorectal cancer: from association to causality. Front Cell Dev Biol 2021; 9: 710165.
28. Zhang S, Yang Y, Weng W, et al. *Fusobacterium nucleatum* promotes chemoresistance to 5-fluorouracil by upregulation of BIRC3 expression in colorectal cancer. J Exp Clin Cancer Res 2019; 38: 14.
29. Bae JM, Kim JH, Kang GH. Molecular subtypes of colorectal cancer and their clinicopathologic features, with an emphasis on the serrated neoplasia pathway. Arch Pathol Lab Med 2016; 140: 406-12.
30. Wen X, Jeong S, Kim Y, et al. Improved results of LINE-1 methylation analysis in formalin-fixed, paraffin-embedded tissues with the application of a heating step during the DNA extraction process. Clin Epigenetics 2017; 9: 1.
31. Freifelder D, Davison PF. Physicochemical studies on the reaction between formaldehyde and DNA. Biophys J 1963; 3: 49-63.
32. Imrit K, Goldfischer M, Wang J, et al. Identification of bacteria in formalin-fixed, paraffin-embedded heart valve tissue via 16S rRNA gene nucleotide sequencing. J Clin Microbiol 2006; 44: 2609-11.
33. Gethings-Behncke C, Coleman HG, Jordao HWT, et al. *Fusobacterium nucleatum* in the colorectum and its association with cancer risk and survival: a systematic review and meta-analysis. Cancer Epidemiol Biomarkers Prev 2020; 29: 539-48.
34. Huangfu SC, Zhang WB, Zhang HR, et al. Clinicopathological and prognostic significance of *Fusobacterium nucleatum* infection in colorectal cancer: a meta-analysis. J Cancer 2021; 12: 1583-91.

JPTM
Journal of Pathology and Translational Medicine 2022; 56: 152-156
https://doi.org/10.4132/jptm.2021.12.09

CASE STUDY

A sinonasal yolk sac tumor in an adult

Jaehoon Shin[1], Ji Heui Kim[2], Kyeong Cheon Jung[3], Kyung-Ja Cho[1]

Departments of [1]Pathology and [2]Otorhinolaryngology-Head and Neck Surgery, Asan Medical Center, University of Ulsan College of Medicine, Seoul; [3]Department of Pathology, Seoul National University Hospital, Seoul National University College of Medicine, Seoul, Korea

Yolk sac tumors (YSTs), which are also called endodermal sinus tumors, are malignant tumors of germ cell origin. These tumors usually occur in the gonads, but 20% of cases have been reported at extragonadal sites. The head and neck is a rarely affected region that accounts for just 1% of all malignant tumors of germ cell origin. In addition, YSTs arise mostly in childhood. We present a rare pathologically pure case of primary adult YST in the sinonasal area. A 45-year-old male patient presented with a rapidly growing mass in the nasal cavity, which caused nasal obstruction and bloody post-nasal drip. The histopathologic features indicated pure YST, and immunohistochemical analysis revealed positive reactivity for Sal-like protein 4 and alpha-fetoprotein. Herein, we discuss the clinical, radiologic, and histologic features of this YST and review other cases of sinonasal YST in adults.

Key Words: Yolk sac tumor; Endodermal sinus tumor; Paranasal sinus; Nasal cavity; Adult

Received: September 6, 2021 **Revised:** December 7, 2021 **Accepted:** December 9, 2021
Corresponding Author: Kyung-Ja Cho, MD, PhD, Department of Pathology, Asan Medical Center, University of Ulsan College of Medicine, 88 Olympic-ro 43-gil, Songpa-gu, Seoul 05505, Korea
Tel: +82-2-3010-4545, Fax: +82-2-472-4560, E-mail: kjc@amc.seoul.kr

Yolk sac tumors (YSTs), which are also called endodermal sinus tumors, are malignant tumors of germ cell origin. These tumors usually occur in the gonads, but 20% of cases have been reported at extragonadal sites. The head and neck is a rarely affected region that accounts for just 1% of all malignant tumors of germ cell origin [1]. In addition, YSTs arise mostly in childhood. To our knowledge, there are only eight reported cases of sinonasal YSTs in adult patients. We report a very rare case of a pathologically pure form of primary adult YST in the sinonasal area.

CASE REPORT

A 45-year-old man was referred to the Department of Otorhinolaryngology at Asan Medical Center in Seoul for persistent right nasal obstruction, bloody rhinorrhea, and post-nasal drip. He reported a history of bloody post-nasal drip for the past four months, facial pain for the last three months, visual disturbance in the right lower field, and diplopia. An endoscopic examination showed a 3-cm-sized mass obstructing the right nasal cavity with partially necrotic tissue.

Initial computed tomography and magnetic resonance imaging revealed a mass that obstructed the right nasal cavity and caused bone destruction of the bilateral frontal and ethmoidal sinuses with intracranial extension. Destruction of the bilateral superomedial orbital wall and invasion of the right medial orbital wall and right nasolacrimal duct and sac were also identified (Fig. 1).

Endoscopic excisional biopsy was carried out. The specimen was removed in three pieces measuring up to 4×3×1.5 cm, with a pinkish brown color and a fleshy gelatinous texture. The submitted specimen was processed for histopathological examination and revealed typical YST features. The tumor showed mostly reticular and microcystic growth patterns with loose myxoid stroma, but there were also areas of glandular, solid sheet-like, and polyvesicular vitelline patterns. Some Schiller-Duval bodies were noted. Intra- and extra-cytoplasmic hyaline globules were identified (Fig. 2). No other tumor components were seen.

Immunohistochemical staining showed diffuse strong nuclear positivity for Sal-like protein 4 and diffuse strong cytoplasmic positivity for α-fetoprotein (Fig. 3). P40 was negative, but integrase interactor 1 (INI1) and Brahma-related gene-1 (BRG1)

pISSN 2383-7837
eISSN 2383-7845

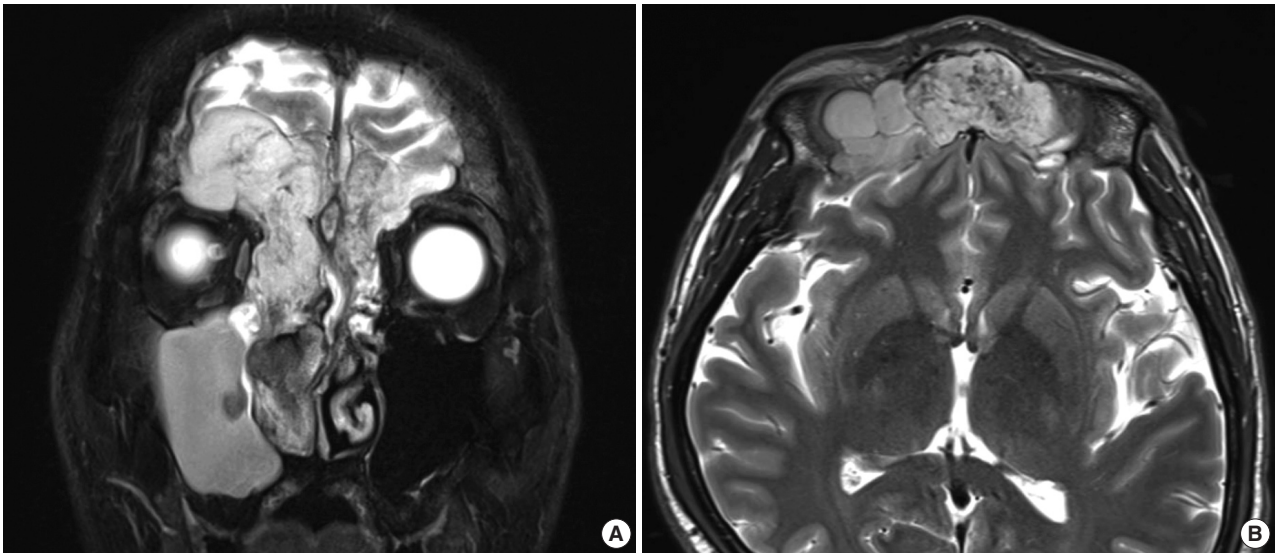

Fig. 1. Coronal (A) and transverse (B) magnetic resonance imaging shows a mass in the right nasal cavity and bilateral frontal sinus.

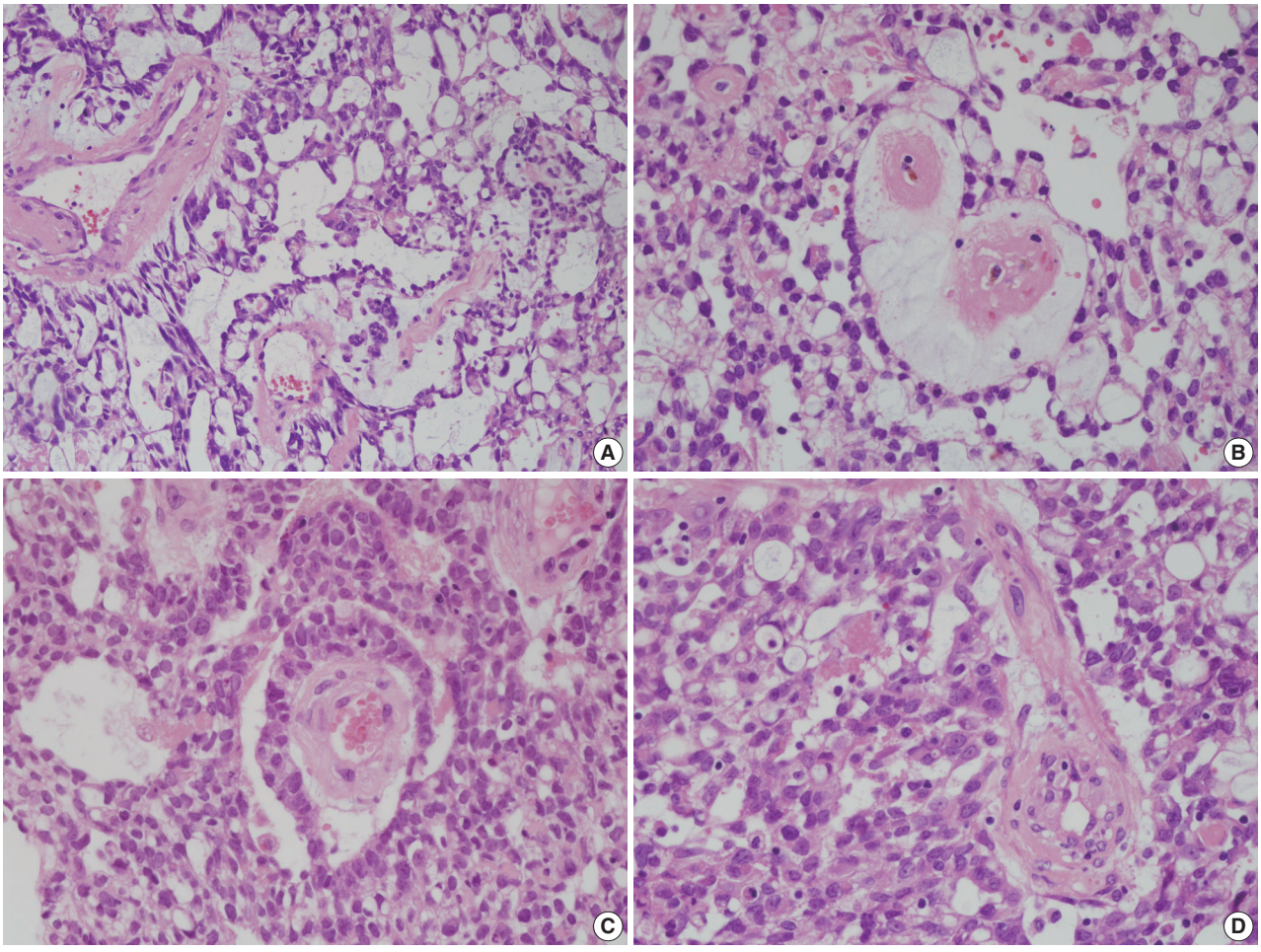

Fig. 2. Histopathologic findings of a sinonasal yolk sac tumor. (A) Reticular and microcystic growth patterns are observed with loose myxoid stroma. (B) A polyvesicular vitelline pattern is occasionally observed. (C) Schiller-Duval bodies are noted focally. (D) Intra- and extra-cytoplasmic hyaline globules are observed.

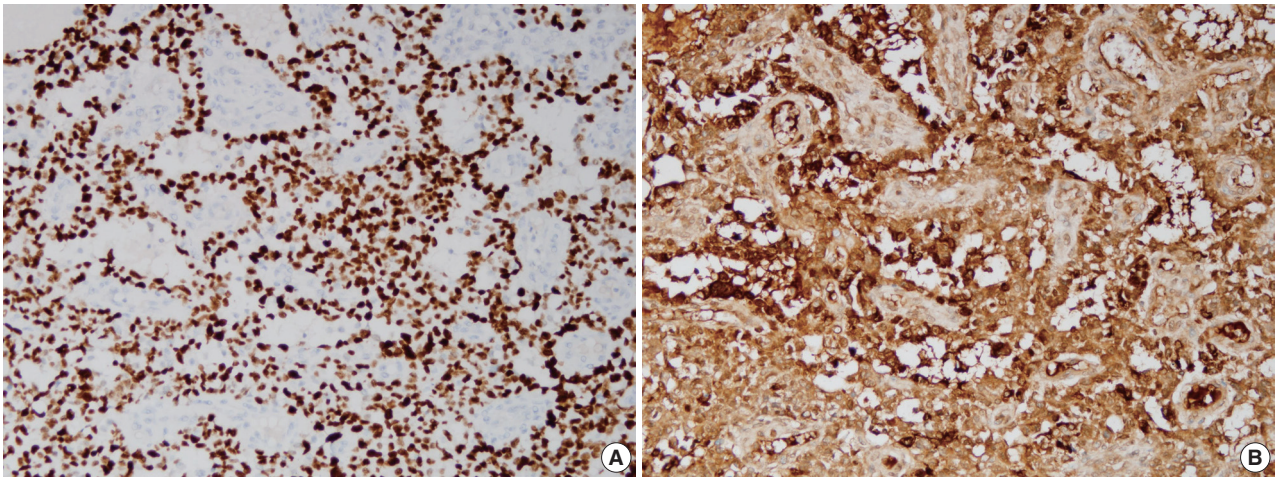

Fig. 3. On immunohistochemical staining, the tumor cells show diffuse strong nuclear positivity for Sal-like protein 4 (A) and diffuse strong cytoplasmic positivity for α-fetoprotein (B).

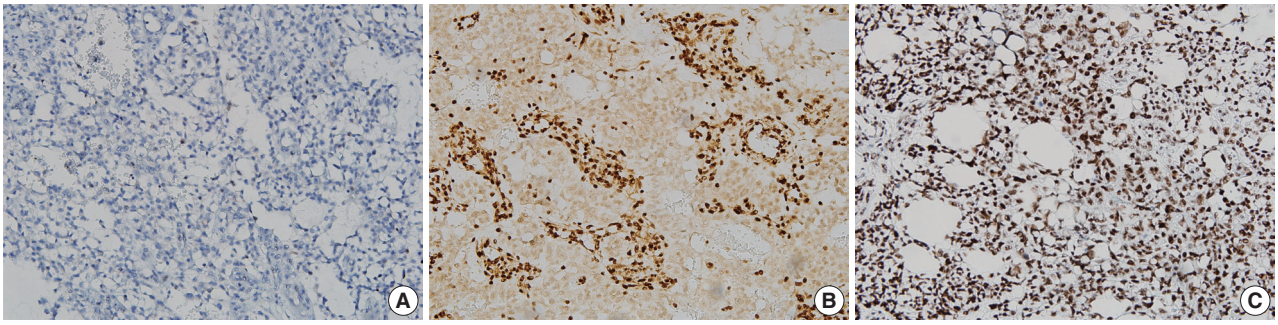

Fig. 4. Immunohistochemical staining revealed that the tumor cells were negative for p40 (A) and diffusely positive for integrase interactor 1 (B) and Brahma-related gene-1 (C).

were both positive (Fig. 4). Therefore, the final diagnosis was pure YST. The patient was started on chemotherapy with a bleomycin, etoposide, and cisplatin regimen and palliative radiation therapy but showed a poor response. He died from the YST at 13 months after diagnosis.

DISCUSSION

YST usually occurs in the gonads and is primarily found in infants and children. Extragonadal sites have included the sacrococcygeal region, retroperitoneum, mediastinum, brain, and very rarely, the head and neck area [2]. In addition, YST is usually accompanied by other germ cell tumor components, like teratoma or embryonal cell carcinoma. For example, the pure form YST of the testis accounts for just 2.4% of the reported adult testicular YSTs [3].

Definite diagnosis of YST can be made by biopsy. Upon microscopy, several histological patterns have been described. The most common is a reticular/microcystic pattern, which is a meshwork of anastomosing spaces and cysts lined by a single layer of tumor cells [4]. Other patterns include endodermal sinus, solid, myxomatous, papillary, glandular, macrocystic, and polyvesicular vitelline [4]. Our case demonstrated reticular, microcystic, and polyvesicular vitelline growth patterns and Schiller-Duval bodies. Shiller-Duval bodies are specific for YST, but they are not essential for diagnosis. The differential diagnoses of this case include sinonasal nonintestinal-type adenocarcinoma, SMARCB1-deficient sinonasal carcinoma with pure yolk sac differentiation, and SMARCA4-deficient teratocarcinosarcoma. Clear cytoplasm, an occasional fibrovascular core, and cytokeratin 7 negativity exclude sinonasal nonintestinal-type adenocarcinoma. SMARCB1-deficient sinonasal carcinoma usually shows high-grade histologic features, including prominent necrosis and mitoses, but relatively uniform cytology [5]. In our case, INI1 positivity excluded the possibility of SMARCB1-deficient sinonasal carcinoma with pure yolk sac differentiation, and BRG1 positivity ruled out the possibility of SMARCA4-deficient teratocarcinosarcoma.

Eight adult-onset YSTs have been reported in the sinonasal

https://doi.org/10.4132/jptm.2021.12.09

Table 1. Previously reported cases of adult-onset yolk sac tumor in the sinonasal area

No.	Age (yr)/Sex	Location	Follow-up	Associated tumor components	Study
1	34/M	Nasopharynx	1 yr (deceased)	Transitional cell carcinoma	Manivel et al. [6]
2	43/M	Orbit, maxillary, ethmoid and frontal sinuses	1.5 yr (pulmonary metastasis)	Transitional cell carcinoma	Manivel et al. [6]
3	48/M	Nasal cavity, ethmoid sinus, cribriform plate	5 yr (disease-free)	Choriocarcinoma	Filho et al. [7]
4	59/M	Orbit, maxillary, ethmoid and frontal sinuses	1 yr (disease-free)	Poorly differentiated carcinoma	Mishra et al. [8]
5	51/F	Nasal cavity, cribriform plate, anterior cranial fossa, and frontal sinus	-	Teratocarcinosarcoma	Thomas et al. [9]
6	58/F	Nasal cavity, ethmoidal sinus, cribriform plate, and nasopharynx	0.8 yr (disease-free)	Transitional cell carcinoma	Mei et al. [10]
7	44/F	Nasal cavity, nasopharynx, ethmoid, sphenoid and maxillary sinuses	-	SMARCB1 (INI1) deficient carcinoma	Zamecnik et al. [11]
8	58/F	Nasal cavity, ethmoid sinus, nasopharynx	3 yr (disease-free)	Transitional cell carcinoma	Wang et al. [12]
9	45/M	Nasal cavity, orbit, frontal and ethmoidal sinuses	13 mo (deceased)	None	Present case

INI1, integrase interactor 1.

area in the English literature (Table 1) [6-12]; four cases were accompanied by a transitional cell carcinoma component. Choriocarcinoma, poorly differentiated carcinoma, teratocarcinosarcoma, and SMARCB1 (INI1)-deficient carcinoma components were present in the remaining four cases, respectively. The reason for the common coexistence of a transitional cell carcinoma component in sinonasal YST remains uncertain. In our case, a transitional cell carcinoma component was not observed, as confirmed by p40 negativity. There are two theories about the origin of extragonadal YST. In the first theory, primordial germ cells are arrested or misplaced during migration from the cranial space to a gonadal site and consequently arrest in the cranial cavity [13]. The second theory holds that extragonadal tumors arise as a result of aberrant somatic differentiation [14]. Previous reports support the second theory. In contrast to previous cases, our case showed histologically pure YST features, which have never been reported. Our case therefore supports the first theory because its histologic features included pure YST not accompanied by other tumor components.

Surgical resection, combined chemotherapy, and radiotherapy are available treatments for YST. Generally, YST is sensitive to chemotherapy. However, the head and neck region, including the sinonasal area as in our case, is very complex and difficult for R0 resection. As a result, the anatomic location seems to affect the prognosis, although the number of sinonasal YST cases is very small [15]. In addition, increasing age is known to negatively affect clinical behavior, and this trend is consistent with our case findings [16].

In conclusion, although adult-onset sinonasal pure YST is extremely rare, differential diagnosis is important. YST can present with many various scenarios in the sinonasal area, so YST should be considered if the clinical findings are histologically suspicious.

Ethics Statement

This case was deemed exempt by the Asan Medical Center Institutional Review Board (IRB #2019-0598). Patient consent waiver was obtained for this study.

Availability of Data and Material

The datasets generated or analyzed during the study are available from the corresponding author on reasonable request.

Code Availability

Not applicable.

ORCID

Jaehoon Shin https://orcid.org/0000-0002-9940-873X
Ji Heui Kim https://orcid.org/0000-0002-9215-6867
Kyeong Cheon Jung https://orcid.org/0000-0002-7741-7184
Kyung-Ja Cho https://orcid.org/0000-0002-4911-7774

Author Contributions

Conceptualization: KJC, KCJ, JS. Data curation: JHK, KCJ, KJC, JS. Methodology: KJC, JS. Writing—original draft: KJC, JS. Writing—review & editing: KJC, JS. Approval of final manuscript: all authors.

Conflicts of Interest

The authors declare that they have no potential conflicts of interest.

Funding Statement

No funding to declare.

References

1. Bernbeck B, Schneider DT, Bernbeck B, et al. Germ cell tumors of the head and neck: report from the MAKEI Study Group. Pediatr Blood Cancer 2009; 52: 223-6.
2. Ronchi A, Cozzolino I, Montella M, et al. Extragonadal germ cell tumors: not just a matter of location: a review about clinical, molecular and pathological features. Cancer Med 2019; 8: 6832-40.
3. Khan S, Jetley S, Pujani M, Neogi S. Pure yolk sac tumor of testis in an adult: a rare occurrence. J Postgrad Med 2014; 60: 351-3.
4. Nogales FF, Preda O, Nicolae A. Yolk sac tumours revisited: a review of their many faces and names. Histopathology 2012; 60: 1023-33.

5. Agaimy A, Hartmann A, Antonescu CR, et al. SMARCB1 (INI-1)-deficient sinonasal carcinoma: a series of 39 cases expanding the morphologic and clinicopathologic spectrum of a recently described entity. Am J Surg Pathol 2017; 41: 458-71.
6. Manivel C, Wick MR, Dehner LP. Transitional (cylindric) cell carcinoma with endodermal sinus tumor-like features of the nasopharynx and paranasal sinuses: clinicopathologic and immunohistochemical study of two cases. Arch Pathol Lab Med 1986; 110: 198-202.
7. Filho BC, McHugh JB, Carrau RL, Kassam AB. Yolk sac tumor in the nasal cavity. Am J Otolaryngol 2008; 29: 250-4.
8. Mishra A, El-Naggar AK, DeMonte F, Hanna EY. Endodermal sinus tumor of the paranasal sinuses. Head Neck 2008; 30: 539-43.
9. Thomas J, Adegboyega P, Iloabachie K, Mooring JW, Lian T. Sinonasal teratocarcinosarcoma with yolk sac elements: a neoplasm of somatic or germ cell origin? Ann Diagn Pathol 2011; 15: 135-9.
10. Mei X, Xia Y, Sasano H, Gao H. Sinonasal yolk sac (endodermal sinus) tumor in an adult female: a case report and review of the literature. APMIS 2015; 123: 810-4.
11. Zamecnik M, Rychnovsky J, Syrovatka J. Sinonasal SMARCB1 (INI1) deficient carcinoma with yolk sac tumor differentiation: report of a case and comparison with INI1 expression in gonadal germ cell tumors. Int J Surg Pathol 2018; 26: 245-9.
12. Wang P, Hou G, Li F, Cheng X. A case of primary sinonasal yolk sac tumor. Clin Nucl Med 2020; 45: 908-9.
13. Oosterhuis JW, Looijenga LH. Human germ cell tumours from a developmental perspective. Nat Rev Cancer 2019; 19: 522-37.
14. Hodgson A, Ghorab Z, Parra-Herran C. Somatically derived yolk sac tumor of the ovary in a young woman. Int J Gynecol Pathol 2021; 40: 296-300.
15. Heerema-McKenney A, Harrison MR, Bratton B, Farrell J, Zaloudek C. Congenital teratoma: a clinicopathologic study of 22 fetal and neonatal tumors. Am J Surg Pathol 2005; 29: 29-38.
16. McKenney JK, Heerema-McKenney A, Rouse RV. Extragonadal germ cell tumors: a review with emphasis on pathologic features, clinical prognostic variables, and differential diagnostic considerations. Adv Anat Pathol 2007; 14: 69-92.

 https://doi.org/10.4132/jptm.2021.12.09

JPTM
Journal of Pathology and Translational Medicine 2022; 56: 157-160
https://doi.org/10.4132/jptm.2021.12.15

CASE STUDY

Juxtacortical chondromyxoid fibroma in the small bones: two cases with unusual location and a literature review

Sun-Ju Oh[1], So Hak Chung[2]

Departments of [1]Pathology and [2]Orthopedic Surgery, Kosin University Gospel Hospital, Kosin University College of Medicine, Busan, Korea

Chondromyxoid fibroma is a rare bone tumor of cartilaginous origin, representing less than 1% of all bone tumors. It preferentially arises in the eccentric location of the metaphysis of a long tubular bone. Juxtacortical locations are reported infrequently in the long bones and even more rarely in short tubular bones, with only three cases documented. Here we present two new cases of juxtacortical chondromyxoid fibroma in the small bones. One was an intracortical osteolytic lesion of the metatarsal bone of the foot with degenerative atypia that histologically should be differentiated from chondrosarcoma. The other was a phalangeal mass protruding into the interphalangeal joint of the hand, which had been labeled mistakenly as a soft tissue mass preoperatively. These cases illustrated that chondromyxoid fibromas have various the manifestations and should be included in the differential diagnosis of an osteolytic lesion or an exophytic mass in the small bones.

Key Words: Chondromyxoid fibroma; Small bones; Juxtacortical

Received: October 11, 2021 **Revised:** December 8, 2021 **Accepted:** December 8, 2021

Corresponding Author: Sun-Ju Oh, MD, Department of Pathology, Kosin University Gospel Hospital, Kosin University College of Medicine, 262 Gamcheon-ro, Seo-gu, Busan 49267, Korea
Tel: +82-51-990-6333, Fax: +82-51-990-3080, E-mail: 10highpowerfield@gmail.com

Chondromyxoid fibroma (CMF) is a rare, benign neoplasm of the bones, mostly affecting people in the second or third decade of life, with a slight male predominance. Long bones, especially the proximal tibia, are the most frequently affected sites, followed by the distal femur, pelvis, and small bones of acral sites [1,2]. The typical CMF eccentrically arises in the medulla of the metaphysis, with sharply circumscribed margins. Infrequent cases of juxtacortical subtypes have been documented in long bones, but only three of the short tubular bones have been reported in the English literature (Table 1). Here we present two new cases of juxtacortical CMF in the hand and foot, respectively.

CASE REPORT

Case 1

A 43-year-old man presented with a swelling on the dorsum of the right foot for more than one year. He complained of intermittent pain for a few months. Plain films demonstrated a well-marginated osteolytic lesion on the second metatarsal bone of the right foot (Fig. 1A). Magnetic resonance imaging (MRI) showed a 2×1.7 cm intracortical mass with expansile growth (Fig. 1B). Medullary bone was partially involved. T1-weighted images revealed an intermediate signal, while T2-weighted images showed a heterogeneous signal with some areas of high intensity. Preoperative diagnosis was a benign bone tumor such as simple bone cyst, and curettage with bone graft was performed.

Histological examination of the lesion showed a lobular architecture on the low-power view (Fig. 2A). Lobules demonstrated hypocellular centers with hypercellular peripheries. Center of the lobules consisted of stellate or spindle-shaped cells with eosinophilic cytoplasmic processes in a myxoid background (Fig. 2B). Cellular areas in the periphery contained round cells with enlarged, hyperchromatic, and pleomorphic nuclei (Fig. 2C). Vacuolization was observed. The nucleocytoplasmic ratio of these cells, however, was low, and no mitosis was found, which implied degeneration rather than malignancy. Overall histologic features rendered a diagnosis of chondromyxoid fibroma. There has been no recurrence for seven months after the surgery.

pISSN 2383-7837
eISSN 2383-7845

Table 1. Reported cases of juxtacortical chondromyxoid fibroma in the small bones

Study	Age (yr)/Sex	Location	Clinical presentation
Baker et al. [2]	65/M	Foot; metacarpal; NA	NA
Slotcavage et al. [9]	29/F	Hand; metacarpal, proximal phalanx; epiphysis, metacarpophalangeal joint	Pain, swelling, movement limitation
Han et al. [7]	17/M	Foot; metatarsal; diaphysis	Pain
Present case 1	43/M	Foot; metatarsal; metadiaphysis	Pain, swelling
Present case 2	43/M	Hand; middle phalanx; epiphysis, interphalangeal joint	Pain, movement limitation

M, male; NA, not available; F, female.

Fig. 1. Radiologic images of the case 1. (A) Oblique radiograph of the foot shows an intracortical lytic lesion (arrow) in the right second metatarsal neck. (B) Sagittal magnetic resonance image shows a hyperintense mass (arrow) with an intact shell of cortical bone.

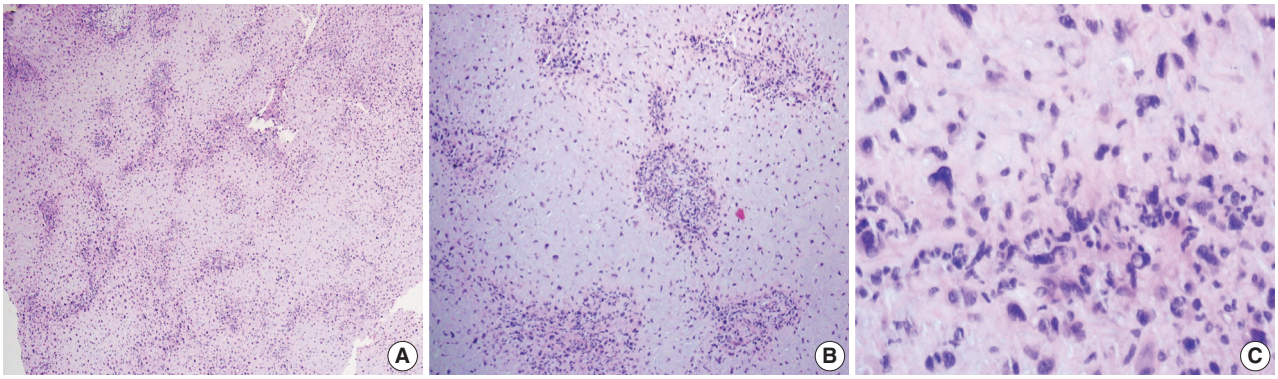

Fig. 2. Histologic findings of the case 1. (A) Low-power view of the tumor shows a prominent lobular patten. (B) The lobules consist of a hypocellular center with abundant myxoid matrix and condensation of tumor cells toward the periphery. (C) The tumor cells in the hypercellular periphery reveal degenerative features including bizarre nuclei, hyperchromasia, and vacuolization.

Case 2

A 43-year-old man presented with dull pain and limitation of movement on the right index finger without any precipitating trauma or injury. Physical examination revealed a soft tissue swelling in the volar aspect of the proximal interphalangeal joint.

Radiographs of the right hand revealed a soft tissue shadow in the proximal interphalangeal joint of the index finger with a small osteolytic lesion in the middle phalanx (Fig. 3A). Multiple calcific deposits were observed. MRI showed a soft tissue mass with high signal intensity in the proximal interphalangeal joint (Fig. 3B). The lesion eroded the epiphysial cortex of the adjacent middle phalanx and was excised under preoperative diagnosis of synovial chondromatosis. In the surgical field, the mass protruded from the head of the middle phalanx and extended toward the soft tissue. A low-magnification view revealed a lobular pattern of tumor cells with zonal architecture (Fig. 3C). The center of the lobules was hypocellular with round and spindle cells, and the periphery was hypercellular containing round cells and multinucleated giant cells (Fig. 3D). One characteristic feature was numerous spotty calcifications, which corresponded to the preoperative radiographs. The histologic diagnosis was juxtacortical chondromyxoid fibroma.

https://doi.org/10.4132/jptm.2021.12.15

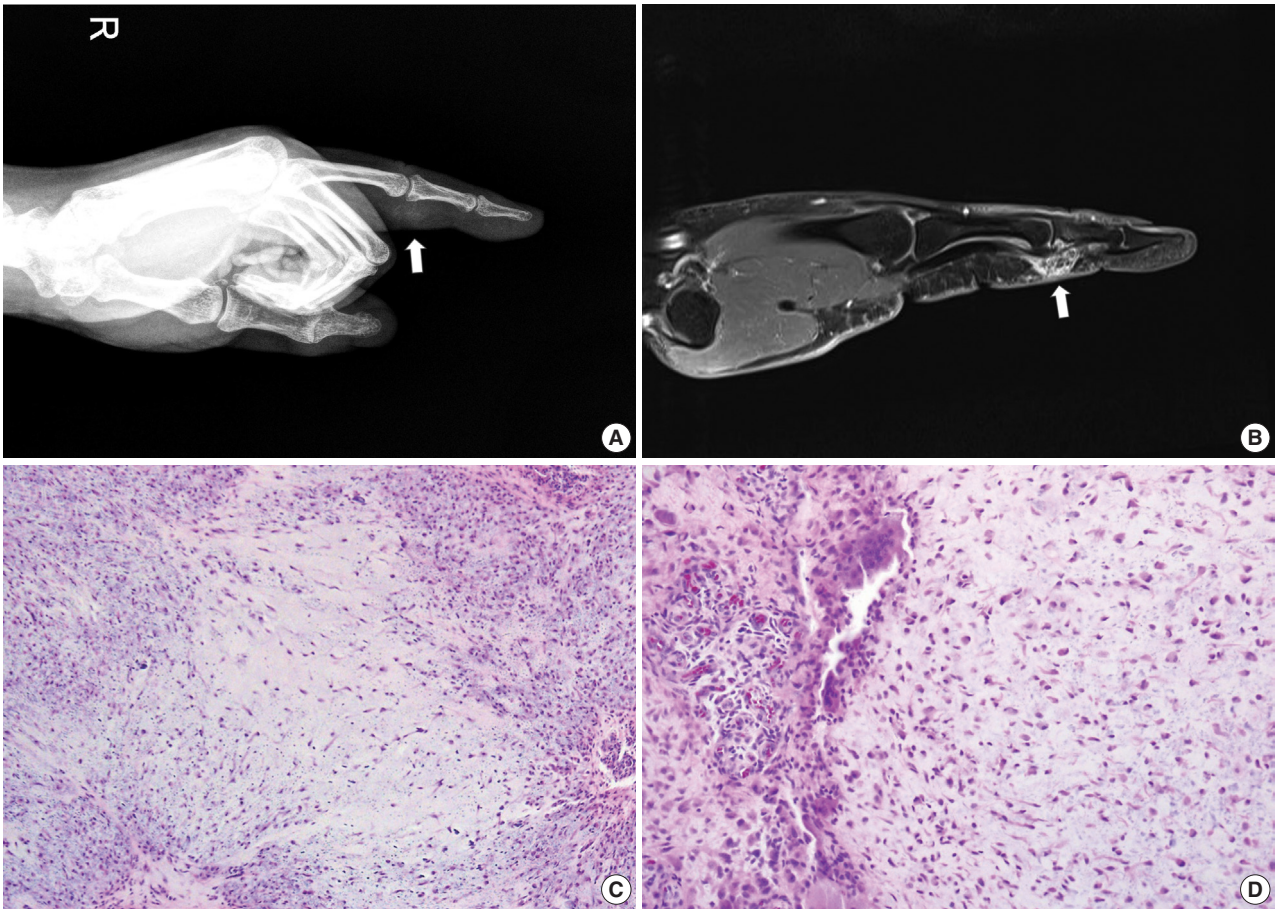

Fig. 3. Radiologic and histologic images of the case 2. (A) Lateral radiograph of the right index finger reveals a soft tissue mass (arrow) with calcification in the proximal interphalangeal joint. The lesion erodes the epiphysis of the mid phalanx. (B) Magnetic resonance image shows a protruding mass (arrow) with heterogeneous intensity. (C) Microphotographs show a characteristic lobular growth pattern. Spotty calcifications are scattered throughout the lesion. (D) Hypercellular area surrounding the hypocellular myxoid lobules occasionally contains multinucleated giant cells.

DISCUSSION

CMF is a rare benign bone tumor, first described by Jaffee and Lichtenstein in 1948 [3]. It accounts for less than 1% of all bone tumors and shows slight male predominance in the second and third decades of life [1]. CMF has a predilection for the metaphysis of a long bone, most often the proximal tibia. Small bones of the feet or flat bones of the ilium are also commonly involved. However, vertebrae, ribs, scapula, skull, and jawbones are rarely involved.

The tumor typically has eccentric location in the bones, with a few cases of juxtacortical subtypes [2,4-9]. Juxtacortical CMFs encompass all surface-type tumors including cortical, subperiosteal, periosteal, or parosteal lesions, and the exact origin is not always identified [2]. Of these juxtacortical cases, most involve long bones, with only three cases affecting small bones of the hands or feet (Table 1) [2,7,9]. Four of five cases including ours involved metacarpal or metatarsal bones. Interestingly, two cases involving the hand appeared in the form of an exophytic mass that involved the joint space; the second current case was mistaken for a soft tissue mass invading the bone on the preoperative radiologic examination.

Pain is the most common symptom in CMFs, as is true of the juxtacortical type of small bones. In addition, soft tissue swelling can manifest due to the thin musculature of hands and feet, and range of motion can be limited when joints are involved.

Histologic features of CMF show a characteristic lobular architecture of a hypocellular center with condensation of tumor cells toward the periphery. The center consists of chondroid and myxoid matrix, containing stellate or spindle-shaped cells often with eosinophilic cytoplasmic process. The lobule is surrounded by fibrous periphery with round cells and scattered multinucleated giant cells. CMFs rarely are accompanied by calcification, but

juxtacortical types can show calcification in the coarse pattern [2]. Tumor cells in CMF are pleomorphic with large nuclei in approximately 20% of cases [10]. Such pleomorphism can be prominent, as in one of our cases, and should be distinguished from chondrosarcoma. The differential findings of CMF are no alteration of nucleocytoplasmic ratio and absence or rarity of unequivocal mitoses.

The main differential diagnosis of CMF is chondrosarcoma, especially with accompanying pleomorphism. The radiologic findings of chondrosarcoma differ markedly from sharply defined CMF even when it slightly erodes the bone. Histologically, chondrosarcoma reveals hypercellularity without zonal architecture. The CMF also differs from chondrosarcoma, with the latter usually producing a large amount of well-differentiated hyaline cartilage and entrapping the pre-existing lamellar bone trabeculae with permeation [11].

Juxtacortical CMFs, especially on the long bones, should be differentiated from the other ominous cartilage-containing neoplasms such as periosteal osteosarcoma and parosteal osteosarcoma [2]. Although the clinical and radiographic features of such neoplasms are usually distinctive, they can show some resemblance to those of CMFs. The most important histologic features of these entities are osteoid formation, which is coarse, lace-like bone present in periosteal osteosarcoma, and well-formed woven bone trabeculae surrounded by cellular fascicles of spindle cells in parosteal osteosarcoma, respectively.

Another benign lesion to differentiate is juxtacortical chondroma or synovial chondromatosis, especially when CMF involves the joint space, as in the current two cases. Juxtacortical chondroma consists of mature chondrocytes lying in lacunae with intervening chondroid matrix. Synovial chondromatosis exhibits nodules of hyaline cartilage, often surrounded by a rim of synovial lining. Juxtacortical chondroma and synovial chondromatosis lack a typical zonal pattern of CMF and show clustering of mature chondrocytes in hyaline cartilage matrix.

En-bloc resection is the mainstay of treatment in CMFs because curettage imposes about 25% risk of recurrence [1]. The prognosis after en-bloc resection is relatively good, though rare cases of recurrence and malignant transformation have been reported [2].

In summary, this study reported two rare presentations of juxtacortical CMFs in the small bones of the hands or feet. Our study indicates that juxtacortical CMFs, although rare, should be considered in the differential diagnosis of a surface-type osteolytic lesion that has well-circumscribed scalloped margins in the short tubular bones or an exophytic lesion radiologically misdiagnosed as soft tissue tumor in the interphalangeal joint.

Ethics Statement

This study was approved by the Institutional Review Board (IRB) of Kosin University Gospel Hospital with a waiver of informed consent (IRB No. 2021-09-030).

Availability of Data and Material

The datasets generated or analyzed during the study are available from the corresponding author on reasonable request.

Code Availability

Not applicable.

ORCID

Sun-Ju Oh https://orcid.org/0000-0001-6013-8579
So Hak Chung https://orcid.org/0000-0003-0689-0270

Author Contributions

Conceptualization: SJO, SHC. Data curation: SJO. Investigation: SJO, SHC. Supervision: SJO. Writing—original draft: SJO. Approval of final manuscript: all authors.

Conflicts of Interest

The authors declare that they have no potential conflicts of interest.

Funding Statement

No funding to declare.

References

1. Unni KK, Inwards CY. Dahlin's bone tumors. 6th ed. Philadelphia: Lippincott Williams and Wilkins, 2010; 50-9.
2. Baker AC, Rezeanu L, O'Laughlin S, Unni K, Klein MJ, Siegal GP. Juxtacortical chondromyxoid fibroma of bone: a unique variant: a case study of 20 patients. Am J Surg Pathol 2007; 31: 1662-8.
3. Jaffe HL, Lichtenstein L. Chondromyxoid fibroma of bone; a distinctive benign tumor likely to be mistaken especially for chondrosarcoma. Arch Pathol (Chic) 1948; 45: 541-51.
4. Takenaga RK, Frassica FJ, McCarthy EF. Subperiosteal chondromyxoid fibroma: a report of two cases. Iowa Orthop J 2007; 27: 104-7.
5. Estrada-Villasenor E, Cedillo ED, Martinez GR, Chavez RD. Periosteal chondromyxoid fibroma: a case study using imprint cytology. Diagn Cytopathol 2005; 33: 402-6.
6. Harrington KA, Hoda S, La Rocca Vieira R. Surface-type chondromyxoid fibroma in an elderly patient: a case report and literature review. Skeletal Radiol 2019; 48: 823-30.
7. Han JS, Shim E, Kim BH, Choi JW. An intracortical chondromyxoid fibroma in the diaphysis of the metatarsal. Skeletal Radiol 2017; 46: 1757-62.
8. Abdelwahab IF, Klein MJ. Surface chondromyxoid fibroma of the distal ulna: unusual tumor, site, and age. Skeletal Radiol 2014; 43: 243-6.
9. Slotcavage RL, Dickson BC, Ogilvie CM. Chondromyxoid fibroma involving the metacarpophalangeal joint. Orthopedics 2009; 32: orthosupersite.com/view.asp?rID=38065.
10. Wu CT, Inwards CY, O'Laughlin S, Rock MG, Beabout JW, Unni KK. Chondromyxoid fibroma of bone: a clinicopathologic review of 278 cases. Hum Pathol 1998; 29: 438-46.
11. Won KY, Lee J, Kim YW, Kim EJ, Kim SW, Park YK. Chondromyxoid fibroma of the ethmoid sinus complicated by a brain abscess: a case report and literature review. Korean J Pathol 2010; 44: 547-50.

JPTM
Journal of Pathology and Translational Medicine 2022; 56: 161-166
https://doi.org/10.4132/jptm.2021.12.28

CASE STUDY

Adrenal hemangioblastoma

Joo-Yeon Koo[1], Kyung-Hwa Lee[1], Joon Hyuk Choi[2], Ho Seok Chung[3], Chan Choi[1]

[1]Department of Pathology, Chonnam National University Research Institute of Medical Science, Bio-Medical Sciences Graduate Program (BMSGP), Chonnam National University Hwasun Hospital and Medical School, Hwasun; [2]Department of Pathology, Yeungnam University Hospital, Daegu; [3]Department of Urology, Chonnam National University Research Institute of Medical Science, Bio-Medical Sciences Graduate Program (BMSGP), Chonnam National University Hwasun Hospital and Medical School, Hwasun, Korea

Hemangioblastoma (HB) is a rare benign tumor that most commonly occurs in the cerebellum. HB is composed of neoplastic stromal cells and abundant small vessels. However, the exact origin of stromal cells is controversial. Extraneural HBs have been reported in a small series, and peripheral HBs arising in the adrenal gland are extremely rare. Herein, we report a case of sporadic adrenal HB in a 54-year-old woman. The tumor was a well-circumscribed, yellow mass measuring 4.2 cm in diameter. Histologically, the tumor was composed of small blood vessels and vacuolated stromal cells with clear cytoplasm. On immunohistochemical stain, the stromal cells were positive for S-100 protein, neuron-specific enolase, and synaptophysin. The tumor did not reveal mutation of VHL alleles. We herein present a case of HB of the adrenal gland and review of the literature.

Key Words: Hemangioblastoma; Adrenal glands; von Hippel-Lindau disease; Immunohistochemistry; Sequencing

Received: December 6, 2021 **Revised:** December 27, 2021 **Accepted:** December 28, 2021
Corresponding Author: Chan Choi, MD, PhD, Department of Pathology, Chonnam National University Research Institute of Medical Science, Bio-Medical Sciences Graduate Program (BMSGP), Chonnam National University Hwasun Hospital and Medical School, 322 Seoyang-ro, Hwasun 58128, Korea
Tel: +82-61-379-7071, Fax: +82-61-379-7099, E-mail: cchoi@jnu.ac.kr

Hemangioblastoma (HB) is a rare benign tumor of the central nervous system that commonly occurs in the cerebellum. While these tumors occur sporadically in most cases, 25% of the patients with HBs are associated with von Hippel-Lindau (VHL) syndrome. Sporadic HBs generally occur in adults between 30 and 65 years of age, whereas VHL-associated tumors present in younger patients, at age 20–30 years [1]. In rare cases, HBs have been reported to occur in extraneural tissue such as the liver, lungs, pancreas, retroperitoneum, soft tissues, and kidney [2-5]. To the best of our knowledge, only five such cases have yet been reported in the literature (Table 1) [3,6-8]. Herein, we present a case of sporadic adrenal HB in a 54-year-old female patient.

CASE REPORT

An adrenal mass was incidentally detected in a 54-year-old woman during a regular medical check-up. She did not have a history of pancreatic tumor, renal tumor, or adrenal tumor. Her family members had no history of such diseases. Laboratory investigations were performed, and 24-hour urinary metanephrine (0.4 mg/day), vanillylmandelic acid (3.3 mg/day), homovanillic acid (4.1 mg/day), and 17-ketosteroid level (16.8 mg/day) were within normal limits. Plasma aldosterone concentration (PAC) was 10.5 ng/dL, plasma renin activity (PRA) was 0.42 ng/mL per hour, and PAC/PRA ratio was 25 ng/dL per ng/mL/hr. Magnetic resonance imaging revealed a $4.2 \times 4.2 \times 3.6$ cm well-defined mass in the left adrenal gland, which was suspected to be a hemangioma (Fig. 1A). The patient underwent partial adrenalectomy. Macroscopic examination revealed that the nodular mass weighed 21 g and displayed a brown-colored cut surface with hemorrhage (Fig. 1B).

On histological examination, the tumor was well encapsulated by a fibrous wall. At low magnification, hypocellular and hypercellular area were present. The tumor was composed of abundant small blood vessels admixed with stromal cells. The blood vessels were lined by thin endothelial cells. The stromal cells had clear and vacuolated or pale eosinophilic cytoplasm (Fig. 2). Their nuclei were round to ovoid, with occasional nuclear atypia. There was no evidence of necrosis. On immunohistochemical stain, the stromal cells were positive for S-100 protein, synaptophysin, and neu-

pISSN 2383-7837
eISSN 2383-7845

Table 1. Reported cases of hemangioblastoma of the adrenal gland in the literature

Case	Age (yr)/ Sex	Clinical feature	Size/Weight	Microscopic findings	Immunohistochemical or special stain/EM	Association with VHL syndrome	Follow-up
Burns et al. (1987) [6]	23/F	Erythrocytosis (hematocrit, 58%)	5.0 cm	Abundant thin-walled blood vessels; stromal cells, large cells with vacuolated clear cytoplasm	Stromal cell with fat vacuole	Yes	NA
Itoh et. al. (1988) [7]	49/M	Incidentally found; elevated noradrenalin (187.4 μg/day) and dopamine (2,308 μg/day) in urine	2.7 cm	Abundant capillary structures; stromal cells, large ovoid	NSE (+), fat stain (+)	No	NA
Nonaka et al. (2007) [3]	30/F	Cerebellar and spinal HB, bilateral adrenal HB	0.9 cm; 0.5 cm	Focal cavernous vascular spaces; stromal cells, vacuolated large with amphophilic cytoplasm, round to oval nuclei	S-100 protein (+, focal), chromogranin (+), CD31 (–), CD34 (–)	Yes	NA
Browning and Parker (2008) [8]	30/M	Bilateral adrenal HB, spinal and cerebellar HB, pancreatic and renal cysts, cystic renal cell carcinoma (suspicious)	Not identified (12.5 g; 8.3 g)	Abundant capillaries; stromal spindled cells. Stromal cells; large, intimately connected with vascular walls	Chromogranin (+), vimentin (+), S-100 protein (–)	Yes	NA
Current case	54/F	Incidentally found	4.2 cm	Abundant capillaries; stromal cells, vacuolated or amphophilic cytoplasm	CD34 (–), CD31 (–), inhibin-alpha (–), EMA (–), CK (–), CA-9 (–), CD10 (–), S-100 protein (+), synaptophysin (+), NSE (+)	No	Alive (1 yr)

EM, electron microscopy; VHL, von Hippel-Lindau; F, female; NA, not available; M, male; NSE, neuron-specific enolase; HB, hemangioblastoma; EMA, epithelial membrane antigen; CK, cytokeratin; CA-9, carbonic anhydrase 9.

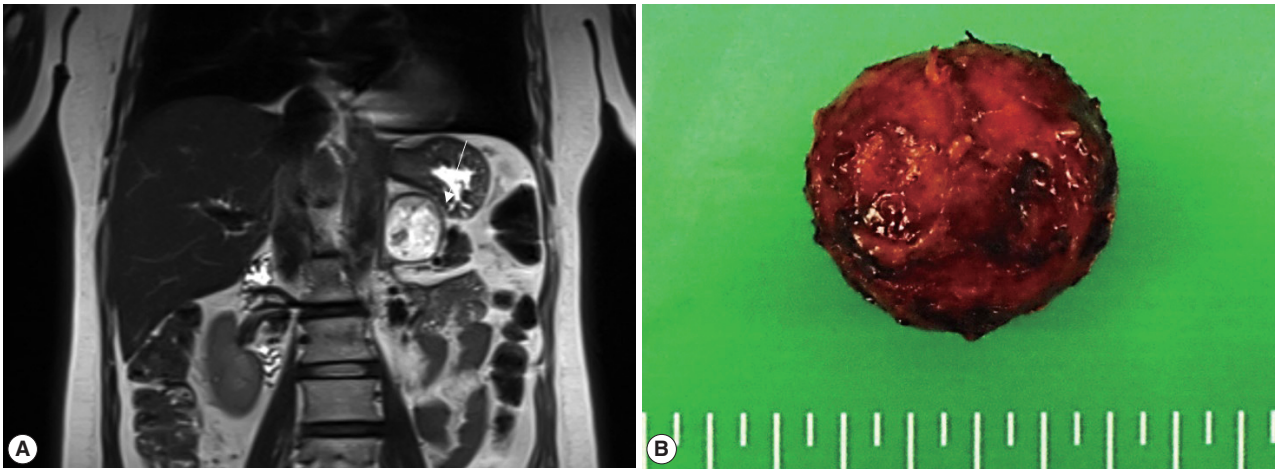

Fig. 1. (A) Magnetic resonance imaging reveals a 4.2×3.6×4.2 cm mass in the left adrenal gland. (B) Gross examination shows an encapsulated nodular mass.

ron-specific enolase (NSE). The endothelial markers, CD34 and CD31, highlighted blood vessels (Fig. 3). The stromal cells were negative for inhibin-α, epithelial membrane antigen (EMA), carbonic anhydrase 9 (CA-9), CD10, glial fibrillary acidic protein (GFAP), GATA3, and chromogranin A. The tumor was diagnosed as HB based on the histological and immunohistochemical findings. The adrenal tissue surrounding the tumor was not submitted.

Targeted sequencing was performed using the ONCOaccuPanel (NGeneBio, Seoul, Korea) which covers 323 genes. Capicua transcriptional repressor (*CIC*), folliculin (*FLCN*), fms related receptor tyrosine kinase 1 (*FLT1*), poly (ADP-ribose) polymerase 1 (*PARP1*), and polybromo 1 (*PBRM1*) were mutated. However, *VHL* was not mutated (Table 2). The patient survived with no evidence of tumor recurrence at 1-year follow-up.

DISCUSSION

HB is a rare benign tumor that generally occurs in the cere-

https://doi.org/10.4132/jptm.2021.12.28

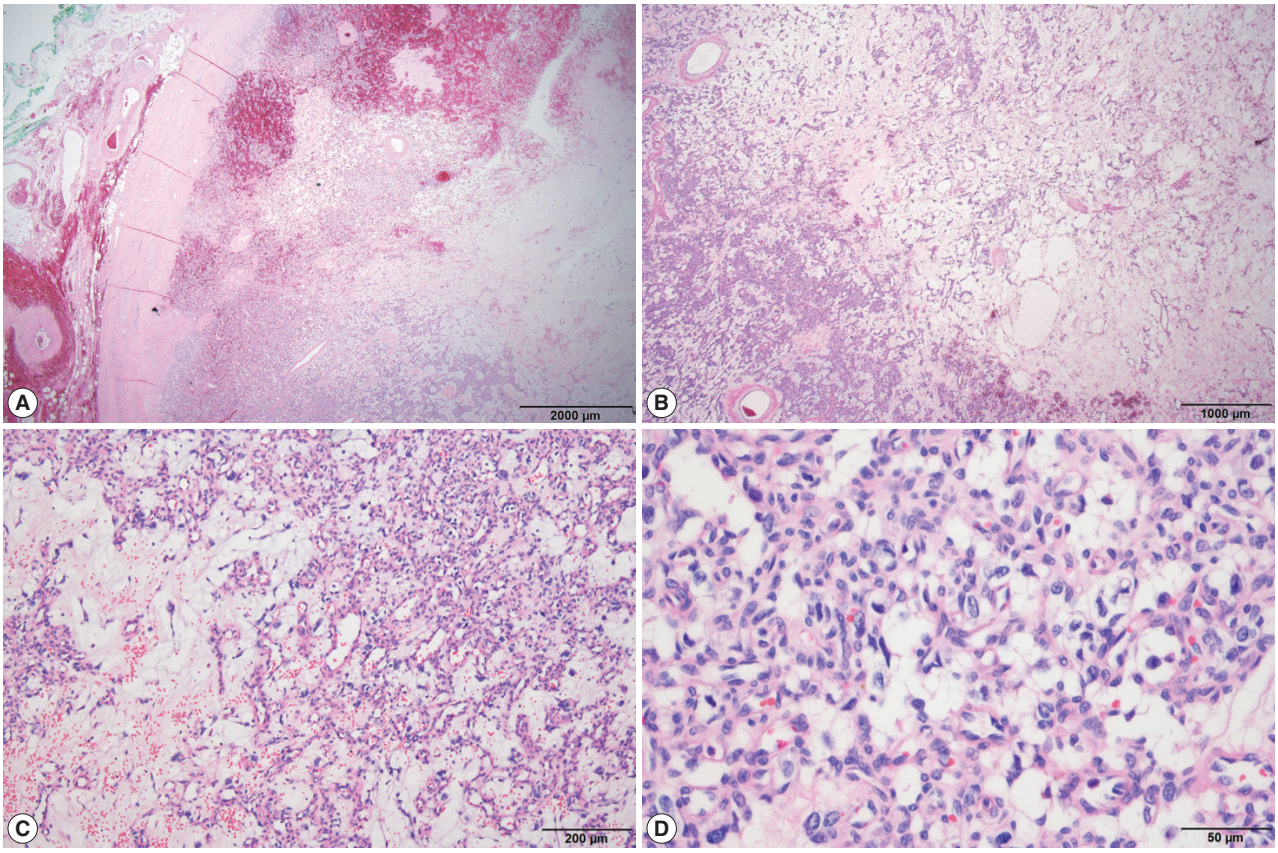

Fig. 2. The tumor is encapsulated by a fibrous wall (A) and is composed of alternating hypercellular and hypocellular areas (B). Vascular structures with vacuolated stromal cells (C, D) are observed.

bellum in adults. In rare cases, HB has been reported to occur at extracerebellar sites. The unusual anatomical locations and histopathological features of HB may pose a diagnostic challenge. HB has been considered as a vascular neoplasm because of the histological findings of its vascular structure. However, various cell lineages such as glial (GFAP), neural (S-100 protein and NSE), vascular, endothelial (factor XIIIa), mesenchymal (vimentin), epithelial (cytokeratin), and smooth muscle/myofibroblastic (desmin and calponin) have been proposed on the bases of immunohistochemical findings [9-12]. Until now, their cell lineage remains unknown.

Somatic inactivation of both *VHL* alleles and the subsequent loss of VHL protein are found in patients with HBs and nonhereditary clear cell renal cell carcinomas (RCCs) [13]. The present case revealed wild-type *VHL* alleles in targeted sequencing. However, mutations of *CIC*, *FLCN*, *FLT1*, *PARP1*, and *PBRM1* were found (Table 2). *CIC* is a member of the high-mobility-group-box superfamily of transcriptional repressors. Mutation of *CIC* is associated with oligodendrogliomas [14], and fusions of *CIC* with *DUX4* (double homeobox 4) and *FOXO4* (forkhead box O) genes have been reported in patients with round cell sarcomas [15]. *FLCN* mutation is associated with Birt-Hogg-Dubé syndrome, which is characterized by benign skin tumors, lung cysts, and kidney lesions [16]. *FLT1* encodes a member of the vascular endothelial growth factor receptor family, which plays an important role in angiogenesis and vasculogenesis. *PARP1* encodes poly(ADP-ribosyl)transferase, which is involved in cell differentiation, proliferation, recovery from DNA damage, and tumor transformation. *PARP1* mutation is associated with Fanconi anemia [17]. *PBRM1* encodes a subunit of ATP-dependent chromatin-remodeling complexes, and *PBRM1* mutation is associated with clear cell RCC [18] and epithelioid sarcoma [19]. It is unclear whether these mutations are specific for HB, and further studies on these mutations in patients with HBs are needed to clarify this issue.

HB should be distinguished from their morphological mimickers, such as pheochromocytomas, perivascular epithelioid cell tumors (PEComas), other vascular tumors, and metastatic RCCs. In cases where vacuolated stromal cells are scant and prominent vascular structures are noted, HB may resemble capillary hem-

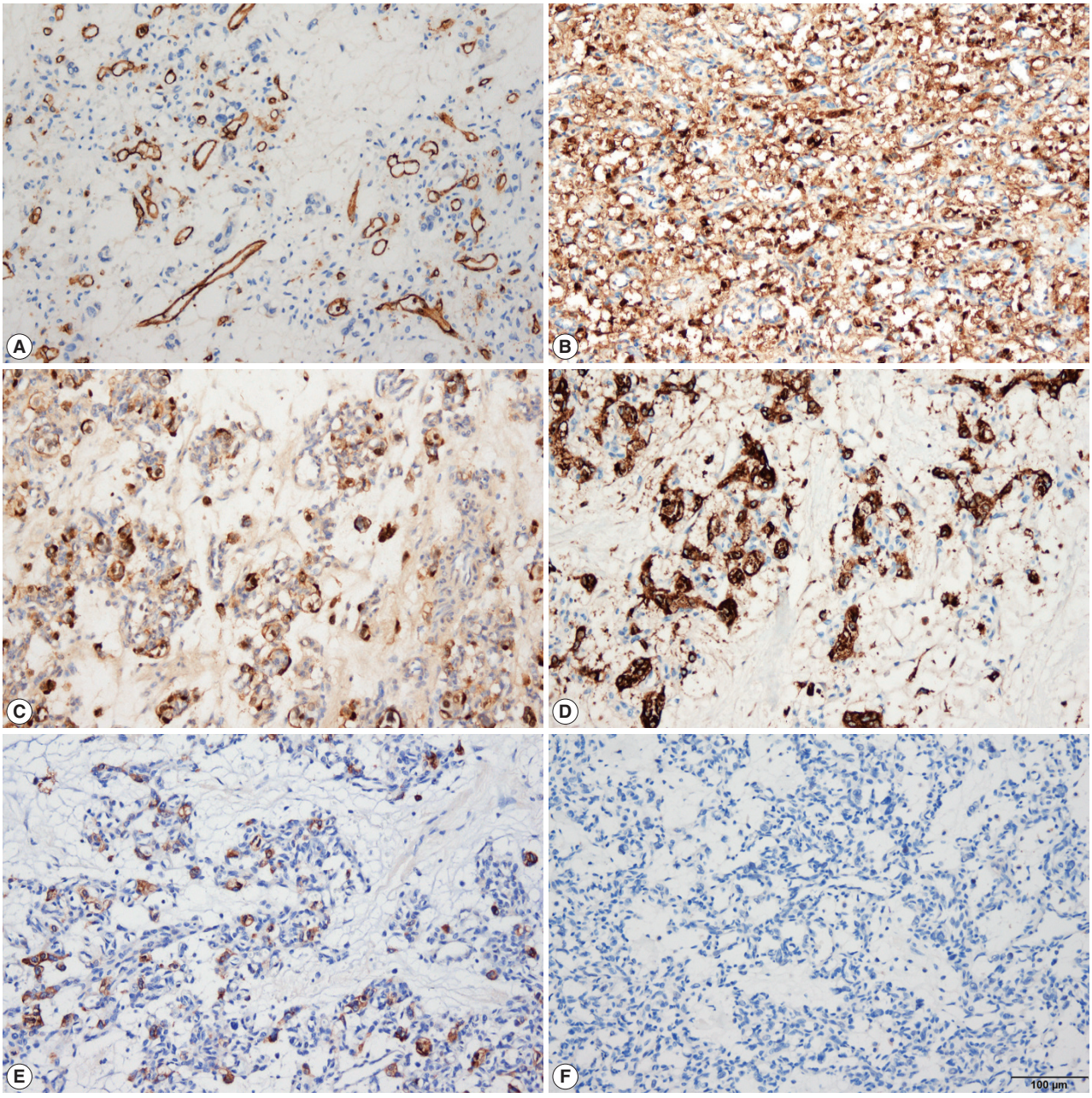

Fig. 3. Immunohistochemical staining shows that the vascular endothelial cells are positive for CD31 (A). The stromal cells are positive for NSE (B), S-100 protein (C), and synaptophysin (D). However, they are negative for chromogranin A (E) and GATA3 (F).

Table 2. The mutated genes found in the targeted sequencing

Gene symbol	RefSeq	Amino acid	Nucleotide	No. of variants/Total	VAF (%)
CIC	NM_015125.3	Pro911Gln	2732C>A	160/365	43.84
FLCN	NM_144997.5	Ser575Leu	1724C>T	165/347	47.55
FLT1	NM_002019.4	Ala673Val	2018C>T	348/734	47.41
PARP1	NM_001618.3	Val991Ala	2972T>C	297/555	53.51

RefSeq, Reference sequence; VAF, variant allele frequency.

https://doi.org/10.4132/jptm.2021.12.28

angioma. However, capillary hemangioma lacks vacuolated or clear stromal cells, and therefore, careful examination is necessary to make a definitive diagnosis. The distinction of RCC from adrenal HB is considered as one of the most difficult differential diagnostic challenges, because RCC can spread to the adrenal gland, and their histological findings may mimic those of HB. Usually, RCC reveals a nested architecture with thin capillaries. Immunohistochemically, RCC is positive for EMA and paired-box gene 8, and negative for inhibin-alpha and S-100 protein. Furthermore, CA-9 is a marker for clear cell RCC, which is the most common subtype of RCC. Pheochromocytoma may arise in the adrenal medulla. Because of their anatomical location and histological findings of microvascular structure and presence of some vacuolated cells, it should be considered as a differential diagnosis of HB. However, the present case did not display a Zellballen pattern, a characteristic feature of pheochromocytomas. Other histological and immunohistochemical features were not consistent with those of pheochromocytomas. PEComa is a mesenchymal tumor with perivascular epithelioid clear cells that generally develop in the kidney, uterus, and soft tissue. Primary PEComa of the adrenal gland is extremely rare and displays a nested growth pattern of epithelioid cells. PEComa typically expresses both smooth muscle and melanocytic markers such as human melanoma black 45 and Melan-A, whereas HB does not express these markers.

In summary, adrenal HB is a rare tumor, and its unusual anatomical location and histopathological features may pose a diagnostic challenge. HB should be distinguished from their morphological mimickers, such as pheochromocytoma, PEComa, other vascular tumors, and metastatic RCC. Considering the rarity of adrenal HB, we present a case report of adrenal HB to provide recommendations for its accurate diagnosis and increased awareness of this disease.

Ethics Statement

This case report was approved by the IRB of Chonnam Natinal University Hwasun Hospital (CNUHH-2021-240). Informed consent was obtained from the participant included in the study.

Availability of Data and Material

The datasets generated or analyzed during the study are available from the corresponding author on reasonable request.

Code Availability

Not applicable.

ORCID

Joo-Yeon Koo https://orcid.org/0000-0003-0551-5954
Kyung-Hwa Lee https://orcid.org/0000-0002-3935-0361
Joon Hyuk Choi https://orcid.org/0000-0002-8638-0360
Ho Seok Chung https://orcid.org/0000-0001-9883-1539
Chan Choi https://orcid.org/0000-0002-9411-9568

Author Contributions

Conceptualization: CC. Data curation: JYK, KHL, JHC. Investigation: JYK. Methodology: YJK, KHL, HSC. Supervision: CC. Visualization: JYK. Writing—original draft: JYK. Writing—review & editing: CC, JHC. Approval of final manuscript: all authors.

Conflicts of Interest

J.H.C., a contributing editor of the *Journal of Pathology and Translational Medicine*, was not involved in the editorial evaluation or decision to publish this article. All remaining authors have declared no conflicts of interest.

Funding Statement

No funding to declare.

References

1. Pakdaman MN, Austin MJ, Bannykh S, Pressman BD. Sporadic hemangioblastoma arising from the infundibulum. J Radiol Case Rep 2017; 11: 1-6.
2. McGrath FP, Gibney RG, Morris DC, Owen DA, Erb SR. Case report: multiple hepatic and pulmonary haemangioblastomas: a new manifestation of von Hippel-Lindau disease. Clin Radiol 1992; 45: 37-9.
3. Nonaka D, Rodriguez J, Rosai J. Extraneural hemangioblastoma: a report of 5 cases. Am J Surg Pathol 2007; 31: 1545-51.
4. Wu Y, Wang T, Zhang PP, Yang X, Wang J, Wang CF. Extraneural hemangioblastoma of the kidney: the challenge for clinicopathological diagnosis. J Clin Pathol 2015; 68: 1020-5.
5. Fanburg-Smith JC, Gyure KA, Michal M, Katz D, Thompson LD. Retroperitoneal peripheral hemangioblastoma: a case report and review of the literature. Ann Diagn Pathol 2000; 4: 81-7.
6. Burns C, Levine PH, Reichman H, Stock JL. Adrenal hemangioblastoma in Von Hippel-Lindau disease as a cause of secondary erythrocytosis. Am J Med Sci 1987; 293: 119-21.
7. Itoh S, Senda K, Sugita Y, Koike A, Takahashi Y. A case of an adrenal capillary hemangioblastoma. Rinsho Hoshasen 1988; 33: 1047-50.
8. Browning L, Parker A. Bilateral adrenal haemangioblastoma in a patient with von Hippel-Lindau disease. Pathology 2008; 40: 429-31.
9. Nemes Z. Fibrohistiocytic differentiation in capillary hemangioblastoma. Hum Pathol 1992; 23: 805-10.
10. Lach B, Gregor A, Rippstein P, Omulecka A. Angiogenic histogenesis of stromal cells in hemangioblastoma: ultrastructural and immunohistochemical study. Ultrastruct Pathol 1999; 23: 299-310.
11. Barresi V, Vitarelli E, Branca G, Antonelli M, Giangaspero F, Barresi G. Expression of brachyury in hemangioblastoma: potential use in differential diagnosis. Am J Surg Pathol 2012; 36: 1052-7.
12. Doyle LA, Fletcher CD. Peripheral hemangioblastoma: clinicopathologic characterization in a series of 22 cases. Am J Surg Pathol 2014; 38: 119-27.
13. Lee JY, Dong SM, Park WS, et al. Loss of heterozygosity and somatic mutations of the VHL tumor suppressor gene in sporadic cerebellar hemangioblastomas. Cancer Res 1998; 58: 504-8.
14. Cahill DP, Louis DN, Cairncross JG. Molecular background of oligodendroglioma: 1p/19q, IDH, TERT, CIC and FUBP1. CNS On-

col 2015; 4: 287-94.
15. Yoshimoto T, Tanaka M, Homme M, et al. CIC-DUX4 induces small round cell sarcomas distinct from Ewing sarcoma. Cancer Res 2017; 77: 2927-37.
16. Schmidt LS, Linehan WM. FLCN: the causative gene for Birt-Hogg-Dube syndrome. Gene 2018; 640: 28-42.
17. Du W, Amarachintha S, Wilson AF, Pang Q. Hyper-active non-homologous end joining selects for synthetic lethality resistant and pathological Fanconi anemia hematopoietic stem and progenitor cells. Sci Rep 2016; 6: 22167.
18. Cancer Genome Atlas Research Network. Comprehensive molecular characterization of clear cell renal cell carcinoma. Nature 2013; 499: 43-9.
19. Li L, Fan XS, Xia QY, et al. Concurrent loss of INI1, PBRM1, and BRM expression in epithelioid sarcoma: implications for the cocontributions of multiple SWI/SNF complex members to pathogenesis. Hum Pathol 2014; 45: 2247-54.

 https://doi.org/10.4132/jptm.2021.12.28

JPTM
Journal of Pathology and Translational Medicine 2022; 56: 167-169
https://doi.org/10.4132/jptm.2021.03.24

BRIEF CASE REPORT

Vascular Ehlers-Danlos syndrome with distinct histopathologic features

Hee Sang Hwang[1], Jin Woo Song[2], Se Jin Jang[1]

Departments of [1]Pathology and [2]Internal Medicine, Asan Medical Center, University of Ulsan College of Medicine, Seoul, Korea

Ehlers-Danlos syndrome is a connective tissue disorders that presents with heterogeneous manifestations depending on the involved genes. Vascular Ehlers-Danlos syndrome (vEDS), also known as Ehlers-Danlos syndrome type IV, is caused by a heterozygous mutation in the *COL3A1* gene that encodes the pro-α1 chains of type III collagen, which attenuates the structural integrity of type III collagen-enriched tissues, such as skin, lung, liver, intestine, and blood vessel. vEDS can result in fatal complications such as arterial or intestinal rupture, but its clinical diagnosis is often challenging. Here, we present a case of vEDS that was diagnosed based on histopathologic and confirmatory genetic examinations.

CASE REPORT

A 19-year-old male was admitted to our hospital for recurrent episodes of spontaneous pneumothorax (6 times), which started about 8 months ago. His father had a history of recurrent pneumothorax and also suffered from spontaneous intra-abdominal bleeding due to aneurysmal rupture of the common hepatic artery 7 years ago. The patient had undergone wedge resection of the lung at another hospital, after which he experienced a secondary pneumothorax, but no specific pathologic diagnosis was made. Thoracic computed tomography at our hospital showed multiple parenchymal cystic lesions with surrounding ground-glass opacity and several small nodular lesions in both lungs (Fig. 1A), suggesting vasculitis with hemorrhage, infected cystic lung disease, or paragonimiasis. However, neither serum anti-nuclear antibody nor anti-*Paragonimus Westermani* antibody titer was elevated. No abnormality in the thoracic greater vessels was identified. Abnormalities of the extrathoracic organs were not evaluated at the time of the admission. Pathological examination of the wedge-resected lung specimen slides sent from an external pathology laboratory revealed intra-alveolar accumulation of red blood cells and hemosiderin-laden macrophages (Fig. 1B, C), indicating recurrent episodes of intra-alveolar hemorrhage. The most diagnostic histologic finding was the presence of several round fibro-osseous nodules scattered in a hemorrhagic background of lung parenchyma (Fig. 1D, E). Disruption of the vascular wall was not identified, even in the examination under van Gieson elastic staining. Due to suspicion of vEDS based on the patient's familial history and the histopathologic findings, *COL3A1* gene sequencing was performed. The sequencing test revealed a heterozygous germline mutation in the spliceosome acceptor site in intron 23 of the *COL3A1* gene (*COL3A1* c. 1662 + 1G > A [p. Gly537_Pro554del]) (Fig. 1F), a known pathogenic mutation in the ClinVar database (https://www.ncbi.nlm.nih.gov/clinvar/variation/101269/). Hence, the patient was diagnosed with vEDS.

DISCUSSION

vEDS comprises about 4%–5% of Ehlers-Danlos syndrome cases and has a high rate of fatal complications related to cardiovascular and gastrointestinal systems, such as cerebrovascular hemorrhage or intestinal rupture. In addition, pregnancy can be fatal in patients with vEDS who might develop ruptures in the uterus or uterine vessels [1]. Therefore, prompt diagnosis is the mainstay of medical management of vEDS to lower the rate of such fatal complications [2]. However, the rarity of vEDS makes its diagnosis challenging, frequently leading to delayed diagnosis. The pathologic diagnosis of vEDS is challenging because the characteristic histopathological findings of vEDS are not widely

Received: December 27, 2020 **Revised:** February 23, 2021
Accepted: March 23, 2021

Corresponding Author: Hee Sang Hwang, MD, PhD
Department of Pathology, Asan Medical Center, University of Ulsan College of Medicine, 88 Olympic-ro 43-gil, Songpa-gu, Seoul 05505, Korea
Tel: +82-2-3010-1869, Fax: +82-2-472-7898, E-mail: hshwang0908@amc.seoul.kr

pISSN 2383-7837
eISSN 2383-7845

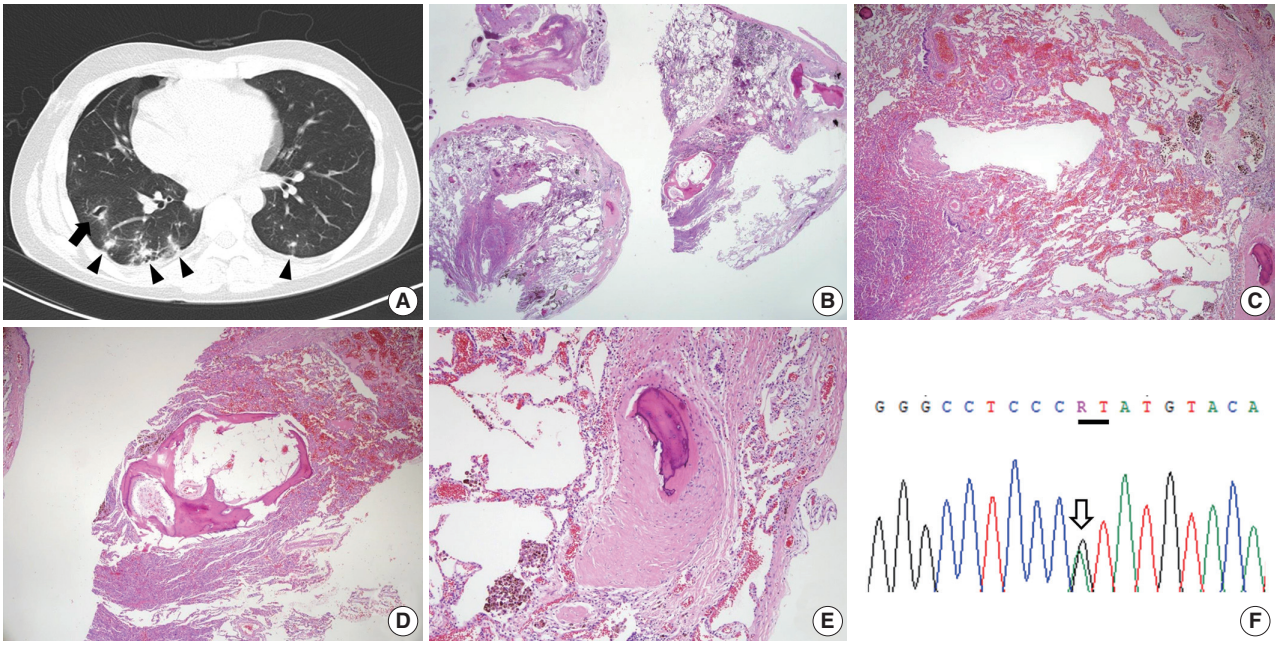

Fig. 1. Radiological and pathological features of the present case. (A) Chest computed tomography, performed after the patient's second episode of spontaneous pneumothorax, showing a parenchymal cystic lesion with an irregularly thickened cavity wall and surrounding ground-glass opacity (arrow). Several ill-defined nodular opacities with adjacent ground-glass opacities, predominant in the basal lungs, were identified (arrowheads). (B) Photomicrogram of the surgical lung biopsy specimen showing multifocal intra-alveolar accumulations of red blood cells and fibro-osseous nodules. (C) Magnified photomicrogram revealing intra-alveolar collections of red blood cells and hemosiderin-laden macrophages. (D, E) Magnifications of a parenchymal fibro-osseous nodule in the background of parenchymal hemorrhage. (F) Sanger sequencing test for the *COL3A1* gene of the patient, showing a heterozygous pathogenic germline mutation (empty arrow) at the spliceosome acceptor site in intron 23 of the *COL3A1* gene (black line) (*COL3A1* c. 1662+1G>A [p. Gly537_Pro554del]).

recognized. Abrupt caliber changes in the muscularis propria with diverticular formation have been identified in colon resection specimens of vEDS patients [3]. Kawabata et al. [4] reported that fragile lung parenchyma with spontaneous laceration, acute hemorrhage and/or hematoma, and fibro-osseous nodules, which are hypothesized to be a consequence of the organization of hematomas, are frequently identified in surgical lung biopsy specimens of vEDS patients, findings which serve as clues for pathologic diagnosis. In line with these findings, a previous report described a case of vEDS that was diagnosed based on identification of fibro-osseous nodules and vascular disruption in the lung parenchyma, suggesting the potential of histopathologic features in clinical diagnosis of vEDS [5]. Therefore, the distinct histopathologic features of vEDS should be considered when assessing surgical lung biopsy specimens from patients with recurrent spontaneous pneumothorax and/or hemorrhagic lung parenchymal cysts.

In conclusion, identifying characteristic histopathologic features in surgical lung biopsy samples, such as parenchymal fragility, spontaneous laceration, parenchymal hemorrhage, and fibro-osseous nodules, can contribute to early clinical diagnosis and proper management of vEDS.

Ethics Statement

This case study was approved by the Institutional Review Board of Asan Medical Center (2020-1889), which waived the requirement for informed consent.

Availability of Data and Material

Data sharing not applicable to this article as no datasets were generated or analysed during the study.

Code Availability

Not applicable.

ORCID

Hee Sang Hwang https://orcid.org/0000-0001-9486-9214
Jin Woo Song https://orcid.org/0000-0001-5121-3522
Se Jin Jang https://orcid.org/0000-0001-8239-4362

Author Contributions

Conceptualization: SJJ, JWS, HSH. Data curation: HSH. Formal analysis: HSH, SJJ. Investigation: HSH. Methodology: HSH, JWS. Resources: SJJ, JWS. Supervision: SJJ. Writing—original draft: HSH. Writing—review & editing: HSH, SJJ. Approval of final manuscript: all authors.

https://doi.org/10.4132/jptm.2021.03.24

Conflicts of Interest

The authors declare that they have no potential conflicts of interest.

Funding Statement

No funding to declare.

References

1. Pepin M, Schwarze U, Superti-Furga A, Byers PH. Clinical and genetic features of Ehlers-Danlos syndrome type IV, the vascular type. N Engl J Med 2000; 342: 673-80.
2. Shalhub S, Black JH 3rd, Cecchi AC, et al. Molecular diagnosis in vascular Ehlers-Danlos syndrome predicts pattern of arterial involveent and outcomes. J Vasc Surg 2014; 60: 160-9.
3. Blaker H, Funke B, Hausser I, Hackert T, Schirmacher P, Autschbach F. Pathology of the large intestine in patients with vascular type Ehlers-Danlos syndrome. Virchows Arch 2007; 450: 713-7.
4. Kawabata Y, Watanabe A, Yamaguchi S, et al. Pleuropulmonary pathology of vascular Ehlers-Danlos syndrome: spontaneous laceration, haematoma and fibrous nodules. Histopathology 2010; 56: 944-50.
5. Berezowska S, Christe A, Bartholdi D, Koch M, von Garnier C. Pulmonary fibrous nodule with ossifications may indicate vascular Ehlers-Danlos syndrome with missense mutation in *COL3A1*. Am J Respir Crit Care Med 2018; 197: 661-2.

JPTM
Journal of Pathology and Translational Medicine 2022; 56: 170-171
https://doi.org/10.4132/jptm.2022.04.25

NEWSLETTER

pISSN 2383-7837 / eISSN 2383-7845

PathologyOutlines.com

What's new in breast pathology 2022: WHO 5th edition and biomarker updates

Kristen Muller[1], Julie M. Jorns[2], Gary Tozbikian[3]

[1]Department of Pathology and Laboratory Medicine, Dartmouth-Hitchcock Medical Center, Lebanon, NH, USA
[2]Department of Pathology, Medical College of Wisconsin, Milwaukee, WI, USA
[3]Department of Pathology, The Ohio State University Wexner Medical Center, Columbus, OH, USA

Received: April 23, 2022
Accepted: April 28, 2022
Corresponding Author: Kristen Muller, DO
Department of Pathology and Laboratory Medicine, Dartmouth-Hitchcock Medical Center, Lebanon, NH, USA
E-mail: kristen.e.muller@hitchcock.org

ORCID
Kristen Muller
https://orcid.org/0000-0003-3166-4523
Julie M. Jorns
https://orcid.org/0000-0002-7777-6670
Gary Tozbikian
https://orcid.org/0000-0002-5941-5652

This article has been published jointly, with consent, in both Journal of Pathology and Translational Medicine and PathologyOutlines.com.

Abstract

The 5th edition WHO Classification of Breast Tumours (2019) has introduced changes to our practices. Highlights are presented below, with a focus on modifications to morphological subtype categorization. In addition, we summarize important updates to ER and PR testing made in the 2020 ASCO/CAP guidelines, and briefly discuss PD-L1 and Ki-67 testing in breast cancer.

GRARE VARIANTS OF INVASIVE BREAST CARCINOMA OF NO SPECIAL TYPE (IBC-NST)

- The prior WHO (4th ed. 2012) classified several tumors as separate entities (listed below). Breast tumors with these "special morphological patterns" now fall under the umbrella category of IBC-NST and are no longer considered to be the following clinically distinct subtypes: oncocytic, lipid-rich, glycogen-rich, clear cell, sebaceous, carcinomas with choriocarcinomatous and pleomorphic patterns, melanocytic, and carcinomas with osteoclast-like stromal giant cells.

INVASIVE BREAST CARCINOMA WITH MEDULLARY PATTERN

- Medullary carcinoma, atypical medullary carcinoma, and carcinoma with medullary features were listed as special subtypes of breast carcinoma in the prior WHO. This diagnostic category has poor interobserver reproducibility; these tumors also show overlapping histologic features with carcinomas that have basal-like molecular profiles and carcinomas with *BRCA1* mutations.
- Tumor infiltrating lymphocytes (TILs) may explain the good prognosis of these cancers.

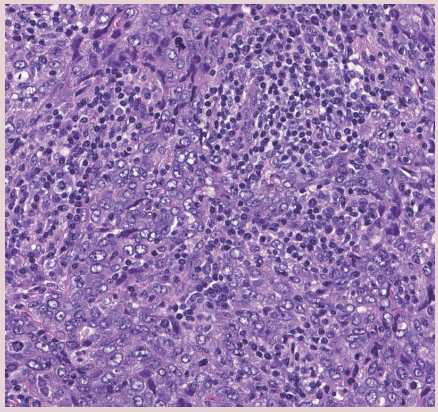

Fig. 1. IBC-NST with medullary pattern. High-grade tumor with a syncytial growth pattern and prominent TILs.

- Carcinomas with a basal-like or medullary pattern (i.e., well-circumscribed, high-grade, syncytial architecture, necrosis, prominent TILs, Fig. 1) now represent one end of the spectrum of TIL-rich IBC-NST; "IBC-NST with medullary pattern" has been proposed to replace "medullary carcinoma."

NEUROENDOCRINE TUMORS

- True primary neuroendocrine (NE) neoplasms of the breast are rare. They are classified as well-differentiated NE tumors (carcinoid-like and atypical carcinoid-like) and poorly differentiated NE carcinomas (small cell neuroendocrine carcinoma and large cell neuroendocrine carcinoma).
- Distinct NE features and expression of NE markers by IHC are needed for diagnosis, since varying degrees of NE differentiation may be seen in IBC-NST, mucinous carcinomas, solid papillary carcinomas, and others.
- Metastasis must be ruled out before considering a primary breast NE tumor.
- Routine staining on IBC-NST that lacks characteristic NE morphological features is not recommended, due to the lack of clinical relevance.

WELL-DIFFERENTIATED LIPOSARCOMA IN PHYLLODES TUMOR

- Malignant heterologous elements are among the diagnostic criteria for malignant phyllodes tumor.
- Adipocytic differentiation in the stromal

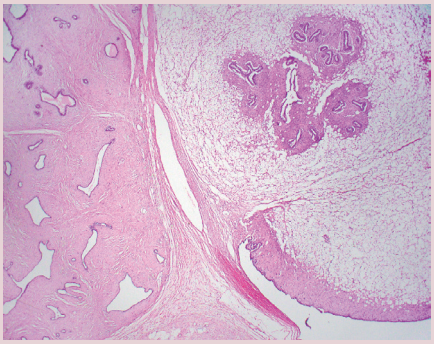

Fig. 2. Phyllodes tumor with liposarcomatous differentiation. Other features (stromal atypia, mitotic activity) in this tumor supported the designation as malignant phyllodes tumor.

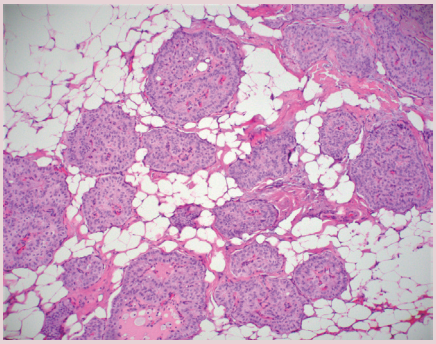

Fig. 3. Tall cell carcinoma with reverse polarity (TCCRP). The tumor is characterized by infiltration of nests of tumor cells with fibrovascular cores and bland columnar cells with apically-located nuclei and abundant eosinophilic cytoplasm.

component of phyllodes tumor, that is morphologically indistinguishable from well-differentiated liposarcoma of soft tissue, has been found to lack the characteristic *MDM2* and *CDK4* amplifications seen in well-differentiated liposarcoma (Fig. 2).

- Based on recent molecular findings and evidence supporting low metastatic risk, the single criterion of well-differentiated liposarcomatous differentiation is no longer recommended for establishing the diagnosis of malignant phyllodes tumor.

MUCINOUS CYSTADENOCARCINOMA

- This recently described, rare, invasive breast cancer subtype is characterized by cystic spaces lined by neoplastic columnar epithelium with papillae and abundant intracellular and extracellular mucin.
- The tumor border is rounded/encapsulated but there is lack of myoepithelium throughout.
- Coexistent DCIS may be present and is helpful in supporting a breast origin.

TALL CELL CARCINOMA WITH REVERSE POLARITY (TCCRP)

- This recently described, rare, invasive breast cancer subtype has characteristic features that include solid nests of tumor, set in fibrous stroma, that have delicate fibrovascular cores lined by bland columnar epithelial cells (Fig. 3).
- Cells have abundant eosinophilic cytoplasm with nuclei present at the apical poles (i.e., reverse polarity) that may have grooves and inclusions.
- Despite low grade morphology, these tumors are positive for CK 5/6 and are triple negative for ER, PR, and HER2. *IDH2* p.Arg172 hotspot mutations have been reported in 84% of tumors studied.

PROGNOSTIC AND PREDICTIVE BIOMARKERS UPDATE

- PD-L1 (clone 22C3)
  - On July 26, 2021, the United States Food and Drug Administration (FDA) approved pembrolizumab for high-risk early-stage triple-negative breast cancer (TNBC) in combination with chemotherapy as neoadjuvant treatment; subsequently it was approved as a single agent adjuvant treatment.
  - The FDA converted the accelerated approval of pembrolizumab, in combination with chemotherapy, for the treatment of locally recurrent unresectable or metastatic TNBC tumors that express PD-L1 (clone 22C3) with a combined positive score (CPS) ≥ 10.
  - CPS is the number of PD-L1 staining cells (tumor cells, lymphocytes, macrophages) divided by the total number of viable tumor cells, multiplied by 100.

$$\text{CPS} = \frac{\text{Number of PD-L1 staining cells (tumor cells, lymphocytes, macrophages)}}{\text{Total number of viable tumor cells}} \times 100$$

- PD-L1 (clone SP142)
  - On August 27, 2021, Genentech withdrew its accelerated indication for atezolizumab plus nab-paclitaxel for the treatment of PD-L1 (clone SP142) positive advanced/metastatic TNBC.
- Ki-67 (clone MIB-1)
  - On October 13, 2021, the FDA approved abemaciclib plus endocrine therapy for hormone receptor positive, HER2 negative, node positive early breast cancer patients with a Ki-67 index ≥ 20%, who are at high risk for recurrence.
  - The FDA approved companion diagnostic to abemaciclib is Ki-67 using the MIB-1 PharmDX/Dako Omnis antibody clone.
- 2020 ASCO/CAP ER/PR Guideline Update Highlights [1]
  - ER low-positive new reporting recommendation: "The cancer in this sample has a low level (1%–10%) of ER expression by IHC. There are limited data on the overall benefit of endocrine therapies for patients with low level (1%–10%) ER expression, but they currently suggest possible benefit, so patients are considered eligible for endocrine treatment. There are data that suggest invasive cancers with these results are heterogeneous in both behavior and biology and often have gene expression profiles more similar to ER-negative cancers."
  - PR testing is optional in DCIS.
  - There is a new recommendation for laboratories to establish a specific protocol to ensure the validity of ER low-positive (1–10%) or negative (0 or < 1%) interpretations and results.

Reference

1. Allison KH, Hammond MEH, Dowsett M, et al. Estrogen and progesterone receptor testing in breast cancer: American Society of Clinical Oncology/College of American Pathologists Guideline Update. Arch Pathol Lab Med 2020; 144: 545-63.

Meet the Authors

Dr. Muller has been an author for PathologyOutlines since 2020 and part of the PathologyOutlines editorial board since 2021. She is currently an Assistant Professor at Dartmouth-Hitchcock Medical Center where she practices Breast and Gynecologic Pathology.

Dr. Jorns has been an author for PathologyOutlines since 2014 and part of the PathologyOutlines editorial board since 2020. She is currently an Associate Professor at the Medical College of Wisconsin where she primarily practices Breast Pathology.

Dr. Tozbikian has been an author for PathologyOutlines since 2018, part of the PathologyOutlines editorial board since 2019, and Deputy Editor in Chief for Breast Pathology since 2021. He is currently an Associate Professor at The Ohio State University Wexner Medical Center where he practices Breast and Genitourinary Pathology.


JPTM
Journal of Pathology and
Translational Medicine